

2. SITE 519¹

Shipboard Scientific Party²

HOLE 519

Date occupied: 1300, 22 April 1980

Date departed: 0600, 25 April 1980

Time on hole: 65 hr.

Position: 26°8.20'S; 11°39.97'W

Water depth (sea level; corrected m; echo-sounding): 3769

Water depth (rig floor; corrected m; echo-sounding): 3779

Bottom felt (m, drill pipe): 3778.5

Penetration (m): 151.6

Number of cores: 37

Total length of cored section (m): 151.6

Total core recovery (m): 138.4

Core recovery (%): 91.3

Oldest sediment cored:

Depth sub-bottom (m): 151.5

Nature: Nannofossil ooze

Age: late Miocene

Basement:

Depth sub-bottom (m): 151.5

Nature: Basalt

Velocity range (km/s): 4.5–6.0

Principal results:

1. Obtained a continuous section of sediments by hydraulic piston corer (HPC) down to the upper Miocene oceanic basement.
2. Biostratigraphical dating of the basal sediment as late Miocene (Tortonian).
3. Established correlation between the biostratigraphy and magnetostratigraphy of the cored section down to the basement.
4. Correlation of the magnetostratigraphy of the sediments with the seafloor lineation down to Chron 10, or Anomaly 5-R.
5. Magnetostratigraphic dating of the basalt basement as 10.3 m.y.

6. Recognition of a Pliocene–Quaternary “ponded facies” or resedimented deposits, overlapping a “draped facies” of upper Miocene pelagic sediments.

7. Identification of a large slump block topped by a turbidite layer, totaling 17 m thick, deposited during the Jaramillo Event of the Matuyama Epoch.

8. Recognition of the realignment of natural remanent magnetization (NRM) during the slumping and turbidite deposition.

9. Establishment for the first time of the lowest occurrences (LOs) of the following species: *Globorotalia cibaoensis* (5.20 m.y.), *Globigerinoides conglobatus* (5.30 m.y.), *Globigerinoides kennetti* (7.50 m.y.), *Catinaster calyculus* (8.95 m.y.), *C. coalitus* (9.6 m.y.), and the highest occurrences (HOs) of the following species: *Globorotalia languaensis* (8.10 m.y.), *Catapsydrax parvulus* (8.20 m.y.), *Catinaster calyculus* (8.35 m.y.), and *C. coalitus* (9.0 m.y.) in a magnetostratigraphically calibrated sequence.

10. Calibration against a magnetostratigraphic time scale of the HOs and/or LOs of the following nannofossil species: *Reticulofenestra pseudoumbilica*, *Pseudoemiliana lacunosa*, *Discoaster tamalis*, *D. surculus*, *D. quinquerramus*, *D. asymmetricus*, *Ceratolithus rugosus*, *Amaurolithus delicatus*, *A. tricorniculatus*, *A. amplificus*, and *A. primus*, and of the following foraminiferal species: *Globorotalia crassaformis*, *G. margaritae*, and *Globigerina nepenthes*.

11. Recognition of peaks of calcite dissolution during late Chron 10 (10 m.y.) and during Chrons 6 to 5 (6–5 m.y.), and a rapid depression of CCD during the early Pliocene (5–4.5 m.y.).

12. Confirmation of the increased influx of terrigenous detritus during the Pliocene and Quaternary (1.5–2.7 m/m.y.) in contrast to the low input during the late Miocene (0.7–1.0 m/m.y.). These rates are comparable to those on the west side of the Mid-Atlantic Ridge during the same two periods (1.7 m/m.y. and 1.1 m/m.y., respectively).

13. Recognition of the late Miocene carbon shift of about $-0.5\text{‰ } \delta^{13}\text{C}$.

14. Recognition of three stages of increases of *Nuttalides umbonifera*, one during Chron 6 (6 m.y.), one just prior to the Gilbert/Gauss transition (3.5 m.y.), and one at about the Gauss/Matuyama transition (2.5 m.y.). The stages signify the first appearance and two intensifications of the activity of the Antarctic Bottom Water (AABW).

15. Recognition of cyclically deposited oozes in the Pliocene and Quaternary, characterized by oscillations in insoluble residue content, in oxygen-isotope values, and in degrees of dissolution that are correlative to the intensities of AABW activity.

16. Postulate of changes in worldwide ocean fertility as the cause of the rise of the calcite compensation depth (CCD) during the Miocene and the depression of the CCD during the Pliocene and Quaternary.

HOLE 519A

Date occupied: 0600, 25 April 1980

Date departed: 1340, 27 April 1980

Time on hole: 55.66 hr.

Position: 26°8.20'S; 11°39.97'W

Water depth (sea level; corrected m; echo-sounding): 3769

Water depth (rig floor; corrected m; echo-sounding): 3779

¹ Hsü, K. J., LaBrecque, J. L., et al., *Init. Repts. DSDP*, 73: Washington (U.S. Govt. Printing Office).

² Ken J. Hsü (Co-Chief Scientist), Geologisches Institut, Eidgenössische Technische Hochschule, CH-8092 Zürich, Switzerland; John L. LaBrecque (Co-Chief Scientist), Lamont-Doherty Geological Observatory, Columbia University, Palisades, New York; Max F. Carman, Jr., Department of Geology, University of Houston, Houston, Texas; Andrew M. Gombos, Jr., Exxon Production Research Company, Houston, Texas; Anne-Marie Karpoff, Institut de Géologie, 67084 Strasbourg Cedex, France; Judith A. McKenzie, Geologisches Institut, Eidgenössische Technische Hochschule, CH-8092 Zürich, Switzerland; Stephen F. Percival, U.S. Geological Survey, Menlo Park, California; Nikolai P. Petersen, Institut für Geophysik, Universität München, D-8000 Munich, Federal Republic of Germany; Kenneth A. Pisciotta, Deep Sea Drilling Project, Scripps Institution of Oceanography, La Jolla, California (present address: Sohio Petroleum Company, 100 Pine Street, San Francisco, California); Richard Z. Poore, U.S. Geological Survey, Menlo Park, California (present address: U.S. Geological Survey, Reston, Virginia); Edward Schreiber, Department of Earth and Environmental Sciences, Queens College (CUNY), Flushing, New York; Lisa Tauxe, Department of Geological Sciences, Lamont-Doherty Geological Observatory, Columbia University, Palisades, New York (present address: Scripps Institution of Oceanography, La Jolla, California); Peter Tucker, Department of Geophysics, University of Edinburgh, Edinburgh, United Kingdom; Helmut J. Weissert, Department of Geological Sciences, University of Southern California, Los Angeles, California (present address: Eidgenössische Technische Hochschule, CH-8092 Zürich, Switzerland); and Ramil Wright, Department of Geology, Florida State University, Tallahassee, Florida (present address: Exxon Production Research Company, Houston, Texas).

Bottom felt (m, drill pipe): 3778.5

Penetration (m): 180.0

Number of cores: 9

Total length of cored section (m): 84.0

Total core recovery (m): 61.4

Core recovery (%): 73.1

Oldest sediment cored:

Depth sub-bottom (m): 151.5

Nature: Nannofossil ooze

Age: late Miocene

Basement

Depth sub-bottom (m): 180.0

Nature: Basalt

Velocity range (km/s): 4.5–6.0

Principal results:

1. Fulfilled the requirement by the JOIDES Planning Committee that drilling into basement should continue until the drill bit wears out.

2. Identified the presence of basalt pillows, basalt breccias, aphanitic basalt, coarse diabase, and other rock types in basement.

3. Confirmed the well-known observations that the mid-ocean ridge basalts (MORB) are tholeiitic and that radiometric dating of MORB is difficult because of argon retention.

4. Established reversed magnetization of the near-surface basalt flow.

5. Measured sonic velocity of basalt.

BACKGROUND AND OBJECTIVES

Site 519 was targeted as the westernmost site of a three-hole traverse along 25° to 30°S on the eastern side of the Mid-Atlantic Ridge to study the paleoceanography and the spreading history of the ridge during the Neogene. The site was to be positioned on Anomaly 5¹ (Epoch 10) short positive between Anomaly 5 and 5A; the seafloor there was expected to have an age of about 10 m.y. The site was selected on the basis of geophysical data provided by the cruise of R/V *Conrad* 801 (13:00 hr., 20 Dec. 1963). A detailed site survey carried out by University of Texas Marine Science Institute (UTMSI) at Galveston in 1979 revealed a small basin perched on the slope of a local ridge underlain by a maximum sediment thickness of about 0.3 s. We chose a site near the edge of the ponded facies, which seemed to have a maximum thickness of pelagic sediments on UTMSI Seismic Line 10 (03:15 hr., 22 Mar. 1979), to avoid erosional unconformities caused by slumping. The site is located 14 km from a minor (18 km offset) left lateral offset fracture zone (the Moore Fracture Zone).

The sediment thickness was estimated to range between 150 and 200 m. The age of the basal sediment was predicted to be early Tortonian. Evaluating the experiences from previous drilling and penetrometer data from Leg 3 cores, we believed that it might be possible to penetrate the entire sediment section by using the hydraulic piston corer (HPC). Consequently it was decided to drill first with the HPC, and then to core the more compact lower section (if any) and the basement with conventional coring after a trip of the drill string to change the core bit. If successful, the cores might provide a detailed and uninterrupted sediment record, at a sedimentation rate of 2.5 to 3 cm/10³ yr., for the last 10 m.y. The sediment cores should yield the samples needed for biostratigraphy (foraminifers, nannofossils, diatoms), for magnetic stratigraphy, and for paleocean-

ography (paleoecology and the stable-isotope analysis of fossils).

Current research indicates that several major events during the last 10 m.y. require further systematic study. They are as follows:

1) 0.7 m.y.—Brunhes/Matuyama boundary. Beginning of Alpine glaciation (Günz) and possible beginning of latest amplification of climatic changes.

2) ~3.5 m.y.—Beginning of major Arctic glaciation.

3) 5 m.y.—End of Messinian salinity crisis. Retreat of the late Miocene Antarctic glacial advance?

4) 6 m.y.—Possible expansion of Antarctic ice cap. Beginning or near the beginning of Mediterranean salinity crisis. Major carbon-isotope shift in world's oceans.

5) 10–12 m.y.—Lowering of calcite compensation depth (CCD), ending the middle Miocene CCD crisis.

We hoped that the cores would provide sufficient material for the investigation of these events.

An uninterrupted section of sediment cores deposited at a relatively fast rate of 2.5 to 3 cm/10³ yr. would provide a further correlation of magnetostratigraphy to biostratigraphy. We might extend refined correlation down from Magnetic Chron 5 or 6 (which has been made possible by hydraulic piston coring during Leg 68) down to Chron 9 or 10. (For the correlation between chrons and magnetic anomalies see Fig. 2 in Hsü, LaBrecque, et al., this vol.) Furthermore, we might improve the absolute chronology of magnetostratigraphy, biostratigraphy, and seafloor anomalies back to a time of 10 Ma from basement radiometric dates near the well identified and spatially narrow Magnetic Anomaly 5¹.

Finally, the question as to whether Cenozoic seafloor spreading has remained at a linear rate has not been completely resolved. Some DSDP sites (e.g., Site 396) drilled in Anomaly 5 reached basement with ages a few million years older than expected. A reduction in the rate of spreading during the middle Miocene has been suspected. A determination of the basement age here compared to that determined at the next two sites would give an accurate rate of spreading for the middle to late Miocene.

The basement objectives were to obtain fresh, unaltered basalt samples for mineralogical, chemical, and paleomagnetic studies. The chemistry of the basalt here, as compared to that of other DSDP holes, should yield information on the possible extent of the heterogeneity of the Earth's mantle. The magnetic properties of the basalt might further our understanding of magnetic lineations on the seafloor and crustal generation.

OPERATIONS

Site Approach

The *Glomar Challenger* approached the targeted site from the west at 1045Z on 22 April 1980. The vessel, sailing at a speed of 10 knots with a heading of 082, passed over a broad magnetic anomaly recognized as Anomaly 5. At 1056Z the speed was reduced to 7 knots. At 1125Z a sonobuoy was thrown overboard for surveying. At 1128Z the vessel passed over a sharp positive anomaly between Anomalies 5 and 5A. At 1139Z we reached the targeted site, a 16-kHz beacon was dropped, and orders

were given to pull in the magnetometer sensor, seismic array, and air gun. At 1155Z all gear was out of the water. The vessel started a turn and at 1202Z took heading 283°, homing on the beacon. At 1230Z the vessel arrived near the site. Three beacons (2 × 13.5 kHz, 1 × 16 kHz) were tested. At 1258Z the vessel was maneuvered on site. A precision depth recorder (PDR) reading was taken and corrected and relayed to the rig floor when the drill crew started to assemble the drill string for the HPC.

Hole 519

The drill bit touched down at 2230Z, and the first core was brought on deck at 0215Z, 23 April (Table 1). Coring operations continued smoothly until 1530Z, when the HPC assembly was dropped because the overshot was sheared. The assembly was retrieved and redressed, and hydraulic piston coring resumed at 1830Z.

Cores were coming up normally at intervals between 1.25 and 1.5 hr. until 0800Z, 24 April, when the HPC

assembly was again dropped and had to be retrieved, with a resultant loss of 2 hr. HPC coring resumed at 1000Z. However, Cores 25 and 26 had broken liners. At 1710Z repair of the rig was necessary, but drilling was resumed at 1830Z. Two shear pins with 1730-lb pressure were now applied. No more liners were broken, and recovery was good. Core 36 failed to achieve full stroke; only 2.6 m were cored. Core 37 was taken after washing down 2.6 m only, but the HPC hit hard basement and recovered only 0.1 m of broken basalt, basalt glass, microfossil debris, and some nannofossil ooze. It was decided to terminate HPC operations in Hole 519. Orders were given to raise the drill string, which cleared the mudline at 0700Z, 25 April. The bottom hole assembly was broken down at 1200Z, and the drill bit reached deck at 1300Z.

Hole 519A

At 1600Z, 25 April, operations were started to run the drill string down. Meanwhile, an air gun survey on station confirmed the basement depth of 150 m at this site. At 2350Z the drill string touched bottom, and Hole 519A was spudded in. After washing down to 67.5 m sub-bottom, the first core was cut. It was raised on deck at 0205Z, 26 April (Table 1). Complete recovery was obtained, but core disturbance was considerable and affected the paleomagnetic results. At 0650Z four cores were obtained back to back, when the drill string registered a sub-bottom depth of 105.5 m. It was decided to wash down for 30 m before cutting Core 5. After 7 m of Core 5 were cut it was discovered that the vessel had drifted 300 m off location. The drilling operation was suspended at 0807Z. Meanwhile, correlation of sediment markers in Holes 519 and 519A indicated that the real depth of Cores 1 to 4 in Hole 519A should be 6 to 10 m less than the registered depth, and that the real depth of the first 7 m of Core 5 should be 10 m less than the registered depth, because of the errors introduced by the drift of the vessel. The discrepancy was confirmed by computations relating apparent depth to drift distance. At 0850Z, drilling was resumed, and the coring of Core 5 was completed. The basement was reached at 151.5 m sub-bottom while Core 6 was being cut, but the core contained only sediments; neither basalt detritus nor basalt was recovered. Drilling characteristics as Core 7 was being cut suggested that loose basalt detritus covering the basement was about 2 m thick before the hard basalt was cored. At 1600Z progress in coring was very slow, indicating that the core barrel was probably jammed. The barrel was raised on deck at 1703Z and was found to contain only 1.5 m of basalt. Two more cores of basalt were cut, with good recovery. Coring in Hole 519A was terminated at 0600Z, 27 April, at 180.0 m sub-bottom after sufficient basalt samples were obtained for shipboard and shore-based studies. The drill string was raised, and the drill bit reached deck at 1315Z, 27 April.

Postdrilling Survey

A postdrilling survey was conducted because of uncertainties concerning the seismic stratigraphy under the

Table 1. Coring summary, Site 519.

Core	Date (April, 1980)	Time (hr.)	Depth from drill floor (m)	Depth below seafloor (m)	Length cored (m)	Length recovered (m)	Recovery (%)
Hole 519^a							
1	23	0210	3778.5–3781.4	0–2.9	2.9	2.9	100%
2	23	0327	3781.4–3785.8	2.9–7.3	4.4	3.7	84
3	23	0440	3785.8–3789.8	7.3–11.3	4.0	4.0	100
4	23	0545	3789.8–3793.8	11.3–15.3	4.0	4.4	100
5	23	0700	3793.8–3797.8	15.3–19.3	4.0	4.5	100
6	23	0804	3797.8–3801.8	19.3–23.3	4.0	4.0	100
7	23	0915	3801.8–3805.8	23.3–27.3	4.0	4.2	100
8	23	1045	3805.8–3809.8	27.3–31.3	4.0	4.2	100
9	23	1145	3809.8–3813.8	31.3–35.3	4.0	4.0	100
10	23	1255	3813.8–3818.2	35.3–39.7	4.4	4.2	95
11	23	1415	3818.2–3822.6	39.7–44.1	4.4	4.2	95
12	23	1525	3822.6–3827.0	44.1–48.5	4.4	4.2	95
13	23	1735	3827.0–3831.4	48.5–53.9	4.4	4.4	100
14	23	1850	3831.4–3835.8	53.9–57.3	4.4	4.1	93
15	23	1951	3835.8–3840.2	57.3–61.7	4.4	3.2	72
16	23	2106	3840.2–3844.2	61.7–66.1	4.4	4.5	100
17	23	2225	3844.6–3849.0	66.1–70.5	4.4	3.7	84
18	23	2350	3849.0–3853.4	70.5–74.9	4.4	3.4	78
19	24	0110	3853.4–3857.8	74.9–79.3	4.4	4.4	100
20	24	0240	3857.8–3862.2	79.3–83.7	4.4	4.4	100
21	24	0350	3862.2–3866.6	83.7–88.1	4.4	3.9	89
22	24	0500	3866.6–3871.0	88.1–92.5	4.4	3.3	75
23	24	0645	3871.0–3875.4	92.5–96.9	4.4	3.5	80
24	24	0750	3875.4–3879.8	96.9–101.3	4.4	4.4	100
25	24	1050	3979.8–3844.2	101.3–105.7	4.4	2.4	54
26	24	1150	3884.2–3888.6	105.7–110.1	4.4	2.2	50
27	24	1350	3888.6–3893.0	110.1–114.5	4.4	2.8	64
28	24	1445	3893.0–3897.4	114.5–118.9	4.0	3.0	68
29	24	1558	3897.4–3901.8	118.9–123.3	4.4	3.7	84
30	24	1710	3901.8–3906.2	123.3–127.7	4.0	4.1	100
31	24	2003	3906.2–3910.6	127.7–132.1	4.4	4.6	100
32	24	2135	3910.6–3915.0	132.1–136.5	4.4	4.6	100
33	24	2245	3915.0–3919.4	136.5–140.9	4.4	4.5	100
34	24	2350	3919.4–3923.8	140.9–145.3	4.0	3.7	94
35	25	0055	3923.8–3928.2	145.3–149.7	4.4	4.3	98
36	25	0340	3928.2–3932.6	149.7–154.1	3.0	2.6	87
37	25	0450	3932.6–3937.0	154.1–158.5	0.1	0.1	100
Total					151.6	138.4	91.3
Hole 519A^b							
0	26	—	0–67.5 ^c	0–3846.0	Washed		
1	26	0205	67.5–77.0 ^c	3846.0–3855.5	9.5	9.3	98
2	26	0345	77.0–86.5 ^c	3855.5–3865.0	9.5	9.2	97
3	26	0520	86.5–96.0 ^c	3865.0–3874.5	9.5	9.7	100
4	26	0650	96.0–105.5 ^c	3874.5–3884.0	9.5	9.4	99
5	26	1000	134.0–143.5 ^d	3984.0–3922.0	9.5	9.8	100
6	26	1115	143.5–153.0	3922.0–3931.5	9.5	2.1	22
7	26	1705	153.0–160.5	3931.5–3939.0	7.5	1.5	20
8	26	2305	160.5–171.5	3939.0–3949.5	10.5	4.8	46
9	27	0600	171.0–180.0	3949.5–3958.5	9.0	5.6	62
Total					84.0	61.4	73

^a Hydraulic piston coring.

^b Rotary coring.

^c Corrected depth minus 6 m because of ship drift.

^d 134–141 m = 124–131 m; 141–143.5 m = true depth (see text on operations).

site. The *Glomar Challenger* got under way at 1330Z, 27 April. The course of the survey is shown in Figure 1. At 1551Z the vessel passed over the beacon again and resumed normal speed (200/200) at 1617Z, proceeding on heading 035° for Site 520.

LITHOLOGY

Sediments

At Site 519, a 151-m-thick sequence of pelagic sediments was continuously cored to basement by using the hydraulic piston corer. Nearly complete recovery and lack of drilling disturbance enabled us to distinguish three lithologic units within this sequence (Fig. 2). The units were differentiated on the basis of color, sedimentary structure, foraminifer content, and calcium carbonate content. Conventional rotary drilling at the same location (Hole 519A) recovered sediments from selected intervals that we tentatively correlated with those at Hole 519 by using prominent marker beds—a diatom-nannofossil ooze layer and a series of distinctive foraminifer turbidites, the latter paired with a sharp color change in the sediments. The depths of cores in Hole 519A are apparent depths, with errors ranging up to 10 m because of a 300-m drift of the vessel (see Operations).

Unit 1 (0–54 m, Cores 1–13, Hole 519) consists of a predominantly white to very pale brown foraminifer-nannofossil ooze. Except for several distinct burrowed intervals, the sediment is homogenous. Foraminifer content varies between 5 and 20% in the ooze. Calcium carbonate content averages about 90% (Fig. 2). A slump deposit is intercalated with the pelagic sequence between

15 and 30 m. The redeposited sediment is characterized by syngenetic folds, chaotic mixtures of white and pale brown ooze, and inclined and faulted beds. The slump is overlain by a graded foraminifer sand. Similar turbiditic foraminifer sands occur in the lower part of Unit 1.

Unit 2 (54–106 m, Cores 14–25, Hole 519; 67–106.5 m, Cores 1–4, Hole 519A) consists of homogeneous white and very pale brown nannofossil ooze. Burrowed intervals occur sporadically. The general paucity of foraminifers in this unit distinguishes it from Unit 1. Discoasters dominate the calcareous flora. As in Unit 1, the calcium carbonate content is high, averaging about 90%. However, between 88 and 94 m the carbonate content drops to 75%. Within this interval a distinct color change from white ooze to pale yellow to brown nannofossil ooze occurs. At 53 to 62 m and at 100 m in Hole 519, we found laminated diatom-nannofossil ooze. We tentatively correlate the upper diatom occurrence with similar sediments in Hole 519A (Core 1). A foraminifer turbidite occurs in the lower part of this unit.

Unit 3 (106–151 m, Cores 26–37, Hole 519; Cores 5–6, Hole 519A) consists of very pale brown, light yellowish brown, brownish yellow, dark yellowish brown, olive brown, and dark brown, marly nannofossil ooze. The abrupt change to darker colors distinguishes Unit 3 from the overlying unit and reflects the downward relative increase in clay and micronodule contents of the sediment. Color alternations within this unit are consistently sharp, with only a few gradational contacts. The calcium carbonate content in the darker sediments is low (60–75%), with the lowest value just above the sedi-

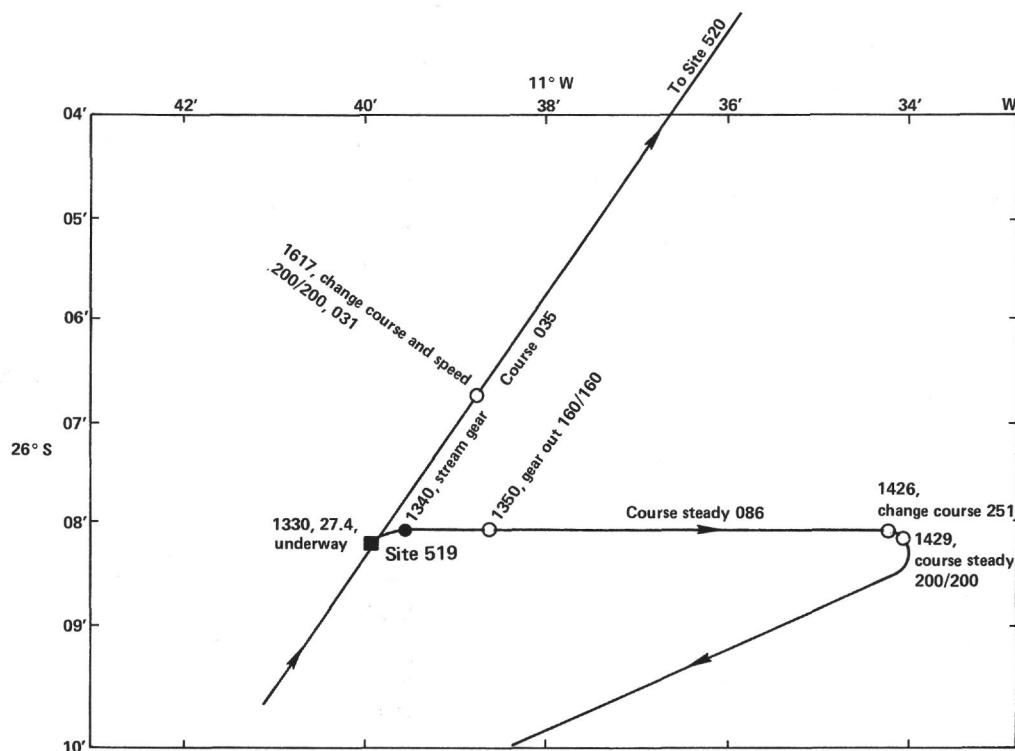


Figure 1. Post-drilling site survey, Site 519.

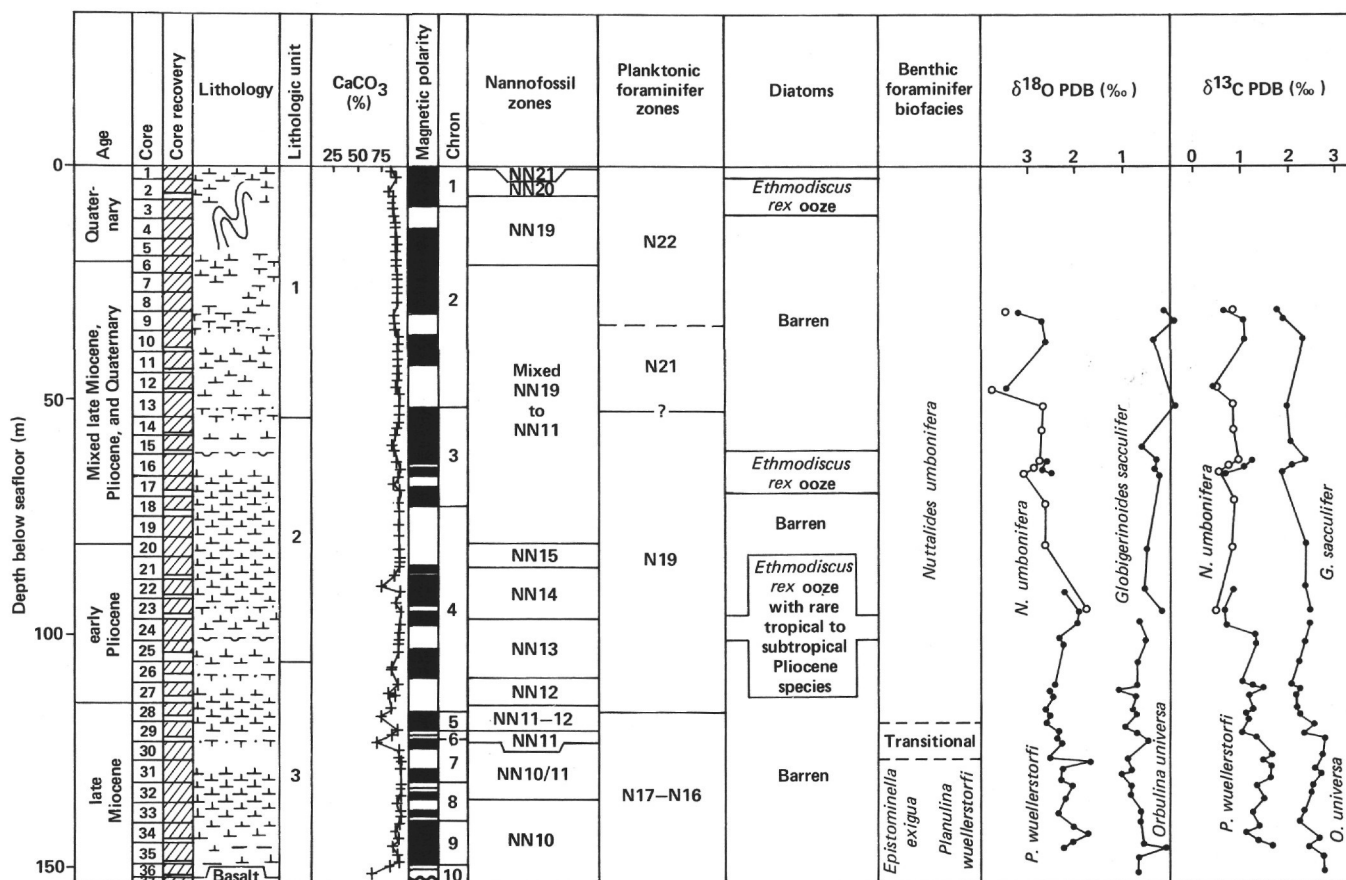


Figure 2. Lithology and stratigraphic summary of Hole 519. Lithology is defined in Hsü, LaBrecque, et al. (this vol.).

ment/basement contact. Unit 3 contains several thin, graded foraminiferal sands.

The observed decrease of foraminifers from Unit 1 to Unit 2 reflects increased dissolution during the late Miocene. Nannofossil preservation parallels this trend; dissolution-resistant discoasters begin to dominate the calcareous flora in Unit 2. Increased dissolution is also reflected in the distinct color change from light-colored to brown and olive brown oozes between Units 2 and 3. These trends suggest that the depth of the foraminifer lysocline in the South Atlantic was shallower during the late Miocene than in Pliocene and Quaternary times.

The pelagic sequence at Site 519 is interrupted by numerous foraminiferal turbidites and slump deposits. These deposits are the results of sedimentary gravity flows and emphasize the significance of relief-controlled sedimentation in pelagic environments.

Igneous Rocks

In a total, 27 m of basalt were drilled in Hole 519A, of which 11.9 m (44%) were recovered. The columnar section of Figure 3 summarizes the details of core and section number, lithology, and designation of flow units. The entire sequence consists of aphyric tholeiitic basalt, all of which is from flow units, with the possible exception of a thin unit near the middle of the cored interval that may be a sill.

Mineralogically, the rocks are all essentially the same, and chemically they are typical ocean floor tholei-

ites (Dietrich et al., this vol.). In the CIPW norm they are plagioclase tholeiites with maximum 4% olivine. They represent rather primitive magmas, with Mg number (Mg/Mg + Fe²⁺) 0.64–0.65, except for Unit 2 (0.67). This assumes that Fe₂O₃/FeO = 0.1. TiO₂, Y, Zr, V, Cr, Ni, Sr, and Ba show concentrations that are distinctive for each petrographic unit (Dietrich et al., this vol.).

Five flow units are distinguished on the basis of structural and textural variations. The approximate thicknesses of the units are 4 m (Units 1 and 2), 0.5 m (Unit 3), 6 m (Unit 4), and 1+ m (Unit 5).

The top of each flow is very fine grained or glassy. The top 70 cm of Flow Unit 1 are pillowed, as shown by glassy and/or very fine quench textures at about 25, 40, and 70 cm and fine quench textures throughout the rest of the top 70 cm. Thus, it is judged that there are three pillows with thicknesses ranging from 15 to 30 cm. They are included in Unit 1 because of their precise chemical identity with the massive unit on which they rest. Distinctive flow-top breccias mark the tops of Units 2 to 5. All units coarsen and show similar characteristic textural changes toward their centers. In Units 1, 2, and 4 the lower margins are more fine grained than the centers. Unit 3, although it coarsens slightly downward, is fine grained throughout, as are the outer several centimeters of the border phases of the thicker flows. Drilling stopped before the base of Unit 5, but the fineness of grain to a depth of about a meter suggests that this is a thin flow and is less than 3 or 4 m thick.

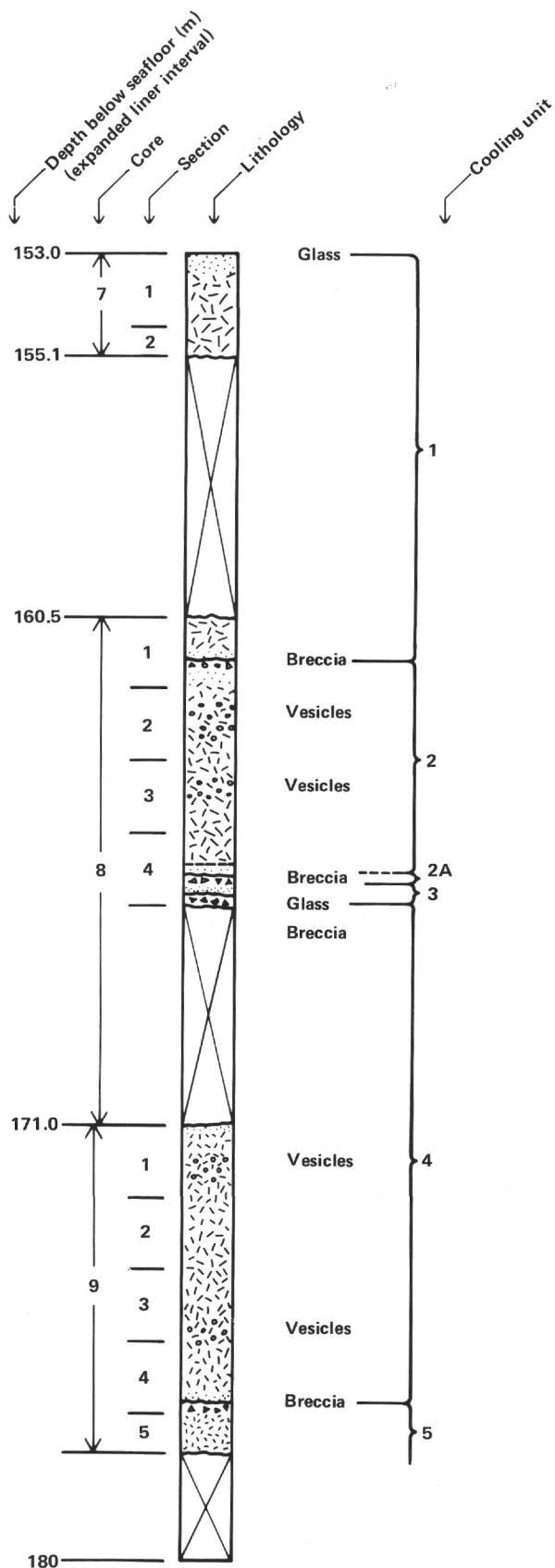


Figure 3. Summary of basaltic rocks at Hole 519A.

Unit 2A is a possible very thin flow or sill, based solely on megascopic examination. In Core 8, Section 4, three pieces (Pieces 3A, B, and 4) all consist of fine-grained aphyric basalt. Pieces 3A and 4 bound, above and below, the larger Piece 3B. Pieces 3A and 4 are badly altered, as are the rocks at all the other contacts. Piece 3A contains an opal-filled vein of a type not seen within any other rocks. Piece 3B is a finely vesicular black basalt that is distinctly fresher than either Piece 3A or 4. Although we lack a thin section to check the quench texture for flow rock characteristics, we are able to interpret these three rocks as being part of a thin sill, a separate flow unit, and part of the lower facies of Unit 2.

Flow Units 2 and 4 each contain vesicular zones 0.5 to 1 m thick in the upper and lower parts of the flow interior. The vesicles are not abundant in these zones, comprising less than 5% of the rock. They range in size from 0.5 to 10 mm, and most are simply calcite filled, although some in the lower zone of Unit 2 contain a clear noncarbonate mineral (zeolite?), and many of those in Unit 4 were lined with olive green to yellowish brown smectite before being filled with calcite.

The central portion of Unit 2 is crossed by a set of conjugate fractures that intersect the core axis at about 60°, and the center of Unit 4 has prominent vertical fractures as long as 1 m. Both of these fracture sets are lined with dark green smectite and black hydrous manganese/iron oxide and filled with calcite. The center of Unit 4 also has horizontal, thin, discontinuous gash fractures that suggest cooling contraction. The fractures are a few centimeters long and 0.25 to 0.5 mm thick. Irregular fractures are common, but sporadic, and most range from small fractions of a millimeter to a few millimeters thick. Most are smectite lined, and many are calcite filled. No obvious differences in lining and filling were observed within or between flow units.

Petrography

All units are aphyric basalts composed of approximately equal parts calcic plagioclase and normal augite, with accessory olivine, pigeonite, titanomagnetite, ilmenite, and rare chrome spinel. In the fine-grained and finer phases, olivine and plagioclase occur as sparse microphenocrysts that range in size from 0.2 to 4 mm. Some of the plagioclase grains are aggregated into glomerocrystic clusters.

Textures show consistent and continuous gradation from cooling boundaries toward the interior of flows. The sequence of textures is glassy, fine to coarse quench (with spherulitic structures), intersertal, subophitic intersertal, and ophitic intersertal.

In the quench texture regions we have somewhat arbitrarily designated six distinctive zones grading from the glass into holocrystalline rock. All phases can be rather easily determined with the microscope. The zones are as follows. Rock with glassy texture is either Zone 1 (glassy; Pl. 1, Fig. 1) or Zone 2 (glassy spherulitic; Pl. 1, Fig. 2). Rock with very fine quench texture is either Zone 3 (coalesced spherulitic; Pl. 1, Fig. 3) or Zone 4 (sheaf-shaped spherulitic; Pl. 1, Figs. 4 and 5). Rock with fine quench texture is Zone 5 (plumose dendritic;

Pl. 1, Fig. 6 and Pl. 3, Fig. 1). Rock with coarse quench texture is Zone 6 (coarse dendritic; Pl. 2, Figs. 1 and 2).

Natland (1979) and Kirkpatrick (1979) have described the same features and established similar zones.

Grain-size increase goes along with these changes, ranging from very fine to medium grained within 2 or 3 cm of a glassy rind in the zones of quench textures, and increasing more gradually thereafter through coarse and very coarse grained. The centers of the thicker flows (Units 1, 2, and 4) are evenly very coarse grained in the range from 0.5 to 2.5 mm over all except the outer few centimeters of each unit. Flow Unit 5 is unique in having flow structure and hyalopilitic texture consisting of thin, tapered, swallow-tailed, and hollow microlites of plagioclase in subparallel alignment and set in an abundant matrix of finely fibrous pyroxene and crypto-crystalline devitrified glass.

Plagioclase is invariably fresh in these rocks. Most of it displays the range of habits to be expected in the textures mentioned, ranging from finely fibrous to skeletal (very thin elongate, tapered, swallow-tailed, hollow, and in radiating sheaves in finer quench zones; thicker, boxy, and hollow, with some chain-link texture in coarse quench portions), and finally to tabular and mostly solid in subophitic and ophitic zones. In some rocks there occurs in the interstices between larger grains a later generation of plagioclase, with finer quench textures. This has perhaps been caused by increased undercooling with the advance of crystallization (Kirkpatrick, 1979, p. 279). The plagioclase is rather strongly zoned, with compositions ranging approximately from An_{75} to An_{50} , and perhaps as low as An_{25} or An_{30} in the outermost extremes of especially strongly zoned grains.

Two types of plagioclase microphenocrysts were detected and designated as being of first or second generations (Pl. 1, Fig. 1 and Pl. 3, Fig. 1). First-generation types are euhedral to subhedral, stubby (width-to-length ratios 1:1–1:10, average 1:3–1:4), simply and coarsely twinned, inclusion-free, slightly to moderately zoned (An_{80-60}), fine- to very coarse-grained (0.04–4.0 mm) crystals, usually occurring in glomerocrystic clusters. Most have thin, more sodic epitaxial rims. On many grains these rims continue as tapering spines from the corners of the microcrysts. None show signs of corrosion or melting, as would be likely if the crystals were out of equilibrium with the enclosing magma. Second-generation types are mostly subhedral, elongate (width-to-length ratios 1:3–1:17, average 1:8–1:10), finely polysynthetically twinned, skeletal (with open ends and inclusion-filled (usually clinopyroxene) centers), strongly zoned (maximum An_{75-30}), fine- to very coarse-grained (0.02–1.3 mm) crystals, often intergrown in subradial clusters with subophitic olivine and/or clinopyroxene. Both types of microphenocrysts are found in the glass of all units examined. The first-generation type is designated as such because of its distinctive morphology, which is typical of relatively slow growth under quiet stable conditions, and its striking difference from grains that have obviously formed after extrusion. First-generation clusters have a distinctively gabbroid or cumulus

aspect. Second-generation types, on the other hand, are clearly morphologically related to groundmass crystals, into which they grade by size; and their textural relations are related to the ferromagnesian minerals.

Pyroxene appears to be mostly normal augite, displaying a range of habits from very finely fibrous and dendritic (in plumose (Pl. 1, Fig. 5) and comb-shaped (Pl. 3, Fig. 1) units) in very fine and fine quench textures, to medium and coarse dendritic grains with serrated cross section in coarse quench textures (Pl. 2, Figs. 1 and 2 and Pl. 3), and coarse to very coarse grains and aggregates of grains in subophitic and ophitic textures. In rocks with the latter two textures there also occur medium to coarse euhedral intergranular augite grains. Augite is largely unaltered, although in the most altered rocks examined it bears iron stains along fractures.

In one rock sample (Sample 519A-7-2, 51 cm (Piece 4)) some intersertal patches contain fine- to coarse-grained pinkish tan pyroxene grains, probably titaniferous augite.

Olivine occurs as euhedral crystals that range from very fine to medium in size. Typically the crystals contain central inclusions (glass?). In rocks with quench textures they sometimes form cores of spherulites, centers of radiating clusters, and sheaves of plagioclase. In other rocks they are concentrated with opaque minerals in interstitial areas between plagioclase-augite intergrowths. The composition of grains fresh enough to measure is magnesium rich, about Fe_{80-85} (based on an estimate of 2V that is consistently close to 90°). Most olivine grains are partially to completely altered to dark greenish brown, yellow brown, or orange phyllosilicates with high birefringence, presumably smectite.

Opaque Mineralogy

Polished thin sections were examined under reflected light by using a Zeiss Photomicroscope to determine the opaque mineralogy. Only the freshest rocks have been examined, and alterations have not been studied. The following minerals could be identified: titanomagnetite, ilmenite, various sulfides, and chromium-spinel.

The most abundant opaque minerals are the titanomagnetites. They make up about 80 vol.% of the opaques. The titanomagnetites are responsible for the magnetization of the basalts; the contribution of the other minerals can be neglected. The grain size of the titanomagnetites varies from almost invisible even under highest magnification (as in Samples 519A-7-1, 72–74 cm [Piece 9], 519A-7-1, 55–57 cm [Piece 7], and 519A-8-2, 47–49 cm [Piece 1E]) to about 100 μm in diameter (Samples 519A-7-2, 50–52 cm [Piece 4], 519A-8-1, 12–14 cm [Piece 1A], and 519A-2-3, 59–61 cm [Piece 2B]). Their shape is predominantly skeletal to subhedral (Pl. 4, Fig. 1), independent of the size of the grains. The titanomagnetites are frequently concentrated in the glassy patches that are interstitial between the feldspar laths. This is particularly evident in the coarse-grained samples with ophitic texture (Samples 519A-7-2, 50–52 cm [Piece 4], 519A-8-1, 12–14 cm [Piece 1A], and

519A-9-3, 59–61 cm [Piece 2B]). This characteristic and the skeletal shape indicate that titanomagnetite was one of the latest minerals to precipitate from the melt. Sample 519A-8-1, 12–14 cm (Piece 1A) seems to be slightly different, inasmuch as there titanomagnetite partly forms perfect octahedrons (Pl. 4, Fig. 2).

The titanomagnetites look fresh under the microscope in all investigated samples, independent of the macroscopic look of the samples, where the brownish colors of many samples signals a certain degree of whole rock alteration. In Samples 519A-8-1, 12–14 cm (Piece 1A) and 519A-9-3, 59–61 cm (Piece 2B), titanomagnetite grains show occasionally exsolved ilmenite lamellae, an indication of deuteric high temperature oxidation.

Discrete primary ilmenite grains occur in most of the samples, but they are volumetrically much less abundant than the titanomagnetites. The ilmenite grains appear under the microscope mostly as laths that are up to 200 μm in length in Sample 519A-8-1, 12–14 cm (Piece 1A). As already mentioned above, in Samples 519A-8-1, 12–14 cm (Piece 1a) and 519A-9-3, 59–61 cm (Piece 2B), secondary ilmenite occurs, which forms exsolution lamellae in titanomagnetite, oriented mostly along parallel lines. This is a rare phenomenon in ocean floor basalts and seems to be restricted to the center parts of thick flow units.

Sulfides are abundant in all samples; they form tiny spherules, indicating the immiscibility of sulfide and silicate melt. Under very high magnification it can be seen that the sulfide spherules consist of a mixture of different components. The dominant mineral is probably pyrrhotite (Pl. 4, Fig. 3).

Chromium–spinel has been observed only in Sample 519A-8-3, 82–84 cm (Piece 2c) (Pl. 4, Fig. 4). It forms the core of isolated titanomagnetite grains.

Conclusion

The similarity of the chemistry, mineralogy, and textures of all these rocks indicates that they have come from a single source, a tholeiitic magma, and probably were erupted over a relatively short time period.

BIOSTRATIGRAPHY

Summary

Foraminifers and calcareous nannofossils were found throughout the 151-m, upper Miocene through Quaternary sedimentary section recovered at Hole 519. In general, calcareous microfossils are abundant and well preserved down through Core 25 (~104 m sub-bottom). Below Sample 519-25,CC, all samples examined show moderate to strong effects of dissolution. Siliceous microfossils were encountered only in Cores 2, 3, 4, 16, and 24.

The Pliocene/Pleistocene boundary is placed near the top of Core 11 because the Olduvai magnetic event occurs in this interval. Identification of the Miocene/Pliocene boundary is equivocal. Calcareous nannofossils suggest placement of the Miocene/Pliocene boundary in Core 28, whereas planktonic foraminifers suggest that

the boundary occurs between Cores 29 and 28. The magnetostratigraphic record and an alternative biostratigraphic interpretation place the boundary near the top of Core 28 (Hsü, Percival, et al., this vol.).

Assemblages of mixed age and inverted zonal sequences are common in the first 20 cores of Hole 519 and are especially pronounced in Cores 5 to 10 and Cores 14 and 15. These anomalous occurrences are believed to have resulted from the slumping of older sediments, although contamination by downhole cavings cannot be entirely ruled out. A summary of biostratigraphic occurrences is given in Figure 4. The magnetostratigraphy in this figure is one of two possible interpretations of the magnetic data. This interpretation is that of Tauxe et al. (this vol.); the alternative interpretation is that there is an unconformity between Chrons 5 and 7 (Poore et al., this vol.).

Calcareous Nannofossils

Hole 519

The first four cores from Hole 519 contain a Quaternary flora. The age of Sample 519-1-1, 50–52 cm is based on the occurrence of *Emiliana huxleyi* (Lohmann). Samples 519-1-1, 64–65 cm to 519-2-3, 74–75 cm represent NN20, which is characterized by the presence of *Gephyrocapsa oceanica* (Kamptner) and the absence of *Pseudoemiliana lacunosa* Gartner. Below this section down to Sample 519-4,CC, NN19 is present, as indicated by *P. lacunosa* Gartner.

Cores 5 to 19 are stratigraphically mixed, with late Miocene sediments occurring within sequences of Pliocene and Quaternary age. The interval from Sample 519-20-2, 67–68 cm to 519-21-2, 80–81 cm is early Pliocene NN15, as indicated by the presence of *Reticulofenestra pseudoumbilica* Gartner. Early Pliocene NN14 starts in Sample 519-21-3, 20–21 cm and continues down to Sample 519-23,CC. This interval contains *Amaurolithus tricorniculatus* (Gartner), with *Discoaster asymmetricus* Gartner. From Sample 519-24-1, 80–81 cm to 519-26,CC, NN13 is found; it is characterized by *Ceratolithus rugosus* Bukry and Bramlette.

Late Miocene zones occur from Sample 519-28-2, 93–94 cm down to Sample 519-36,CC. From Sample 519-27-1, 50–51 cm to 519-28-1, 98–99 cm, NN12 is found, as indicated by the absence of the genus *Ceratolithus*. The interval from Sample 519-28-2, 93–94 cm to Sample 519-29-2, 76–77 cm is assigned to NN11/12 because of the occurrence of *A. amplificus* (Bukry and Percival). The absence of *A. amplificus* (Bukry and Percival) and the presence of *Amaurolithus* spp. places Sample 519-29-3, 36–37 cm to Sample 519-29,CC in NN11. The absence of *Amaurolithus* spp. and *Catinaster calyculus* Martini and Bramlette assign the interval from Sample 519-30-1, 93–94 cm to 519-33-1, 68–69 cm to NN10/11. The presence of *C. calyculus* Martini and Bramlette from Sample 519-33-2, 45–46 cm to 519-34-1, 80–81 cm indicates NN10. Similarly, the presence of *C. coalitus* Martini and Bramlette from Sample 519-34-2, 70–71 cm to 519-35-2, 79–80 cm indicates NN10. The in-

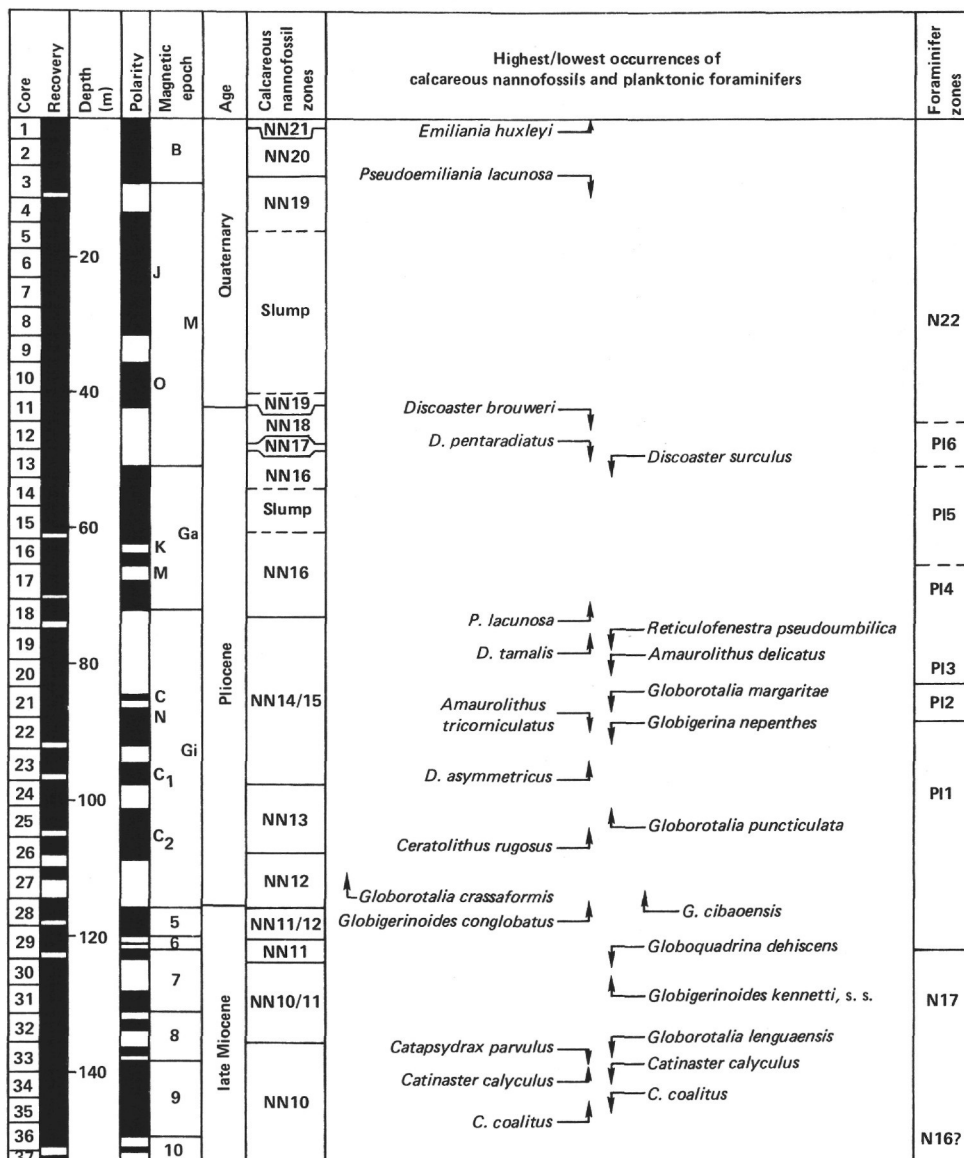


Figure 4. Biostratigraphic summary of significant calcareous and planktonic microfossils, Hole 519. Magnetic epochs are Brunhes (B); Matuyama (M), Jaramillo (J), Olduvai (O); Gauss (Ga), Kaena (K), Mammoth (M); and Gilbert (Gi), Cochiti (C), Nunivak (N), C₁ and C₂ Events.

terval from Sample 519-35-3, 80–81 cm to 519-36,CC is assigned to NN10 because of the absence of *D. hamatus* Martini and Bramlette.

Hole 519A

The four cores from Hole 519A contain mixed Pliocene and late Miocene zones. Therefore they do not show a complete stratigraphic sequence.

Planktonic Foraminifers

Planktonic foraminifers are generally abundant and well preserved in the upper 104 m of Hole 519 (Cores 1 through 25). Dissolved assemblages occur, however, in Samples 519-14,CC, 519-19,CC, and 519-21,CC. All samples below Core 25 show indications of strong dissolution.

Cores 1 through 4 contain rich Quaternary low-latitude assemblages. Taxa that occur commonly in this interval include: *Globorotalia truncatulinoides*, *G. tumida*, *Globigerinoides sacculifer*, *G. ruber*, *G. conglobatus*, and *Orbulina universa*. Cores 5 to 8 contain mixed Pliocene and Quaternary assemblages, with the Pliocene component being dominant. *Globorotalia truncatulinoides* occurs with *Sphaeroidinellopsis* spp. and *Globoquadrina altispira* in Sample 519-5,CC, and *Globorotalia truncatulinoides* occurs with *Globigerina nepenthes* and *Globorotalia conomiozea* in Sample 519-7,CC. Sample 519-8,CC contains an unmixed Quaternary assemblage, and Samples 519-9,CC through 519-13,CC appear to be late Pliocene.

Samples 519-14,CC through 519-28,CC are early Pliocene. Several inversions of Pliocene Zone P11 with com-

bined Pliocene zonal interval P12 to 3 are seen from 57 m sub-bottom (Core 14) through 88 m sub-bottom (Core 21). These inverted sequences, as well as the mixed assemblages seen higher in the hole, are due to the downslope slumping and flow of older sediments.

Identification of the Miocene/Pliocene boundary is equivocal because of the dissolved nature of the assemblages and downhole contamination. For example, *G. truncatulinoides* and *Globoquadrina dehiscens* occur in Sample 519-31, CC. The last consistent downhole occurrences of *Globorotalia crassaformis* in Section 1 of Core 28 and *Globigerinoides conglobatus* in Sample 519-28, CC are used to place the Miocene/Pliocene boundary between Cores 29 and 28. Planktonic foraminifers from the lower portion of the sedimentary column of Hole 519 are indicative of upper Miocene Zones N16 or N17.

Diatoms

Diatoms are sporadic and poorly preserved in Hole 519. Fragments of the giant diatom *Ethmodiscus rex* are common in Sample 519-2, CC and are rare in Sample 519-3, CC. In Sample 519-4, CC, only two specimens of *Coscinodiscus marginatus* were observed, with no *E. rex* fragments. Cores 5 through 15 are barren of diatoms. In Sample 519-16-1, 63 cm, *E. rex* ooze with a trace of *C. nodulifer* occurs. In Sample 519-16-1, 125 cm, pure *E. rex* ooze, with no trace of other species, is present. *E. rex* is common, along with clay particles, in Sample 519-17, CC. Cores 18 through 23 are barren of diatoms. Sample 519-24, CC contains a moderately diverse, yet poorly preserved diatom assemblage that includes abundant *E. rex* and rare *Hemidiscus cuneiformis*, *C. nodulifer*, *C. lineatus*, *C. vetustissimus* v. *javanicus*, *Nitzschia marina*, and *Thalassionema* spp. These forms conform to the Pliocene age indicated by calcareous microfossils. Cores 25 through 37 are barren of diatoms.

Benthic Foraminifers

The benthic foraminifers in Hole 519 are typical bathyal and abyssal Neogene faunas. The dominant species are *Nuttalides umbonifera*, *Cassidulina subglobosa*, *Oridorsalis umbonatus*, *Epistominella exigua*, *Planulina wuellerstorfi*, and *Pullenia* spp. (*P. osloensis*, *P. subcarinata*, and *P. bulloides*). The fauna are well preserved, abundant, and moderately diverse.

The Pliocene-Quaternary fauna is dominated by *N. umbonifera*, which makes up to 60% of the assemblage. Based on analogs with the present-day distribution of benthic foraminifers in the South Atlantic (Lohmann, 1978) and other parts of the world (Schnitker, 1980), the dominance of this species suggests the presence of Antarctic Bottom Water (AABW).

In the lower part (late Miocene) of Hole 519, *N. umbonifera* becomes much less dominant and is replaced in importance by *E. exigua* and *P. wuellerstorfi*. This transition occurs over the interval from Sample 519-29-2, 64 cm (120.64 m sub-bottom) to Sample 519-31-1, 100 m (127.90 m sub-bottom), an interval that represents approximately 1.8 m.y. The late Miocene benthic foraminifer fauna is most similar to a modern fauna typical of

lower North Atlantic Deep Water (NADW). However, the existence of NADW during the late Miocene is uncertain, and until such time as it can be adequately documented, this late Miocene water mass might be better labeled as Miocene South Atlantic Deep Water (MSADW).

The transition from MSADW to AABW in Hole 519 occurred between 5.7 and 7.5 m.y. and may represent a major shift in water mass during the late Miocene. An equally plausible explanation, however, is the subsidence of the site through the boundary between the shallower MSADW and deeper AABW at this time. A back track curve constructed for this site (Fig. 5) reveals that the water depth during this transitional interval was between 3250 and 3450 m. In the South Atlantic today, the dominance of *N. umbonifera* is noticeable below 3500 m (Lohmann, 1978).

Dissolution

Figure 6 shows the downcore distribution of two measures of dissolution, the ratio of benthic to planktonic foraminifers and the degree of fragmentation among planktonic foraminifer tests. The curves behave sympathetically, with the percentage of fragments being a more sensitive measure of dissolution during episodes of low to moderate dissolution and the percentage of benthics being more sensitive during episodes of moderate to intense dissolution.

In Hole 519, a mild episode of dissolution is indicated at 85 to 90 m sub-bottom (Cores 21 and 22). A moderate

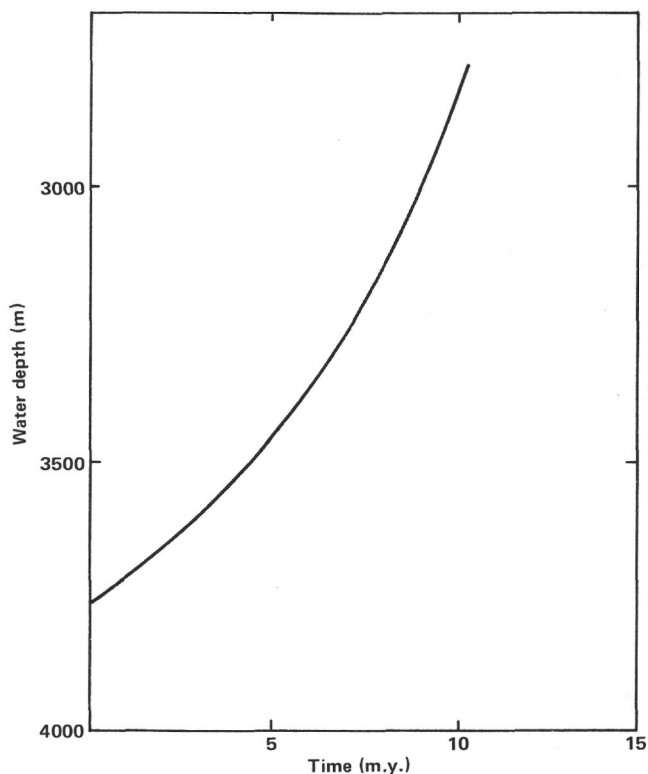


Figure 5. Bathymetry of Site 519 based on subsidence curves (which are corrected for sediment load).

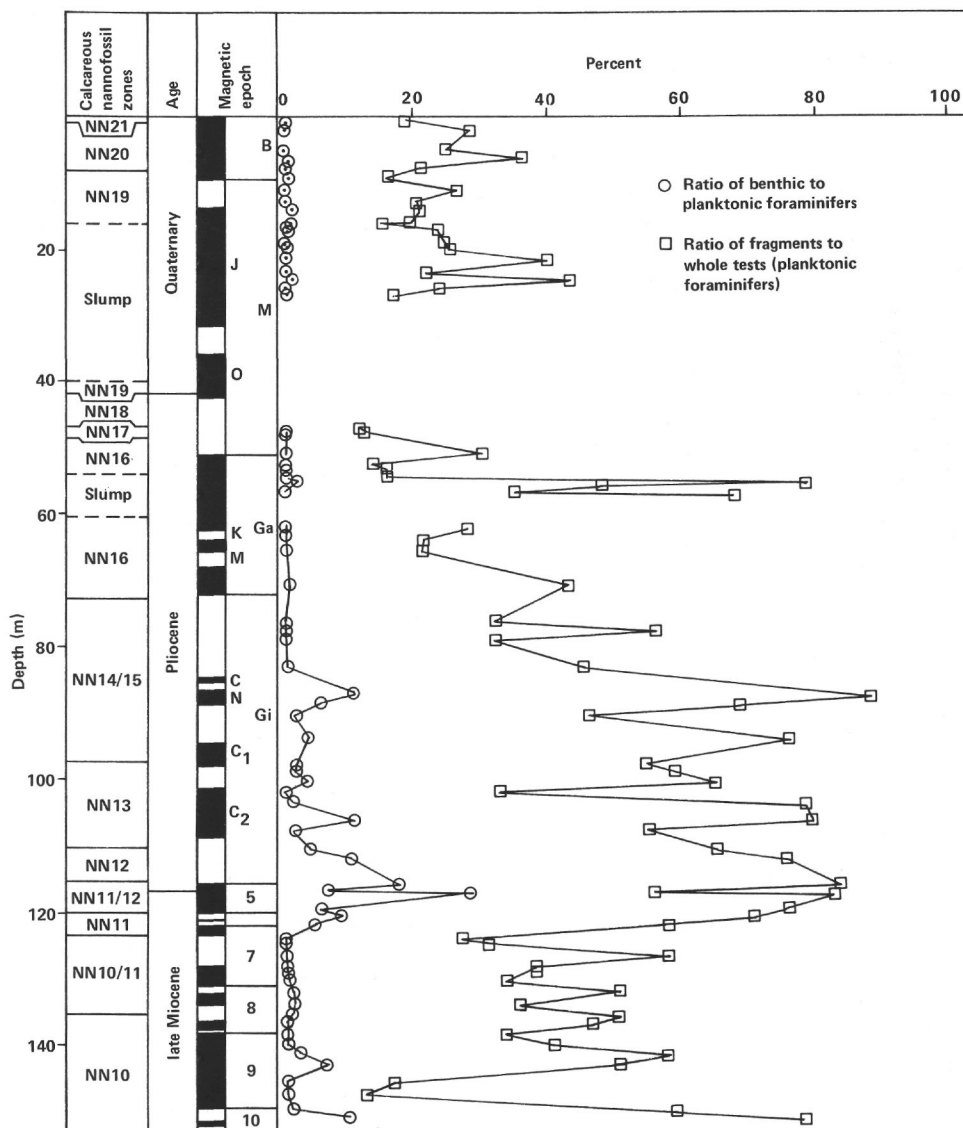


Figure 6. Dissolution indices, Hole 519. See text for description. Magnetic epochs as in Fig. 4.

episode occurs at 115 to 117 m sub-bottom (Core 28). These two intervals of dissolution are seen also in the plot of percent carbonate (Fig. 2).

Sedimentation Rates

Sedimentation rates at Hole 519 are estimated from both calcareous nannofossil datums and magnetic polarity events (Fig. 7). The chronology of the paleomagnetic datums is that of LaBrecque et al. (1977) as modified by Mankinen and Dalrymple (1979), who used the new decay and abundance constants recommended by the International Union of Geological Sciences Subcommittee on Geochronology. The presence of slump structures in the sediments in the interval between 15 and 32 m sub-bottom is reflected in the high sedimentation rates through this interval. Turbiditic foraminiferal sands accompanied by biostratigraphically mixed faunal and floral assemblages in the interval from 32 to 80 m sub-bottom indicate that further mixing and slumping took place, although not with the same intensity as in the up-

per interval. This lower part of the mixed zone (32–80 m sub-bottom) accumulated at a rate similar to that of the biostratigraphically coherent interval below (80–120 m sub-bottom).

The lower sedimentation rates in the upper Miocene sequence reflect the increased dissolution during that interval.

PALEOMAGNETISM

Sediments

The long core spinner gave very disappointing results. The results from the first three cores were reliable, but for the lower cores the declination results were in general too scattered to permit any interpretation. Regions of rust contamination in the core were correlated with anomalously high intensities (10^3 – $>10^4$ μG) compared with uncontaminated sediment (10 – 3×10^2 μG). This effect was especially pronounced around the occasional splits in the core liners.

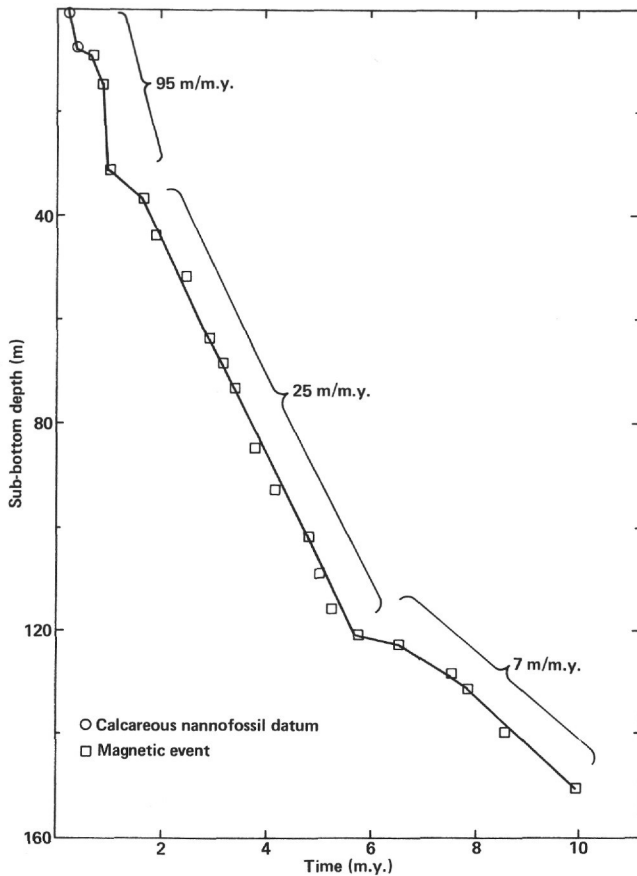


Figure 7. Sedimentation rates, Hole 519.

To obtain meaningful data it was necessary to subsample the core. In undisturbed sediment routine samples were taken every 20 to 30 cm. To resolve finer scale features of the paleomagnetic record, selected areas (notably around polarity transitions) were resampled more densely. In all, 475 minicores were taken. In general, the top 50 cm of each core were too disturbed to give consistent results. There was often a shift of up to 60° in the measured declination between adjacent cores. The discrepancy is believed to indicate an inadequacy in the orientation technique. Solution of this problem should be given high priority.

For much of the sedimentary sequence, a considerable Brunhes overprint was present. That is, a normal polarity signal was recorded on top of the true field record. The overprint was magnetically soft and was removed after demagnetization in alternating fields of 100 Oe. Typical results of demagnetization are shown in Figure 8. For non-overprinted material, the remanence direction remained stable for demagnetization up to 700 Oe, the median destructive field being around 250 to 300 Oe.

The natural remanent magnetization (NRM) was measured routinely. The samples from Cores 21 to 30, 33, and 36, plus other representative samples, were then demagnetized and remeasured. The results and interpretation are summarized in Figure 9. Only after alternating field (AF) demagnetization were some of the fine-scale features in the record fully resolved. The polarity transitions were usually sharply defined (Fig. 10), although

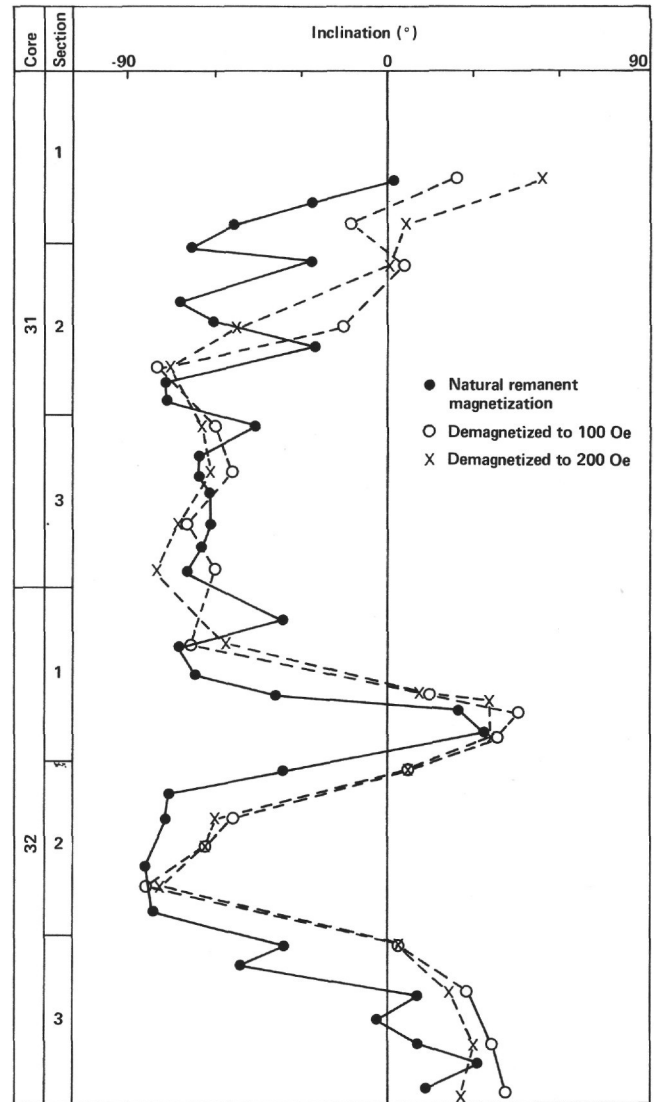


Figure 8. Example of typical demagnetization responses of several sediment cores from Hole 519.

they often moved position on demagnetization (Fig. 8). An intensity minimum was associated with the transition. At the present time it is not known if this and the other characteristic features of the transition represent the true behavior of the geomagnetic field or are caused by the magnetization process itself.

The magnetic record was good for Cores 1 to 3. From mid-Core 4 to mid-Core 8, the remanence directions stayed remarkably constant (with normal polarity). This is thought to reflect the resetting of the magnetization of this whole section as a result of slumping. The slump must have taken place in a normal polarity interval (almost certainly the Jaramillo Event). The record from Core 12 to Core 24 and Cores 27 to 36 was good except for one or two gaps (e.g., at the top of Core 11). Cores 25 and 26 were very disturbed, and although samples taken from their least disturbed sections showed consistent normal polarity, there is some doubt as to the authenticity of the inferred event. Possible action events were identified in Cores 3, 14, 33, and 36.

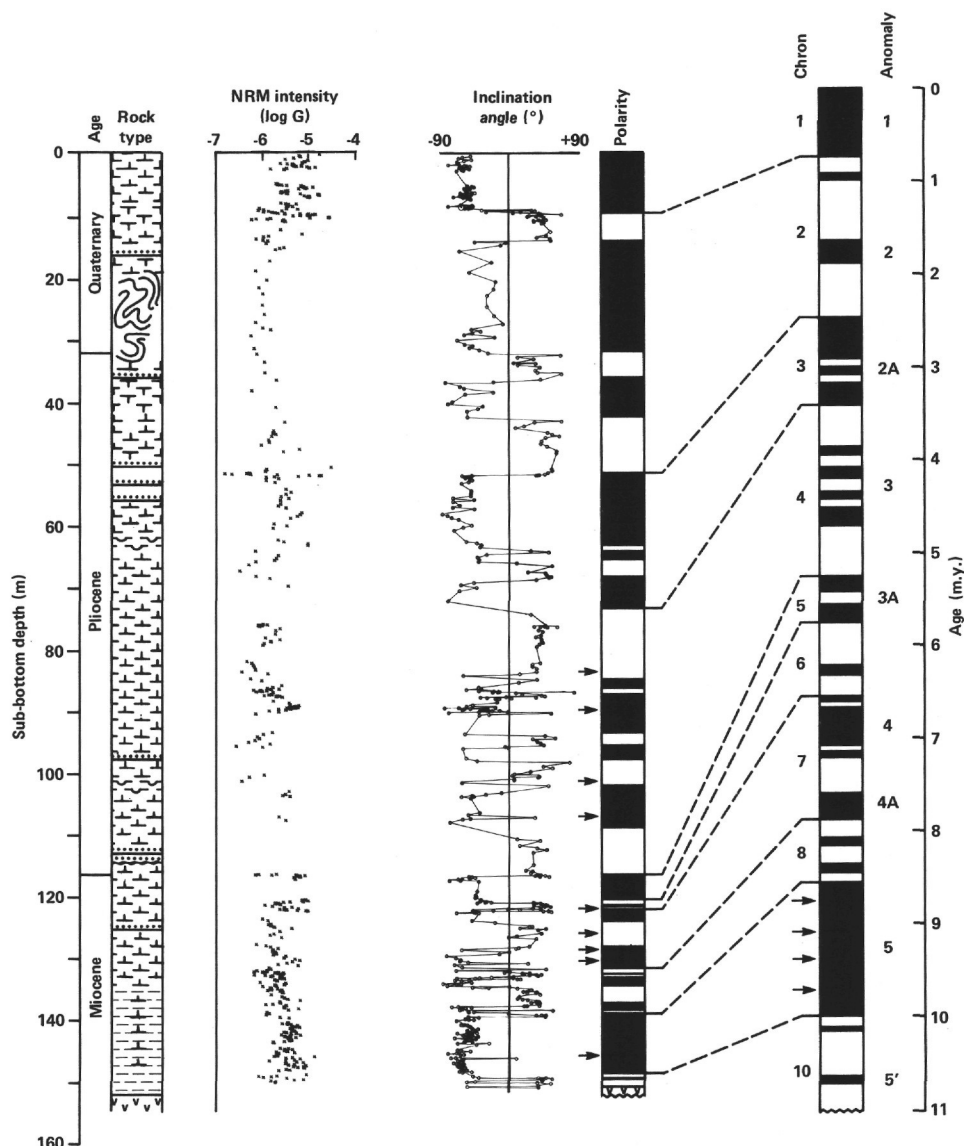


Figure 9. Summary of magnetic polarity record at Site 519. Lithology is defined in Hsü, LaBrecque, et al. (this vol.). Solid blocks denote intervals of normal polarity. Arrows identify the positions of polarity units that are defined by single samples and are therefore tentative (see Tauxe et al., this vol.).

Igneous Rocks

The primary goal of the paleomagnetic investigations of the basalts was to determine the original magnetic remanence direction acquired by the igneous material during cooling. This type of remanence is a thermoremanent magnetization. It is often not the only kind of remanence that may be present in the rock. During the interval between cooling and measurement in the laboratory, the rock may acquire secondary remanences, such as chemical and viscous magnetizations, but also remanences imposed by the drilling process, the so-called drilling remanence. The latter is probably imposed on the rock by the combined action of pressure, vibration, and magnetic field. It always seems to be directed along the axis of the drill core.

In order to eliminate these secondary magnetizations and to establish the direction of remanent magnetiza-

tion, a program of stepwise alternating field demagnetization was employed. Peak fields as high as 1000 Oe were employed, although fields at which stable directions were reached are commonly much lower.

In order to characterize the igneous samples more fully, the susceptibilities were measured, and the Koenigsberger Q -factor was calculated according to the relation:

$$Q = \frac{J_{\text{NRM}}}{\chi H}$$

where J_{NRM} is the volumetric NRM intensity, χ is the susceptibility, and H is the Earth's magnetic field at this location ($H = 0.27$ Oe).

Determination of the stable direction of magnetization of a sample was accomplished by examining the change in inclination as the sample was progressively de-

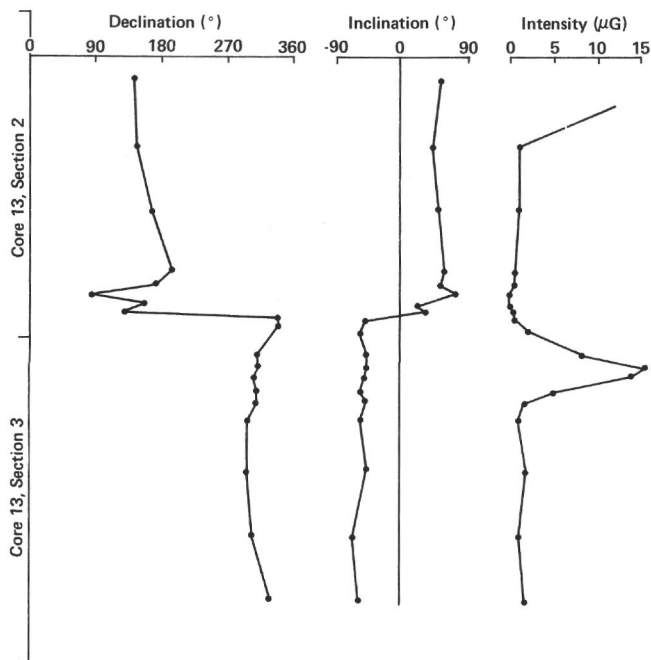


Figure 10. Example of sharp polarity transitions typical of Site 519.

magnetized. If during the demagnetization the inclination of remanent magnetization reached a value that did not change significantly for several steps, this was termed the stable inclination (see Fig. 11). Change in declination was also considered but was not used as the determining parameter. Because the rock samples can be oriented only with respect to the vertical axis, only the inclinations can be determined absolutely. Declinations are relative values, and are referred to the face of the split core.

As a measure of the degree of inherent stability of the remanent magnetization, the medium destructive field (MDF) was found for each sample. This is the alternating current field necessary to eliminate half of the original intensity of magnetization (see Fig. 11).

The location of Hole 519A is near a polarity transition on crust of age Chron C-5-R. The results of the rock magnetic measurements are listed in Table 2. The inclination varies from 80° in the upper part of the basalt sequence to about 0° in the lower part, with an abrupt change from 45° to 0° (positive inclination means reversed polarity on the Southern Hemisphere) at the boundary between Cores 8 and 9. This change corresponds to a break in lithology (see the section on igneous petrology). The magnetic polarity of the upper part of the basalts has the same sign as the lowermost portion of the sediments of Site 519 (see section on sediment paleomagnetism).

The inclination of the Earth's magnetic dipole field at the latitude of the drill site is 43°. The magnetic inclination of the sediments come much closer to this value than that of the basalts.

It has often been observed that the magnetization inclination becomes shallower with increasing depth in basalt drill cores from the Atlantic. We observe the same phenomenon in our cores from Hole 519A. One

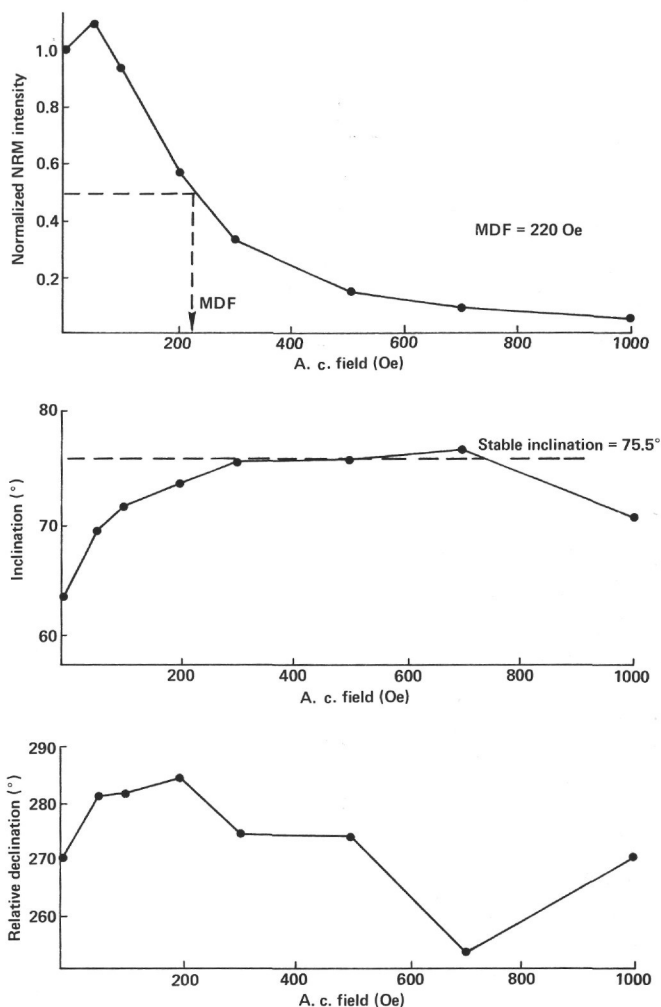


Figure 11. Determination of the medium destructive field (MDF) and stable magnetic inclination of the natural remanent magnetization (NRM). Sample 519A-7-1 (110-112 cm).

Table 2. Paleomagnetism of basalts at Hole 519A.

Core-Section (interval in cm)	NRM			MDF (Oe)	Susceptibility (10 ⁻⁴ G Oe ⁻¹)	Q-factor
	Intensity (10 ⁻⁴ G)	Inclination ^a (°)	Stable inclination ^a (°)			
7-1, 53-55	19.51	76.7	79	—	2.4	30
7-1, 72-74	27.58	76.0	76.5	850	2.7	38
7-1, 110-112	12.87	66.1	75.5	220	5.5	9
7-2, 5-7	10.09	77.6	75	—	4.8	8
7-2, 11-13	8.02	66.4	71	—	4.8	6
7-2, 50-52	11.56	72.7	79	—	4.5	9
8-1, 12-14	9.81	-3.1	68	60	19.7	2
8-1, 57-59	9.89	24.2	69	—	13.5	3
8-1, 77-79	10.69	68.7	58	—	3.7	11
8-1, 95-97	38.94	79.6	—	—	8.8	16
8-1, 122-124	51.80	82.4	81.5	350	4.1	47
8-2, 11-12	25.40	75.6	—	—	7.3	13
8-2, 53-55	13.12	63.7	68	340	5.3	9
8-2, 129-131	17.96	38.7	53	160	6.7	10
8-3, 82-84	10.03	38.1	50	310	3.7	10
8-4, 15-17	7.86	15.2	42	150	4.0	7
8-4, 133-135	4.85	46.1	45.5	320	2.7	7
9-1, 34-36	13.08	-9.3	-5.0	460	3.5	14
9-2, 20-22	15.63	-6.0	3.0	110	10.6	5
9-3, 48-50	13.44	-30.3	0	70	9.9	5
9-4, 96-98	7.12	-30.4	-0.5	70	16.3	2
9-5, 6-8	10.59	-4.5	-2.0	400	13.9	3
9-5, 37-39	12.44	0.6	-1.0	380	9.2	5

Note: Dashes signify no data.

^a Positive inclination means reversed polarity on the Southern Hemisphere.

possible explanation for this phenomenon is that the basalts record a transition of the Earth's magnetic field from normal to reversed. However, we do not observe a corresponding variation of magnetization intensity, which makes it unlikely for a magnetic field transition to be the cause. Another explanation is the tilting of the basement block in this area. However, the process of tilting has to be complex to account for the observed variation of inclination. It cannot be explained by a single rotation—at least two subsequent rotations would be necessary. Independent of any possible rotation model that could explain the observation, the rotation angles have to be large, at least 40° for each of the subsequent rotations.

The magnetization intensity varies relatively little in the measured profile apart from one very high magnetization value in Core 8, Section 1. The values of the Koenigsberger Q -factor run more or less parallel to the magnetization intensity, with most values well above 1.

PHYSICAL PROPERTIES

Only soft sediment consisting of foraminifer-nannofossil ooze was recovered from Hole 519. The particles were dominantly silt-sized throughout. Sediment stiffness increased generally with depth, but the stiffer sediments were interrupted repeatedly by segments of soft ooze throughout the entire length of the section. Except for the upper portion of the hole, where sediments were soft, the physical properties of the stiffer sediments in the section were measured.

The results of the measurements performed on the sediments recovered from Hole 519 are presented in Figure 12. These data show a number of interesting trends. The physical properties are constant with increasing depth, generally showing scatter about a mean value up to a depth of 130 m sub-bottom. In the intervals from 65 to 78, 83 to 95, and 105 to 108 m sub-bottom, drilling disturbance was considerable, which is reflected in the physical properties. At a depth of about 130 m sub-bottom there appears to be a small shift in the mean value of the velocity, possibly indicating the presence of the hiatus noted in both the core and the seismic record. This is seen as a small shift in the compressional velocity from a mean value of 1.49 km/s to 1.51 km/s, and it has no expression in the other physical measurements.

Results of the measurements on the basalts recovered from Hole 519A are summarized in Table 3. All the basalt pieces showed some anisotropy in compressional velocity, with the horizontal direction (perpendicular to core axis) having generally lower velocity than the vertical direction. Core 8, Section 2 is an exception; it shows a greater velocity in the horizontal direction.

The densities determined by 2-min. gamma ray attenuation porosity evaluator (GRAPE) all yield higher values when measured in the vertical direction. The differences between a value of density in any pair of measurements is considerable, and this is reflected in the associated porosity values.

Thermal conductivity values range between 1.5 and 2.2, with an inexplicably high value recorded for the sample from Core 8, Section 4.

Figure 13 illustrates a series of cross plots for these basalts. In the lower part of the figure, velocity, water content, and thermal conductivity are plotted as functions of wet bulk density. Water content is used rather than porosity because the former is calculated on the basis of wet sample weight; porosity is referred to the weight of the dry sample. Sound velocity shows the expected linear increase with increasing density and decreasing water content. Thermal conductivity appears to be independent of density over this narrow range. It also appears to be independent of porosity and of water content, as seen in the upper part of Figure 13, although a slight increase in conductivity appears to accompany lower water contents and porosities.

In plotting Figure 13, the densities, water content, and porosities obtained from the gravimetric data were used, rather than values obtained from the 2-min. GRAPE data. In most instances, the gravimetric wet bulk density is in reasonable agreement with the 2-min. GRAPE value in the vertical direction. The density anisotropy indicated by the 2-min. GRAPE data is not consistent with the observed velocity anisotropies, however.

INORGANIC CHEMISTRY

Table 4 lists the results of three analyses of interstitial water squeezed from sediments at Site 519. All the values remain constant with depth aside from a possible slight increase in calcium and depletion in magnesium concentrations. These results suggest that neither basalt alteration nor diagenetic reactions within the sediments have had much effect on interstitial water compositions, at least in the upper 115 m, at this site.

CORRELATION OF DRILLING RESULTS TO GEOPHYSICAL DATA

Holes 519 and 519A are located on the older reversal transition of Magnetic Anomaly 5¹, a short wavelength positive magnetic anomaly between Anomalies 5A and 5. Holes 519 and 519A were spudded on the sides of a small perched basin (Fig. 14) to avoid the problem of major turbidite deposits.

The seismic data may be interpreted to extend our understanding of the Site 519 drilling results. Figure 14 shows a line drawing of the site. The most interesting feature of the data is a zone of apparent reflector convergence, which is located above and nearly conformable with the basement reflector (R_2). This zone of convergence is manifested by reflector (R_1) approximately 0.1 s (two-way travel time) above basement (R_2). Few coherent reflectors can be seen between R_1 and R_2 . Reflectors located above R_1 are generally horizontal though discontinuous. These horizontal reflectors may be reflections from the observed turbidite layers within Unit 2. Reflector R_1 is interpreted to be a zone of onlap between pelagic drape facies below and ponded facies above.

Below Site 519 near the sediment/water interface, a zone of irregular reflections that is not conformable with the surface and which appears to shoal to the north is present. This zone may be the slump deposit that was noted in Cores 3 to 13.

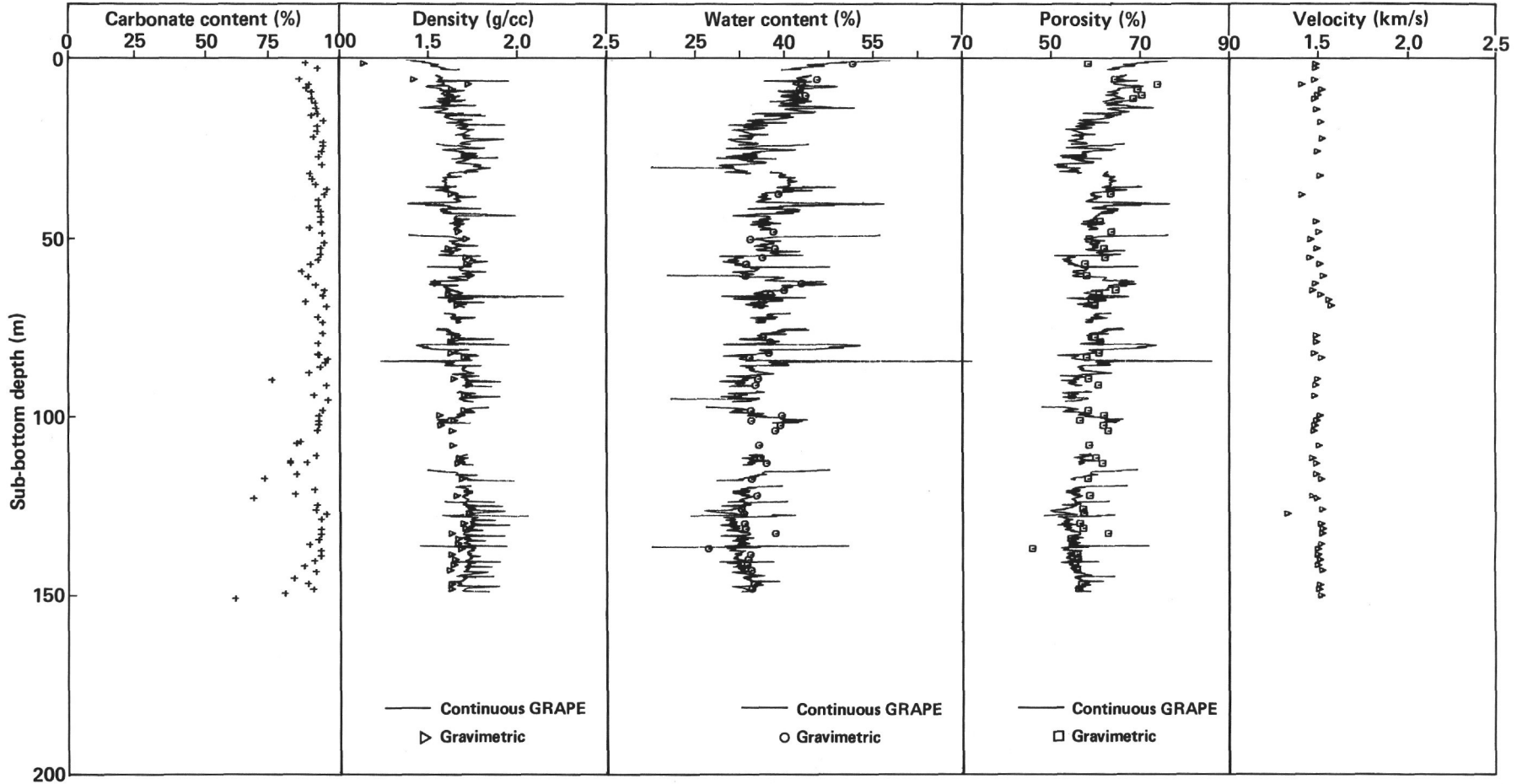


Figure 12. Summary of sediment physical properties, Hole 519. Velocity data are for perpendicular beds.

Table 3. Physical properties of basalts, Hole 519A.

Core-Section (interval in cm)	Velocity (km/s)		Gravimetric data			Uncorrected 2-min. GRAPE ρ (g/cc)		Corrected 2-min. GRAPE				Thermal conductivity, K (W/m ² C)
	Vertical	Horizontal	ρ (g/cc)	H ₂ O (%)	ϕ (%)	Vertical	Horizontal	ρ (g/cc)		ϕ (%)		
								Vertical	Horizontal	Vertical	Horizontal	
7-2, 11-13	5.456	5.483	2.839	3.84	10.9	2.867	2.588	2.865	2.570	1.87	17.6	—
8-1, 91-93	4.565	4.467	2.715	4.58	12.4	2.862	2.390	2.860	2.360	2.13	28.3	1.603
8-2, 87.5-89.5	5.515	5.925	2.835	2.68	7.6	2.837	2.526	2.833	2.504	3.57	21.1	1.536
8-3, 88-90	5.882	5.786	2.860	1.72	4.9	2.915	2.563	2.916	2.543	0.85	19.0	2.040
8-4, 120-122	5.316	4.784	2.807	3.39	9.5	2.775	2.425	2.767	2.397	7.09	26.8	4.268
9-1, 58-60	5.964	5.553	—	—	—	2.911	2.574	2.911	2.574	0.59	17.4	1.927
9-2, 39-41	5.509	5.493	2.801	1.09	3.1	2.882	2.569	2.881	2.550	1.01	18.8	2.159
9-3, 59-61	5.865	5.604	2.797	1.22	3.4	2.902	2.538	2.902	2.538	0.11	19.3	1.895

Note: Dashes signify no data; ρ = density; ϕ = porosity.

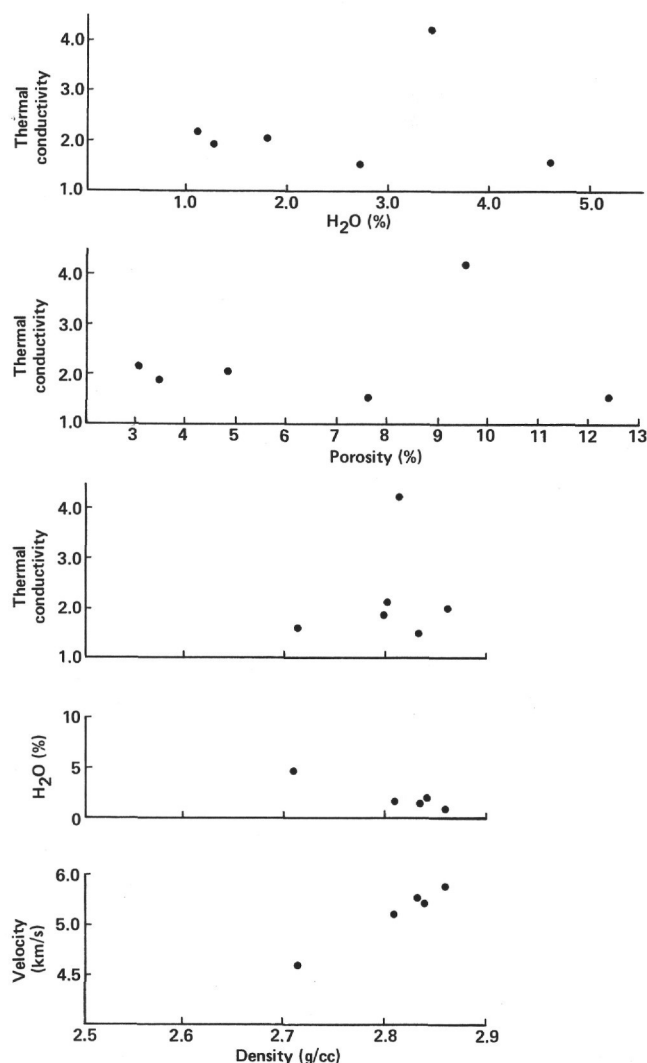


Figure 13. Cross plots of selected physical properties of basalts recovered from Hole 519A. Velocity data are for perpendicular beds; density, water content, and porosity were obtained from gravimetric data.

Laboratory measurements on the recovered sediments give seismic velocities of 1.48 to 1.5 km/s. We can assume an average velocity of 1.49 km/s for the section. This seismic interpretation suggests the following sedimentological subdivision of recovered sediment correlated to the proposed lithologic subdivisions: Unit 1—

Table 4. Interstitial water chemistry, Site 519.

Core-Section (interval in cm)	Depth below seafloor (m)	pH	Alkalinity (meq/l)	Salinity (‰)	Ca (mmol/l)	Mg (mmol/l)	Chlorinity (‰)
7-2, 140-150	28-31.5	7.4	2.95	37.4	10.6	49.9	19.6
17-2, 133-150	66.1-70.5	7.4	2.96	35.5	10.8	53.3	20.1
27-2, 112-122	110.1-114.5	7.4	3.071	35.5	11.5	51.8	20.1

ponded facies from 0 to 15 m, slump from 15 to 40 m; Unit 2—ponded facies from 40 to 110 m; Unit 3—pelagic facies from 110 to 151 m.

The zone of onlap between the pelagic facies and the ponded facies may represent either a depositional hiatus (missing section) and/or an increase in sedimentation rate, depending in part on the degree of erosion active prior to onlap. The pelagic drape sequence should correlate to the observed Magnetic Chrons 7, 8, 9, and 10 (C-3A to C-5). Chrons 5 to 6 may correlate to the zone of onlap and dissolution prior to onlap.

SUMMARY AND CONCLUSIONS

The main purposes of drilling this site are to sample for paleoceanographical studies and to relate the seafloor spreading history to patterns of sedimentation. To achieve these aims, precision stratigraphy is a prerequisite. We have five sets of data: (1) seafloor lineations registered as magnetic anomalies, (2) natural remnant magnetism of sediments, (3) nannofossil biostratigraphy, (4) planktonic foraminifer biostratigraphy, and (5) stable-isotope stratigraphy. Diatom and benthic foraminifers were studied, but they seldom yield critical biostratigraphical information. Calcite dissolution, which is related to ocean fertility and ocean chemistry, has been studied. The framework of precision stratigraphy permits an accurate dating of some of the major Neogene events at this site.

Lithostratigraphy and Lithology

Site 519 is located on the edge of a local basin on the east side of the Mid-Atlantic Ridge. Seismic profiling data indicated that the sedimentary sequence in the basin can be divided into an upper ponded facies, a lower ponded facies, and a pelagic sediment sequence draped over the basement. Drilling indicated that those seismostratigraphic units at this site are at depths from 0 to 40 m, 40 to 110 m, and 110 to 151 m, respectively. Those intervals correspond roughly to the three lithologic units (foraminifer-nannofossil ooze, 0-54 m; nannofossil

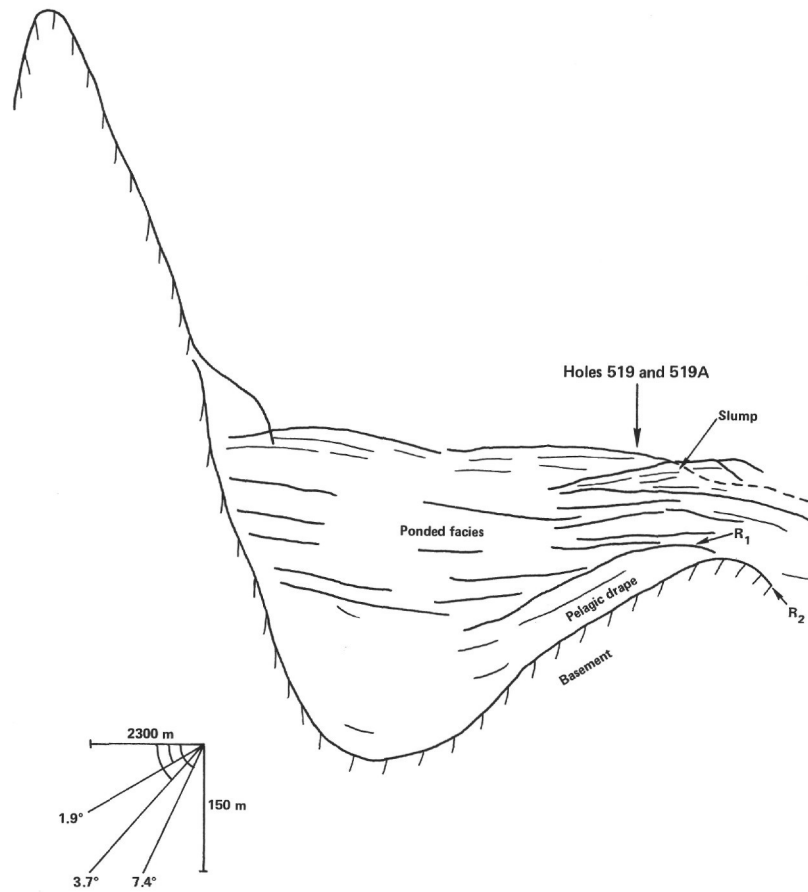
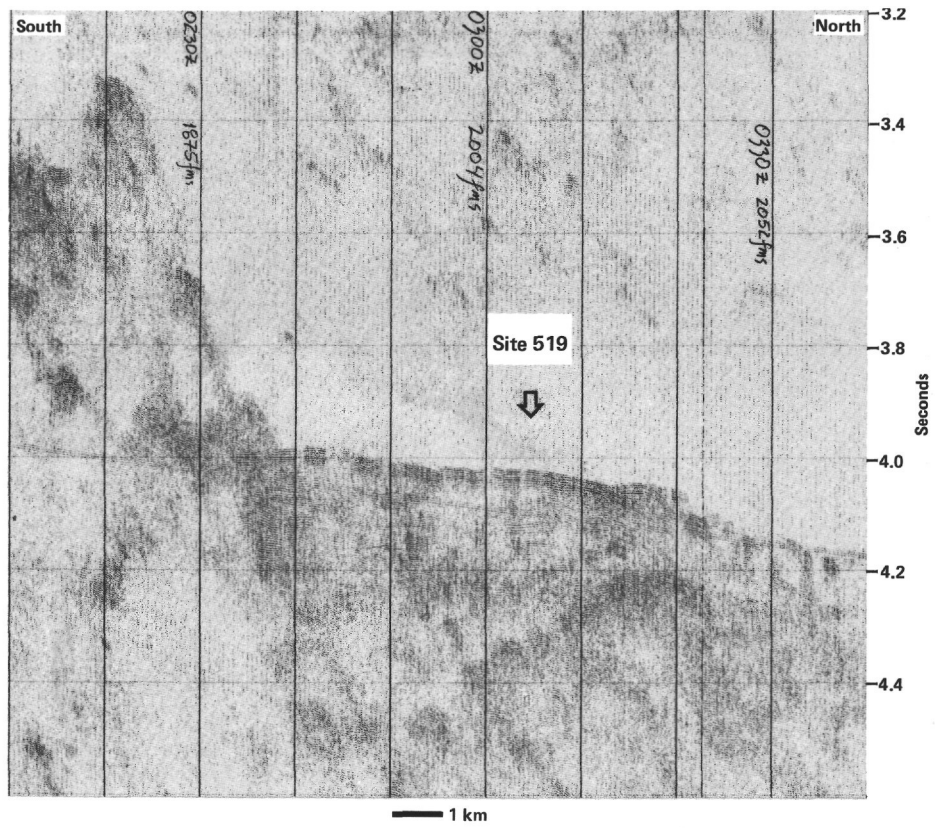


Figure 14. Seismic profile and interpretation of seismic data at Site 519. In the lower figure, the vertical scale was computed by assuming a sediment velocity of 1.5 km/s. The horizontal scale was calculated by using a ship speed of 7.5 knots.

ooze, 67–106.5 m; and brown marly ooze, 106.65–151 m).

Turbidites are common in the ponded facies. One re-sedimented deposit about 17 m thick (14.0–31.0 m) was laid down during the Jaramillo Event of the Matuyama Epoch. The deposit is sedimentologically very similar to that produced by a historical catastrophic slumping in Lake Zurich (Kelts and Hsü, 1980). The bulk consists of contorted beds of soft sediments not completely disaggregated during the downslope movement. Homogeneous ooze, or apparently disaggregated slump sediment, is present only at a few thin intervals between the contorted beds. The very top of the deposit is a foraminifer sand (base of Core 4, Section 2 and top of Core 4, Section 3), which is characterized by graded bedding and was laid down by the turbidity current that was generated by the mass movement. The slumped sequence includes practically the whole of the Pliocene and contains nannofossils belonging to NN12 to 16. However, the natural remnant magnetism has been realigned, probably as a result of slumping, although the degree of realignment is not perfect (see Tucker, this vol.).

The pelagic sediments, especially the brown marl oozes, have been subjected to some dissolution. They are on the whole eolytic or oligolytic (see Violanti et al., 1979); only one upper Miocene sample contains slightly more than 30% of insoluble residue (Fig. 15).

The pattern of ponded sediments overlying draped sediments is typical of the Neogene ridge-flank basins of the South Atlantic. Resedimented deposits of Miocene

age were accumulated in the central depression, as we found at our next site. On the flank of a basin such as the site here, the overlapping of the ponded over the draped sediments first took place in the Pliocene–Quaternary time, when much of the basin had been filled by resedimented deposits.

Biostratigraphy and Magnetostratigraphy

The correlation of biostratigraphy and magnetostratigraphy is shown by Figure 16. The only uncertainty concerns the recognition of Chron 6. We all agree that the upper upper Miocene sequence at this site is very condensed because of dissolution. Four samples from the lower part of Core 29, at 121.0 to 122.0 m sub-bottom, are reversely magnetized. The lowest occurrence of *Amaurolithus amplificus* (very rare) is found in a sample 120.76 m sub-bottom (near Core 29, Section 2, 76 cm). The lower occurrences of *A. primus* and *A. delicatus* (both very rare) are in the core-catcher sample of Core 29. Poore, our specialist in planktonic foraminifers, noted that the first occurrence datum of *A. primus* has been reported from Chron 7 at some localities. He suggested, therefore, that the sediments in the lower part of Core 29 (from the reversely magnetized interval on down) are of Chron 7. He believed that the uppermost Chron 7 and all of the Chron 6 sediments were removed by erosion. The interpretation shown by Figure 16 is that suggested by our shipboard paleomagnetists (see Tauxe et al., this vol.); they assume that the reversely magnetized interval is a condensed section of Chron 6

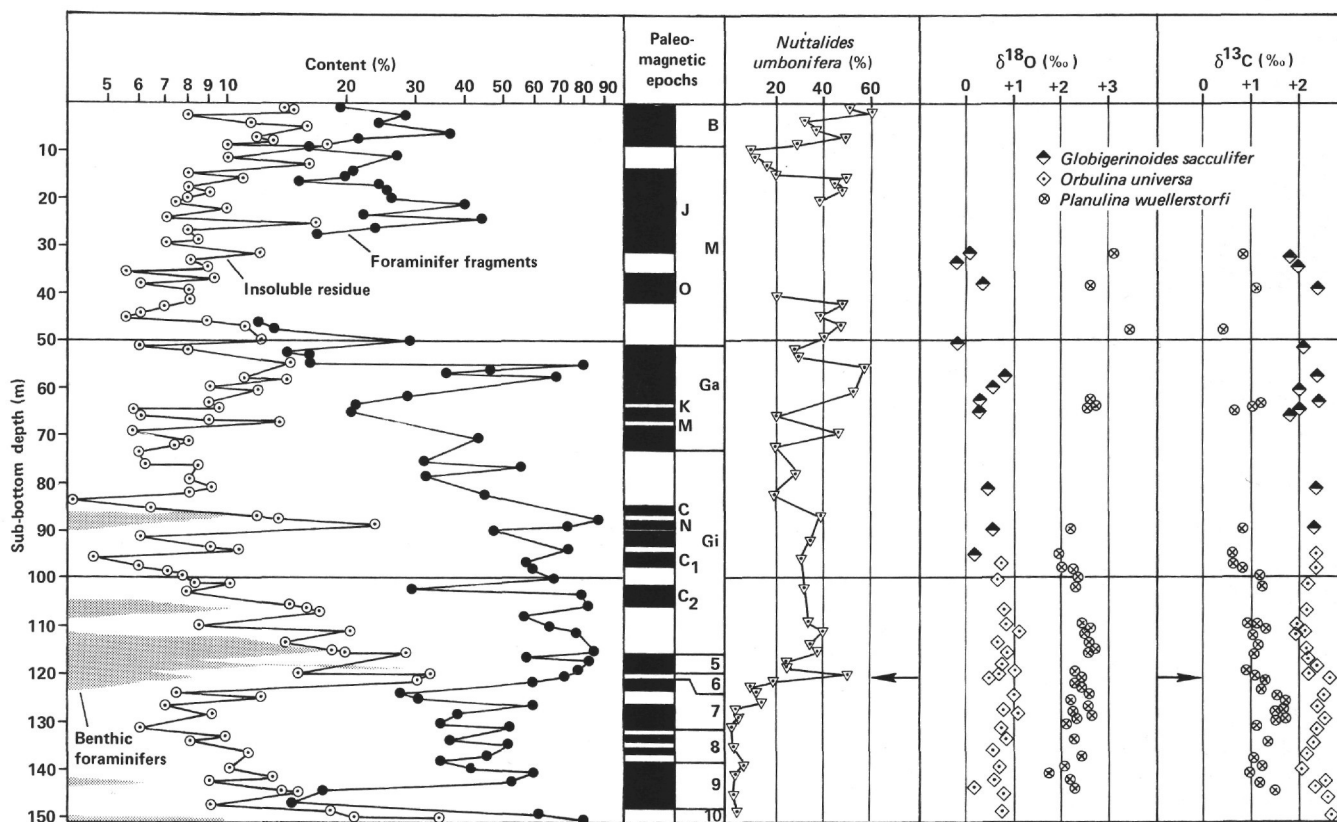


Figure 15. Paleoceanographic data, Site 519. See text for discussion. Magnetic epochs as in Fig. 4.

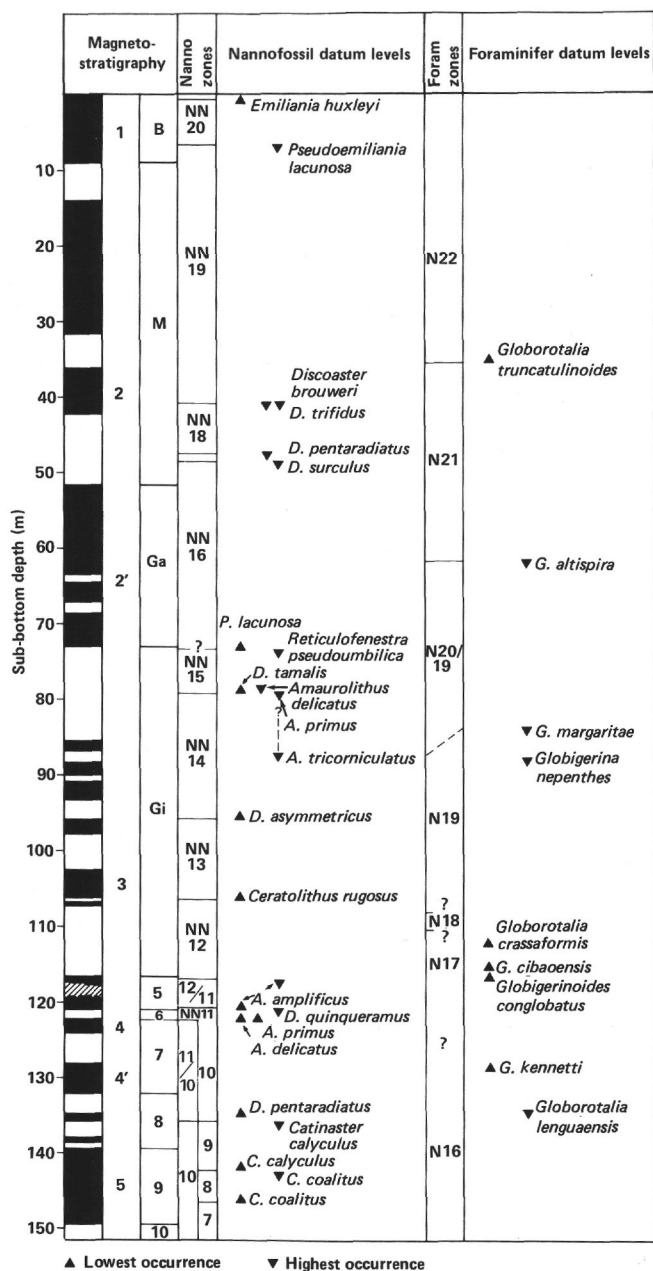


Figure 16. Magnetostratigraphy and biostratigraphy at Site 519. See text for explanation of alternative correlations. Magnetic epochs as in Fig. 4.

sediments and that the underlying normally magnetized Core 29 core-catcher sediments belong to the top of Chron 7. Such an interpretation is in agreement with nannofossil stratigraphy, because the lowest occurrence (LO) of *A. amplificus* (at 120.76 m sub-bottom) lies just above the top of Chron 6 (at 121.0 m sub-bottom), as does the reported FAD of this species elsewhere. The presence of *A. primus* and *A. delicatus* in the Core 29 core-catcher sample (at 122.9 m sub-bottom) cannot be used to evaluate these interpretations: they may have made their true first appearances in Chron 7 time. Furthermore, those very rare occurrences may have resulted from contamination, which is very common in all core-

catcher samples obtained by hydraulic piston coring (see Poore et al., this vol.). The trend of the isotope signals from Site 519 samples is very similar to that given by the samples from a continuous section at Site 16 on the west side of the Mid-Atlantic Ridge (see McKenzie et al., this vol.). The chief scientists, therefore, elected to illustrate the second interpretation in Figure 16, although we might add that the disagreement is a minor issue and does not affect any major conclusions.

With the help of biostratigraphic information, the magnetic reversals in the sediments could be definitely correlated to the geomagnetic reversal pattern down to Anomaly 3 of the Gilbert Epoch, except that the sediments deposited during the Nunivak Event seem to be a little thicker than usual, and one of the Nunivak samples is negatively polarized. The sediments deposited during Anomaly 3A (Chron 5 and 6) are unusually thin because of calcite dissolution. The correlations to Anomalies 4 and 4A (Chron 7 and 8) are adequate, and that to Anomaly 5 (Chron 9 and Chron 10) is again unquestionable. The seafloor at this site falls within the Anomaly 5-R interval. Extrapolating on the basis of 8.6 m.y. and 10.0 m.y. ages for the tops of Chrons 9 and 10, respectively, the seafloor age should be 10.3 m.y.; this is almost exactly the age predicted on the basis of the assumption of a linear rate of seafloor spreading during the Cenozoic (LaBrecque et al., 1977). The NRM of the basement basalt has a negative polarity; it formed during Chron 10 (or C-5-R). The chronology of the highest and lowest occurrences (HOs and LOs) of the various foraminiferal and nannoplankton taxa could be determined on the basis of the magnetostratigraphic time scale. The first directly controlled estimates for the following events have been made at this site (see Poore et al., this vol.): LO *Globorotalia cibaoensis*, 5.20 m.y.; LO *Globigerinoides conglobatus*, 5.30 m.y.; LO *G. kennetti*, 7.50 m.y.; LO *Catinaster calyculus*, 8.95 m.y.; LO *C. coalitus*, 9.6 m.y.; HO *Globorotalia languaensis*, 8.10 m.y.; HO *Catapsydrax parvulus*, 8.20 m.y.; HO *Catinaster calyculus*, 8.35 m.y.; and HO *C. coalitus*, 9.0 m.y.

The LOs and HOs thus determined present a number of problems. The LO of *Globigerinoides conglobatus* is considerably younger than its FAD in Chron 7 in the Pacific (Poore et al., this vol.). There might be several explanations, such as late appearance because of migration, or truncation of the lower range by dissolution. The HOs and LOs of *C. calyculus* and *C. coalitus* present a greater problem. Both species have their LOs in the single NN8 sample of DSDP Hole 62-1. However, at Site 63-1, the LO of *C. calyculus* is somewhat higher than that of *C. coalitus*. Martini (1971) eventually chose the LO of *C. coalitus* to define the base of the nannofossil zone NN8 (p. 1475) and remarked that the LO of *C. calyculus* should be just above the base of NN8 (p. 1477). The HO of the former was given as the middle of NN9 and that of the latter as near the top of NN9. However, Percival noted that the HOs of the two species ranged up into NN10. His interpretation gave a correlation of NN10 with Chron 9, a correlation that deviates only slightly from that postulated by Ryan et al. (1978,

p. 14). On the other hand, if we follow Martini, and consider the LOs of the two species at this site reliable datum levels to define nannofossil zones, we would come up with an age of NN7 for the Anomaly 5 basement here. Such an alternative interpretation will lead to further problems, because the LO of *C. coalitus* found by Martini and Bramlette in Core EM 8-13 of the experimental Mohole of the Pacific (1963) is associated with an ash bed dated radiometrically by Dymond (1966) to be 11.4 ± 0.6 m.y. This age is appreciably older than the 9.6 m.y. age found for the LO of this species on the basis of magnetostratigraphic calibration.

The HOs and LOs of a number of other key species used in biostratigraphic zonations are also shown in Figure 16. The HO of *Reticulofenestra pseudoumbilica* at this site in sediments older than the LAD of species in the Pacific resulted in the placement of the top of NN15 at a level corresponding to the Gilbert/Gauss epoch boundary (or about 3.4 m.y.). At Site 397, Mazzei et al. (1979) noted the HO of this species at a horizon corresponding to the Gauss/Matuyama boundary (~2.4 m.y.). The HO of the species during the late Gauss chron (~3 m.y.) was recorded by the Pacific cores (Gartner, 1973). Poore attributed the discrepancies to a taxonomic problem, because the smaller *R. pseudo-umbilica* in some samples may have a range different from that of the typical forms (Poore et al., this vol.).

The LOs of *Pseudoemiliania lacunosa* and *Discoaster tamalis* and the HO of *D. surculus* are comparable to previously recorded FADs and LADs. The HO of *D. quinqueramus* is about the same as its LAD in the Pacific and seems a little higher at this site than the HO at Site 397. The LOs of *Ceratolithus rugosus* and *D. asymmetricus* are about the same as the LOs of those species at Site 397, but on the other hand they are slightly older than the LOs in the Pacific (see Mazzei et al., 1979; Poore et al., this vol.). Perhaps the data at Site 519 should be considered in revising the FAD of those nannofossil taxa.

As for the datum levels for the planktonic foraminifers, the HO of *Globigerina nepenthes* here is about the same as the HO of the species in the Pacific, but the HO of *Globorotalia margaritae* is slightly older, perhaps because dissolution has truncated the upper range of this species at this site. The LO of *G. crassaformis* is significantly older here than the FAD determined by previous calibrations; Poore suggested that this species evolved in the temperate region and then migrated to equatorial oceans.

Calcite Dissolution and Sedimentation Rates

The percentage of insoluble residues (IR) in pelagic sediments gives a measure of the degree of sediment dissolution if the terrigenous influx does not vary significantly. Two other parameters used to evaluate calcite dissolution are the percentage of benthic foraminifers (BF) in microfaunal assemblages and the percentage of fragmented foraminiferal tests (FFT). The IR (or carbonate content) analyses were carried out on board by Leg 73 sedimentologists and on shore by DSDP techni-

cians. The BF and FFT analyses were made by Ray Wright. The results are shown graphically in Figure 15.

The oldest sediments of Chron 10 age (10 m.y.) show considerable dissolution, containing 34% IR, 10% BF, and 78% FFT. The overlying sediments of Chrons 9 to 7 (8–10 m.y.) have undergone less dissolution, even though the ridge crust subsided rapidly from 2600 to 3200 m during the deposition of those early late Miocene sediments. It is assumed that the mesolytic sediments of Chron 10 were deposited near the top of the lysocline, so the CCD must have been depressed at a higher rate than crustal subsidence during the subsequent 2 m.y. Dissolution reaches a minimum (6% IR) at about the Chron 7/8 boundary, or about 8 m.y., when the lysocline rose again. The peak dissolution occurred during Chron 6 at about 6 m.y. (according to the IR data; 32% IR) or during Chron 5 at about 5.5 m.y. (according to BF data). The lysocline must have risen to a level above the paleodepth of 3300 m at that time. The lysocline then rapidly became depressed again, reaching another minimum at about early Gilbert time (4.5 m.y.), so that a sediment deposited during the C₁ Event has a minimum IR of 4.6%. The lysocline remained depressed during the next 1.5 m.y., except for one short dissolution event during the Cochiti Event. During the late Gauss and the Brunhes, subordinate peaks of IR may indicate either slightly increased dissolution (as suggested by high FFT) or a substantial increase of terrigenous input (as suggested by the low BF percentages).

The extent of calcite dissolution is reflected in the sedimentation rates, as shown by the time–depth plot for this site (Fig. 17). The average accumulation rates for sediment bulk and for IR are also tabulated for various intervals in Table 5. The rates of IR deposition were 0.7 to 1.0 m/m.y. for the late Miocene but 1.5 to 2.7 m/m.y. for the Pliocene–Quaternary, confirming the general observation that the terrigenous influx to the Atlantic was unusually high during the glacial times. The lower upper Miocene sediments deposited during Chrons 9 to 7 have about the same IR percentages as the Pliocene–Quaternary sediments, but they have suffered on the whole twice as much dissolution, as indicated by the rates of bulk sedimentation (7.0–10.4 m/m.y. vs. 15–26.7 m/m.y.). This more advanced degree of dissolution is also shown by the FFT data (Fig. 15). The upper upper Miocene sediments deposited during Chrons 6 to 5 have about three times as much IR as the Pliocene–Quaternary average (25% vs. ~8%), but they have undergone a fivefold more severe dissolution, as indicated by their bulk sedimentation rates (4.2 m/m.y. vs. ~20 m/m.y.).

A comparison with the results of the dissolution studies made at Site 16 yields interesting results. That site, which was on the west flank of the ridge, was drilled on Anomaly 5 and bottomed in basalt below Tortonian sediments slightly (<1 m.y.) younger than the oldest sediments at Site 519. The Pliocene–Quaternary (Albatross) ooze is a chalk ooze deposited at the rate of 18 m/m.y., with a terrigenous influx of 1.7 m/m.y.; those rates are similar to those of the correlative sedi-

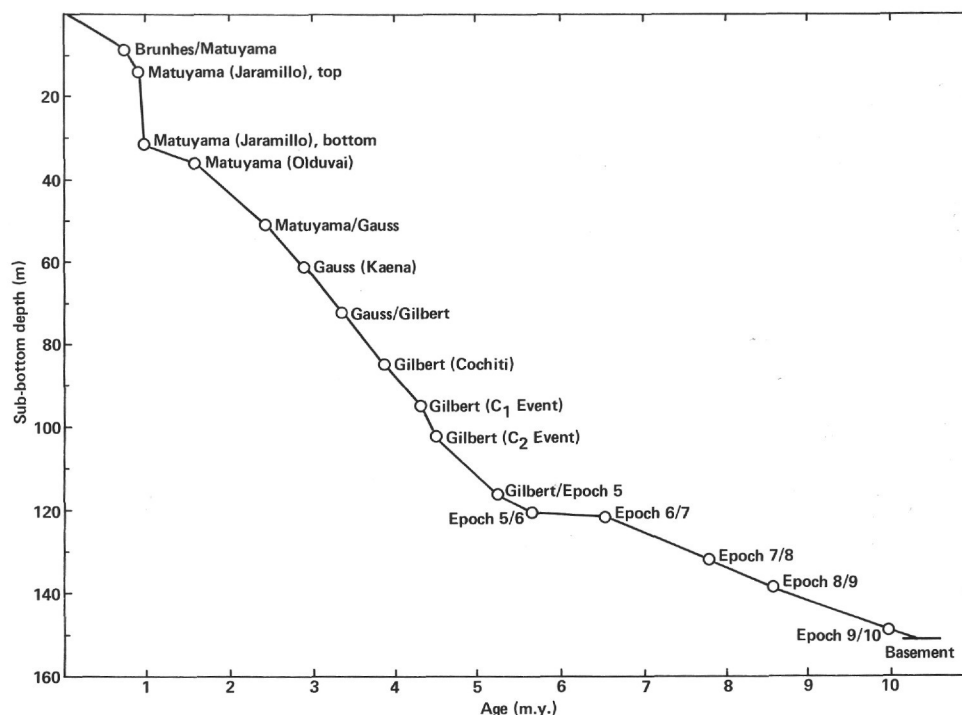


Figure 17. Sedimentation rate summary, Site 519. See text for explanation.

Table 5. Sedimentation rates, Site 519.

Datum	Depth (m)	Age (m.y.)	Insoluble residue (%)	Sedimentation rate (m/m.y.)	
				Interval	Insoluble residue
Jaramillo, top	14	0.91	12	15.4	1.9
Jaramillo, bottom		0.98	—	(Slump block)	—
Kaena, top	62	2.92	10	15	1.5
Gauss/Gilbert	73	3.41	7.5	22.6	1.7
Cochiti, top	85	3.86	7.5	26.7	2.0
C ₁ , top	95.5	4.35	12	21.4	2.6
C ₂ , top	102	4.52	7	38.2	2.7
Gilbert/Chron 5	116.5	5.26	17	6.1	1.0
Chron 6/Chron 7	121.9	6.54	25	4.2	1.0
Chron 7/Chron 8	132.1	7.88	9	7.6	0.70
Chron 8/Chron 9	139.2	8.56	9.5	10.4	1.0
Chron 9/Chron 10	149.1	10.00	12	7.0	0.84

ments at Site 519. A lithologic change could be found in the lowest Pliocene sediments at Site 16 (as at Site 519). The Messinian (Blake) ooze is a remarkably white chalk ooze that contains, on the average, exactly as much insoluble residue (9.3%) as the Pliocene-Quaternary ooze there, even though the Messinian has undergone 50% more dissolution as deduced from comparative sedimentation rate (12 m/m.y. vs. 18 m/m.y.). The bulk compositions of the two different oozes are coincidentally identical because of a proportionally slower rate of terrigenous influx (1.1 m/m.y.) in the more dissolved sedi-

ments. The late late Miocene rate of IR accumulation is about the same at Sites 16 and 519; a comparison of the IR and the bulk sedimentation rates indicates that the ooze of this age on the east side of the Mid-Atlantic Ridge has undergone three times as much dissolution as that on the west side, although the difference in the paleodepth of the two sites is less than 300 m. The older upper Miocene (*Challenger*) ooze at Site 16 was deposited at the rate of 10 m/m.y., whereas the IR accumulated at the rate of 1.0 m/m.y. These rates are similar to those of the synchronous sediments at Site 519, indicating the same degree of dissolution at both sites during the time interval from Chrons 7 to 9 (6.5–8.5 m.y. ago).

Paleoceanography

In addition to calcite dissolution data, studies of the benthic microfauna and analyses of the light isotopes of foraminiferal tests yield information on ocean chemistry and ocean fertility. Both those factors influence the level of the calcite compensation depth.

The severe dissolution of the middle Miocene sediments of the South Atlantic was first discovered during Leg 3 and still represents one of the major findings of the Deep Sea Drilling Project. The initial attempt to explain the dissolution by changes in seafloor depth (Maxwell et al., 1970, pp. 445–453) was soon abandoned in favor of the idea that calcite compensation depth had changed, a theory proposed by the shipboard staff of the next cruise (Benson et al., 1970, pp. 672–673). The reason for the CCD changes has remained a question of much debate. In principle, compensation requires supply to replace dissolution loss. Rises in CCD could result from more corrosive bottom water or from a reduction in supply.

One favorite hypothesis is that increased dissolution is related to the more vigorous circulation of a presumably more corrosive Antarctic Bottom Water. The rise of the CCD in the Cape Basin during the middle late Miocene was related by Melguen (1978) to pulsations of the deep Antarctic current. Wright recognized that *Nuttallides umbonifera* is a benthic taxa that is commonly found in regions in the flow path of the AABW. The first occurrence of the species in sediments of any site should signify the first intrusion of the AABW, and its relative abundance in benthic fauna assemblages may indicate the relative strength of the current, which is presumably stronger in colder times. Wright's study indicates that *N. umbonifera* first occurred in significant numbers during Chron 6 (~6 m.y.), when the site had subsided to a depth of 3400 m and when Site 16 on the other side of the ridge was down to 3000 m. The mere presence of this species may not be a true indicator of AABW, however; it may merely indicate deep oceanic depth, because the species is also found in moderate amounts in benthic populations at shallower depths where the bottom water is the North Atlantic Deep Water. However, the dominance of the species (30 to 50% of BF) suggests the first intrusion of AABW at that time. There was another remarkable increase in the population of *N. umbonifera*, about 3.5 m.y. ago (just below the Gilbert/Gauss boundary), signifying another intensification of the AABW. This intensification would be synchronous with the reported expansion of the Antarctic Ice Sheet and the beginning of the Arctic Glaciation during the mid-Pliocene (Shackleton and Opdyke, 1977; Keigwin, 1979). A detailed investigation indicates oscillations of the *N. umbonifera* population in cyclically deposited late Pliocene sediments with corresponding oxygen-isotope oscillations. This facts suggest pulsations of the AABW in response to alternating glacial and interglacial stages (Weissert et al., this vol.). Still another increase of *N. umbonifera*, with a corresponding oxygen shift, took place at about 2.5 m.y. (Gauss/Matuyama boundary), indicating a still further intensification of the AABW, corresponding to another expansion of polar ice caps (see Shackleton and Opdyke, 1977).

Weissert et al. (this vol.) studied the cyclically deposited Pliocene ooze at this and other sites. They found that the darker oozes contain more IR, higher percentages of BF, more FFT, and more abundant *N. umbonifera* and are characterized by a more positive $\delta^{18}\text{O}$. Although the high IR could be interpreted in part, at least, as having resulted from a higher influx of terrigenous detritus, the other indicators suggest higher degrees of dissolution of the marl oozes deposited during glacial stages, when the AABW was also more active. The periodicity of the Pliocene cycles has been estimated to be about 10^5 yr. (Weissert et al., this vol.), and it seems that Melguen's postulate (which relates dissolution to AABW pulsations) might be applicable to CCD changes of such shorter durations. However, one could hardly apply the same principle to explain the long-term changes with a periodicity of about 10^7 yr. True, the peak dissolution started during Chron 6, or about 6 m.y. ago, co-

inciding with the timing of the first abundant occurrence of *N. umbonifera* at this site. Yet the degree of dissolution of the Chron 6 and 5 sediments at Site 16 on the west side of the Ridge, where the AABW should have been more active, was less intensive than at Site 519. Furthermore, no significant increases in dissolution took place during the 3.5- and 2.5-m.y. events; the CCD either remained more or less the same or even became depressed during those times (when AABW flow intensified). Investigations at other sites also failed to show a correlation between the rise of CCD and either AABW indicators or oxygen-isotope shifts (see Hsü et al., this vol.).

The intensification of calcite dissolution during Chron 6 coincided in timing with the so-called late Miocene carbon shift (see Vincent et al., 1980). We noted that the carbon shift of about -0.5% at Site 519 is much smaller than the shift of -1% or more in the North Pacific. The difference suggests that the bottom waters of the South Atlantic became younger and more nutrient rich, whereas the North Pacific bottom waters became older and more nutrient poor during Chron 6 time, when the shift took place (Bender and Graham, 1981). There may have been a significant reorganization in the bottom circulation of the world's oceans when the present circulation pattern first became established. However, we could not conclude that the intrusion of younger, more nutrient rich water at that time was responsible for the late Miocene CCD crisis, because such younger, more nutrient rich water had come at earlier times (e.g., the Oligocene), when the CCD was not raised, but significantly depressed.

To conclude, it seems that postulating the presence of more corrosive water does not explain the CCD crisis. We have to look into the supply side of the equation. As proposed by the cruise synthesis chapter, the presently available data suggest that the higher levels of the CCD which occurred during the Eocene and Miocene in the world's oceans generally and in the South Atlantic particularly, had to be related to significantly reduced ocean fertility during those times, when many nutrients were tied up in phosphate deposits on continental shelves that were submerged upon a worldwide rise in sea level (see Hsü et al., this vol.).

Basement Petrology and Tectonics

All the basement basalt samples have similar chemistry, mineralogy, and texture, indicating that the basalts have come from a single source, a tholeiitic magma that probably erupted over a relatively short time during a period of reversed polarity within Chron 10 (or Anomaly 5-R or Chron C-5-R). Inclinations of NRM in the samples suggest tilting of the basement fault blocks. The potassium-argon dating of a basalt sample was not satisfactory; retention of primary argon led to an apparent age of 115 m.y. for this 10.3-m.y.-old basement (McKee, this vol.).

REFERENCES

- Bender, M. L., and Graham, D. W., 1981. On late Miocene abyssal hydrography. *Mar. Micropaleontol.*, 6:451-464.

- Benson, W. E., Gerard, R. D., and Hay, W. W., 1970. Summary and conclusions. In Bader, R. G., Gerard, R. D., et al., *Init. Repts. DSDP*, 4: Washington (U.S. Govt. Printing Office), 659-673.
- Dymond, J. R., 1966. Potassium-argon geochronology of deep-sea sediments. *Science*, 152:1239-1241.
- Gartner, S., 1973. Absolute chronology of the late Neogene calcareous nannofossil succession in the equatorial Pacific. *Geol. Soc. Am. Bull.*, 84:2021-2033.
- Keigwin, L. D., 1979. Late Cenozoic stable isotope stratigraphy and paleoceanography of DSDP sites from the east equatorial and north-central Pacific Ocean. *Earth Planet. Sci. Lett.*, 45:361-382.
- Kelts, K., and Hsü, K. J., 1980. Resedimented facies of 1875 Horgan slumps in Lake Zurich and a process model of longitudinal transport of turbidity currents. *Eclogae Geol. Helv.*, 73:271-281.
- Kirkpatrick, R. J., 1979. Processes of crystallization in pillow basalts, Hole 396B, DSDP Leg 46. In Dmitriev, L., Heirtzler, J., et al., *Init. Repts. DSDP*, 46: Washington (U.S. Govt. Printing Office), 271-282.
- LaBrecque, J. L., Kent, D. V., and Cande, S. C., 1977. Revised magnetic polarity time scale for Late Cretaceous and Cenozoic time. *Geology*, 5:330-335.
- Lohmann, G. P., 1978. Abyssal benthonic foraminifera as hydrographic indicators in the western South Atlantic Ocean. *J. Foraminiferal Res.*, 8:6-34.
- Mankinen, E. A., and Dalrymple, G. B., 1979. Revised geomagnetic polarity time scale for interval 0-5 m.y.B.P. *J. Geophys. Res.*, 84:615-626.
- Martini, E., 1971. Standard Tertiary and Quaternary calcareous nannoplankton zonation. In Farinacci, A. (Ed.), *Proc. Second Planktonic Conf.*: Rome (E. Tecnoscienza), pp. 739-785.
- Martini, E., and Bramlette, M. N., 1963. Calcareous nannoplankton from the experimental Mohole drilling. *J. Paleontol.*, 37:845-856.
- Maxwell, A. E., Von Herzen, R. P., Andrews, J. E., Boyce, R. E., Milow, E. D., and Shipboard Scientific Party, 1970. Summary and conclusions. In Maxwell, A. E., Von Herzen, R. P., et al., *Init. Repts. DSDP*, 3: Washington (U.S. Govt. Printing Office), 441-471.
- Mazzei, R., Raffi, I., Rio, D., Hamilton, N., and Cita, M. B., 1979. Calibration of late Neogene calcareous plankton datum planes with the paleomagnetic record of Site 397 and correlation with Moroccan and Mediterranean sections. In von Rad, U., Ryan, W. B. F., et al., *Init. Repts. DSDP*, 47, Pt. 1: Washington (U.S. Govt. Printing Office), 375-390.
- Melguen, M., 1978. Facies evolution, carbonate dissolution cycles in sediments from the eastern South Atlantic (DSDP Leg 40) since the Early Cretaceous. In Bolli, H. M., Ryan, W. B. F., et al., *Init. Repts. DSDP*, 40: Washington (U.S. Govt. Printing Office), 981-1024.
- Natland, J. H., 1979. Crystal morphologies in basalts from DSDP Site 395, 23°N, 46°W, Mid-Atlantic Ridge. In Melson, W. G., Rabinowitz, P. D., et al., *Init. Repts. DSDP*, 45: Washington (U.S. Govt. Printing Office), 423-445.
- Ryan, W. B. F., Bolli, H. M., Foss, G. N., Natland, J. H., Hottman, W. E., and Foresman, J. B., 1978. Objectives, principal results, operations, and explanatory notes of Leg 40, South Atlantic. In Bolli, H. M., Ryan, W. B. F., et al., *Init. Repts. DSDP*, 40: Washington (U.S. Govt. Printing Office), 5-28.
- Schnitker, D., 1980. Quaternary deep-sea benthic foraminifers and bottom water masses. *Annu. Rev. Earth Planet. Sci.*, 8:343-370.
- Shackleton, N. J., and Opdyke, N. D., 1977. Oxygen isotope and paleomagnetic evidence for early Northern Hemisphere glaciations. *Nature*, 270:216-219.
- Vincent, E., Killingley, J. S., and Berger, W. H., 1980. The magnetic epoch-6 carbon shift; a change in the oceans' $^{13}\text{C}/^{12}\text{C}$ ratio 6.2 m.y. ago. *Mar. Micropaleontol.*, 5:185-203.
- Violanti, D., Premoli Silva, I., Cita, M. B., Kersey, D., and Hsü, K. J., 1979. Quantitative characterization of carbonate dissolution facies of the Atlantic Tertiary sediments. An attempt. *Ital. Paleontol.*, 85:517-548.

Date of Initial Receipt: August 12, 1982

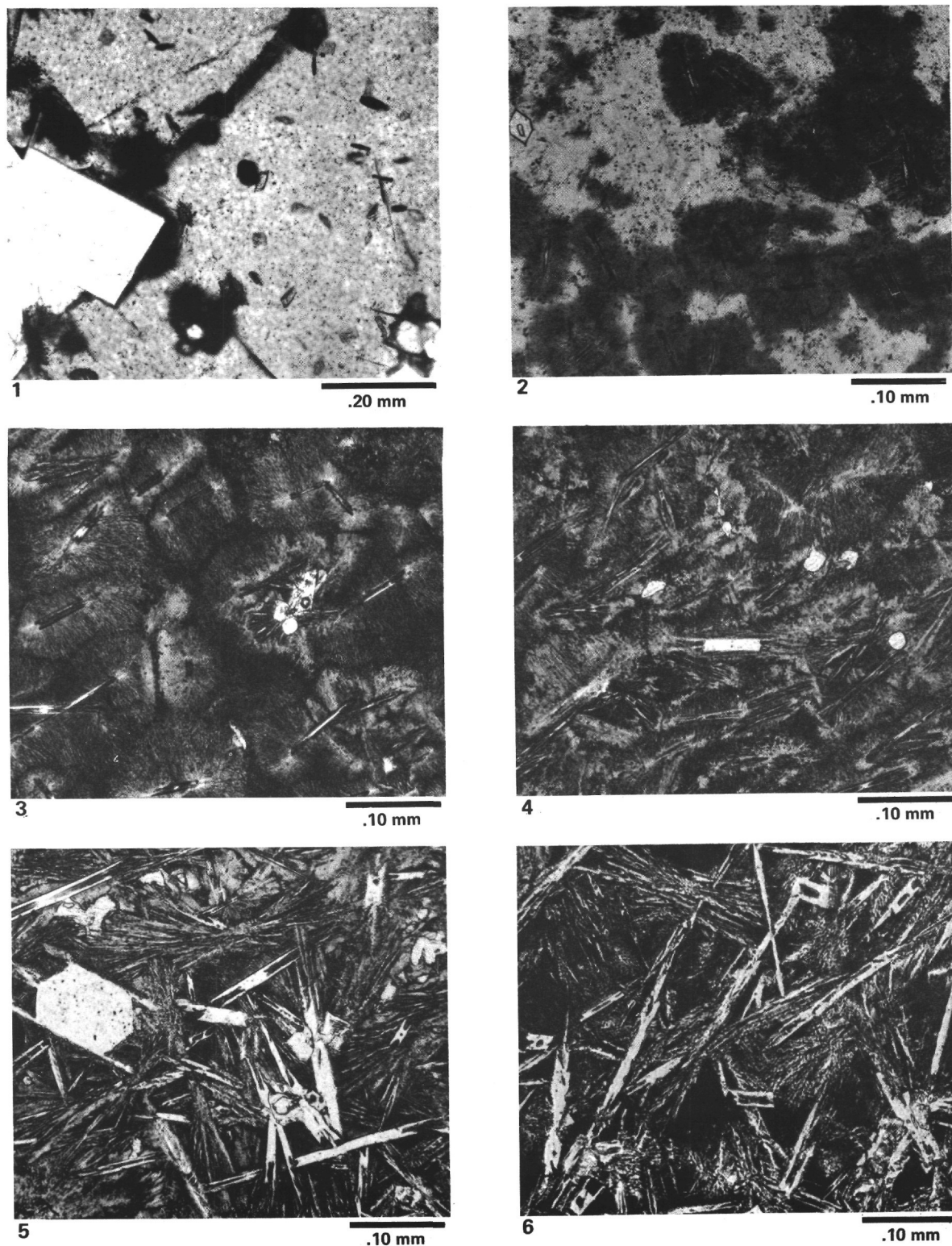
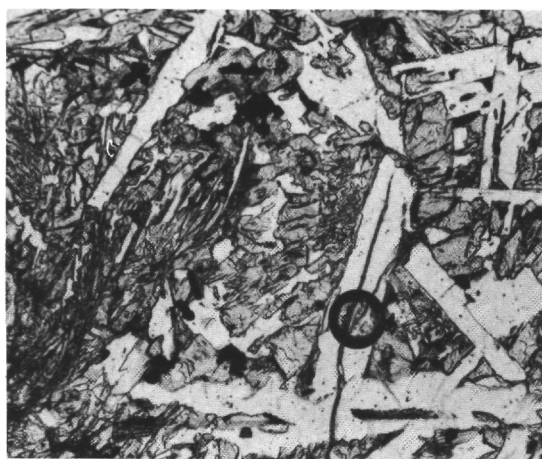
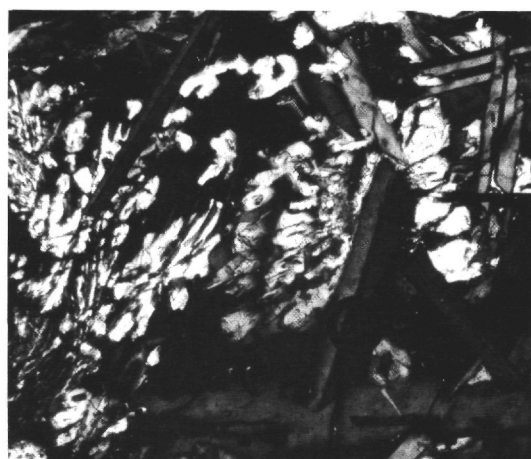


Plate 1. Photomicrographs of igneous rocks, Hole 519A. 1. Microphenocrysts in glass, Zone 1 (glassy). Top of Flow Unit 1, Sample 519-37, CC. First-generation plagioclase phenocrysts with spherulitic overgrowths. 2. Spherulites in glass, Zone 2 (glassy spherulitic). Top of Flow Unit 1, Sample 519A-7-1, 15-18 cm (Piece 3). 3. Solid spherulites with very fine quench texture, Zone 3 (coalesced spherulitic). Same sample as Fig. 2, 0.75 mm from glassy zone. 4. Spherulites and fine quench texture, Zone 4 (sheaf-shaped spherulitic). Same sample as Fig. 2, 2.8 mm from glassy zone. 5. Fine quench texture with subordinate, partial spherulites, Zone 4 (sheaf-shaped spherulitic). Same sample as Fig. 2, 10 mm from glassy spherulitic zone. 6. Fine quench texture, Zone 5 (plumose dendritic). Interior of Flow Unit 1, 0.5 m below top. Sample 519A-7-1, 55-57 cm (Piece 7). Plumose clinopyroxene and skeletal plagioclase. See Pl. 3, Fig. 1 for magnification of plumose clinopyroxene.



1

.10 mm



2

.10 mm



3

.10 mm



4

.10 mm



5

.50 mm



6

.50 mm

Plate 2. Photomicrographs of igneous rocks, Hole 519A. 1. Coarse quench texture, Zone 6 (coarse dendritic). Interior of Flow Unit 4, near top, 0.5 m below margin. Sample 519A-9-1, 58-60 cm (Piece 1C). Plain light. Note skeletal plagioclase with open ends. 2. Same as Fig. 1. Note thick dendritic augite (white) enclosing ends of plagioclase (dark gray, twinned). Crossed nichols. 3. Subophitic intersertal texture. Interior of Flow Unit 1, 1.5 m below top. Sample 519A-7-3, 5-7 cm (Piece 1A). Plain light. Plagioclase white, augite light gray, intersertal areas dark gray to black. 4. Same as Fig. 3. Subophitic augite white. Crossed nichols. 5. Same sample as Fig. 3, but same magnification as Fig. 6 for comparison. Intersertal areas are darkest. 6. Ophitic intersertal texture. Interior of Flow Unit 1, 2 m from top. Sample 519A-7-2, 50-52 cm (Piece 4). Plain light. Plagioclase white, augite light gray, intersertal areas dark gray to black. All augite in lower half of figure is a single grain.

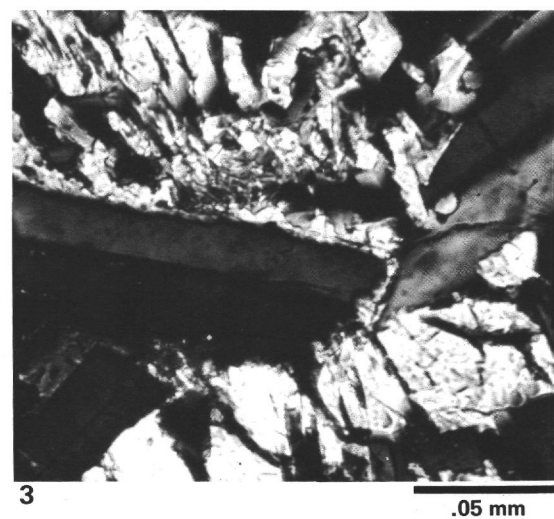
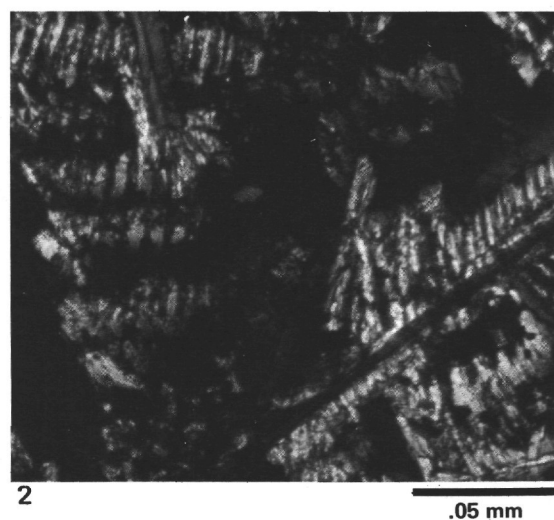
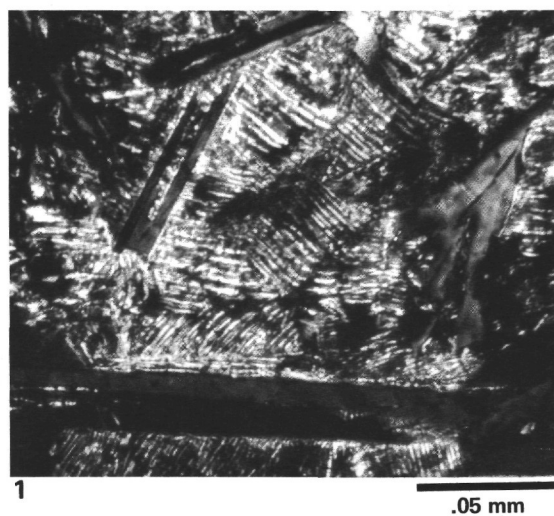
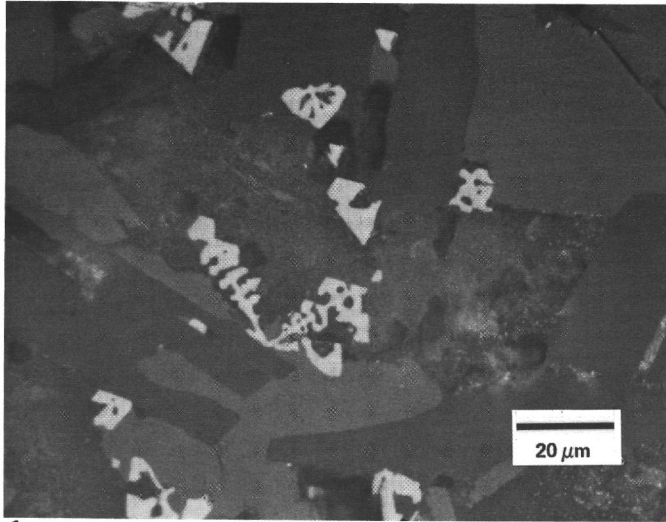
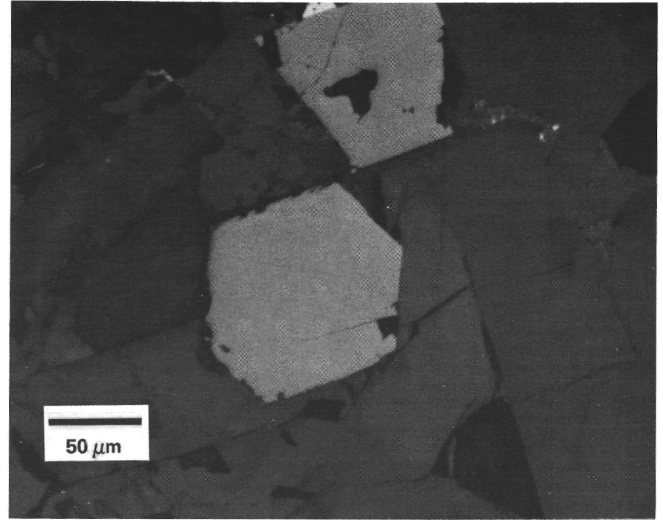


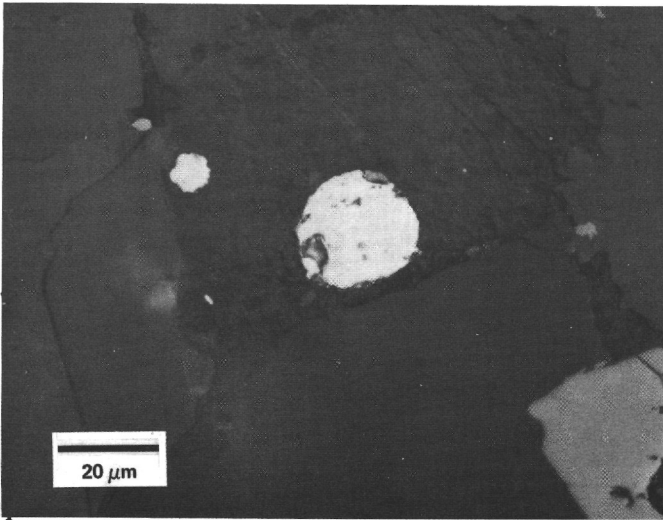
Plate 3. Photomicrographs of igneous rocks, Hole 519A. 1. Dendritic augite (white) in fine quench texture, Zone 5 (plumose dendritic). Interior of Flow Unit 1, 0.75 m below top. Sample 519A-7-1, 70-74 cm (Piece 9). Second generation plagioclase across bottom half of figure. Crossed nichols. 2. Dendritic augite (white) in coarse quench texture, Zone 6 (coarse dendritic). Interior of Flow Unit 2, 1 m below top. Sample 519A-8-2, 47-49 cm (Piece 1E). Crossed nichols. 3. Thick dendritic augite (white) in coarse quench texture, Zone 6 (coarse dendritic). Interior of Flow Unit 4, 0.5 m below top. Sample 519A-9-1, 58-60 cm (Piece 1E). Crossed nichols.



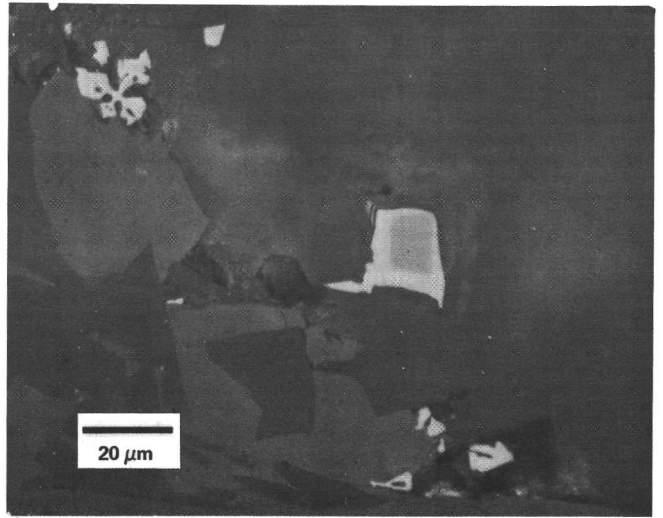
1



2

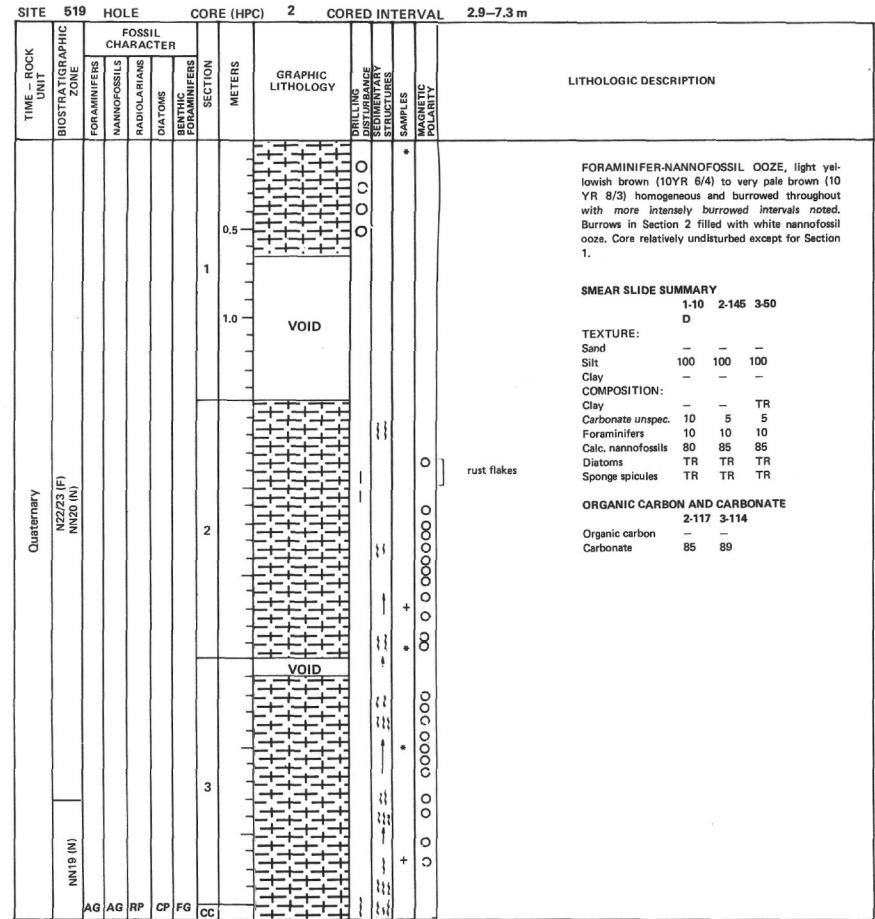
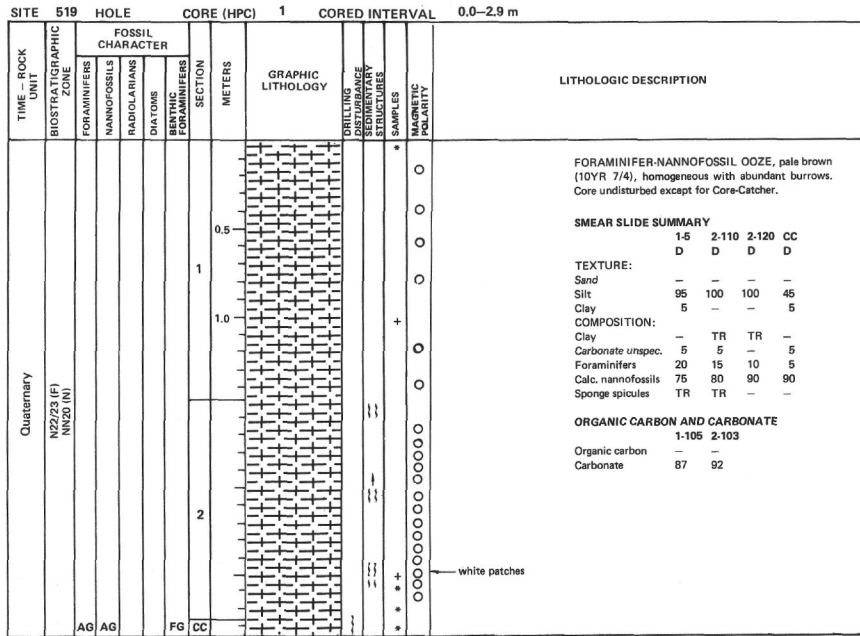


3

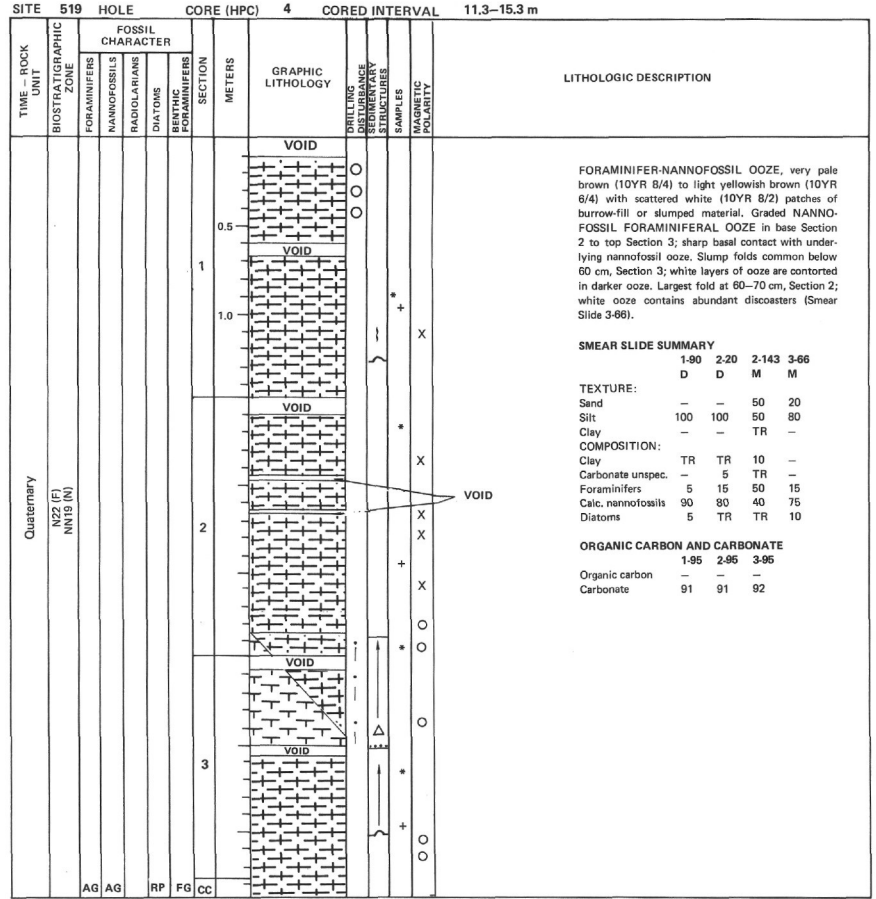
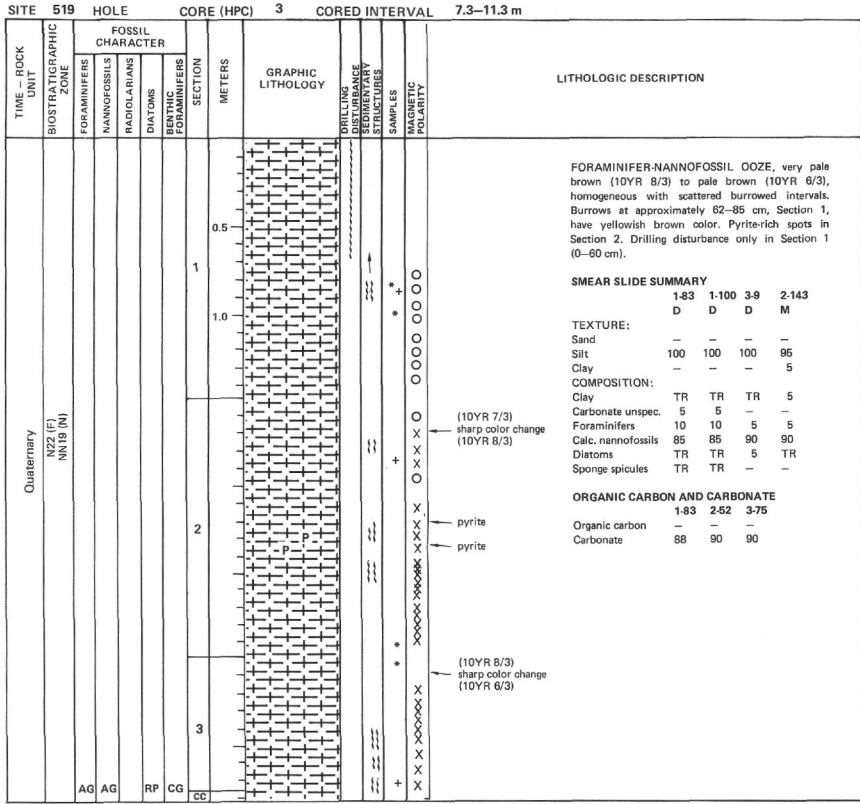


4

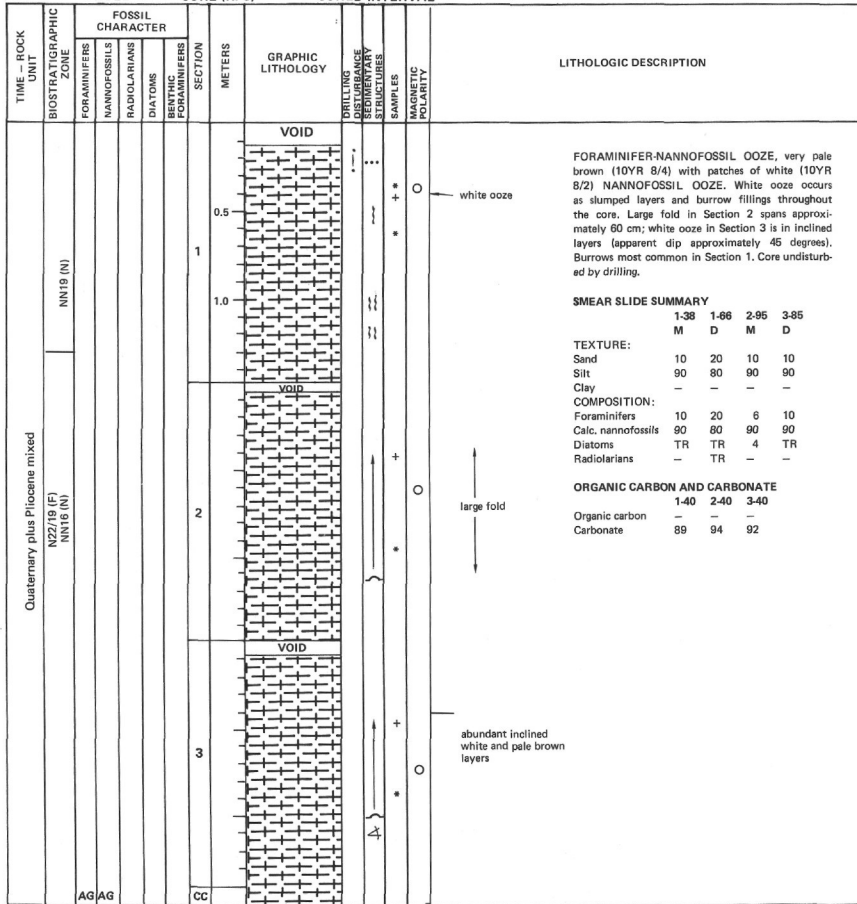
Plate 4. Opaque mineralogy (reflected light) of basaltic rocks, Hole 519A. 1. Titanomagnetite grains with typical skeletal shape (light gray). 2. Euhedral titanomagnetite grain (light gray). 3. Sulfide spherule consisting mostly of pyrrhotite. 4. Euhedral titanomagnetite grain (center, light gray), with core of chromium-spinel (gray). In the upper left corner, skeletal titanomagnetite (light gray).



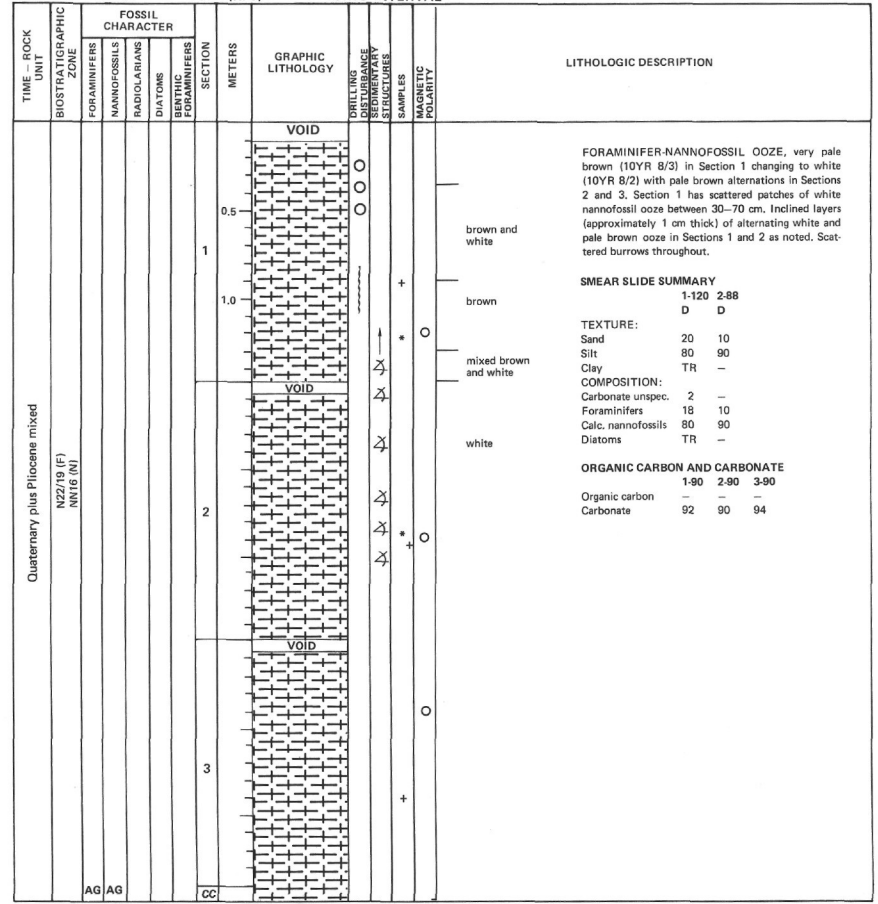
Information on core description sheets, for ALL sites, represents field notes taken aboard ship under time pressure. Some of this information has been refined in accord with post-cruise findings, but production schedules prohibit definitive correlation of these sheets with subsequent findings. Thus the reader should be alerted to the occasional ambiguity or discrepancy.

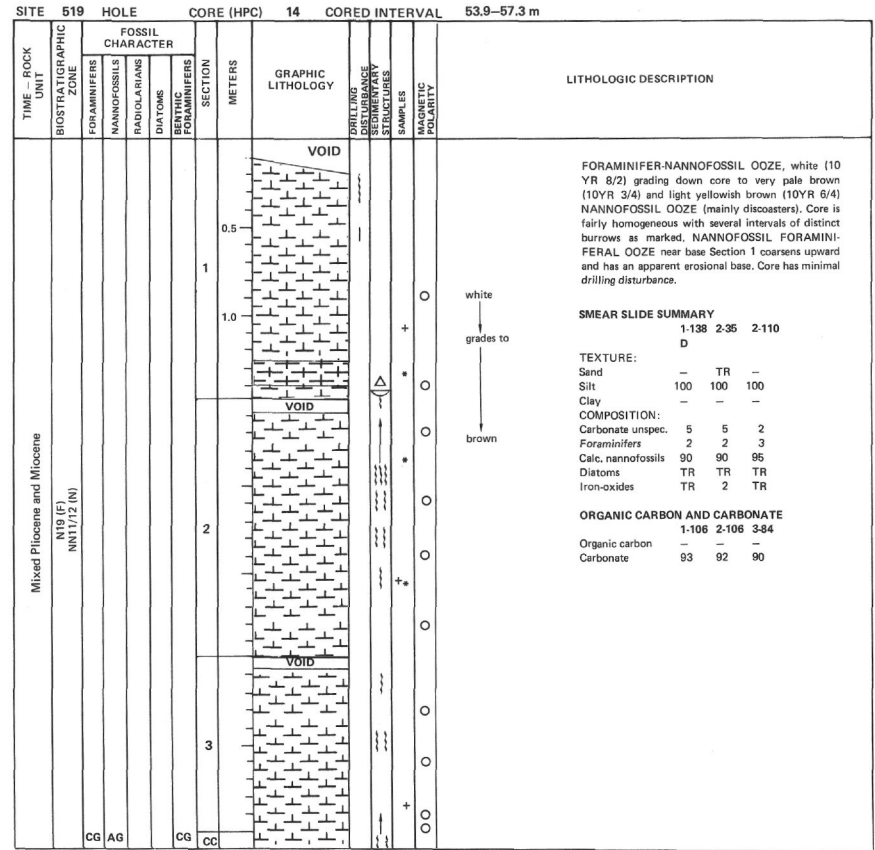
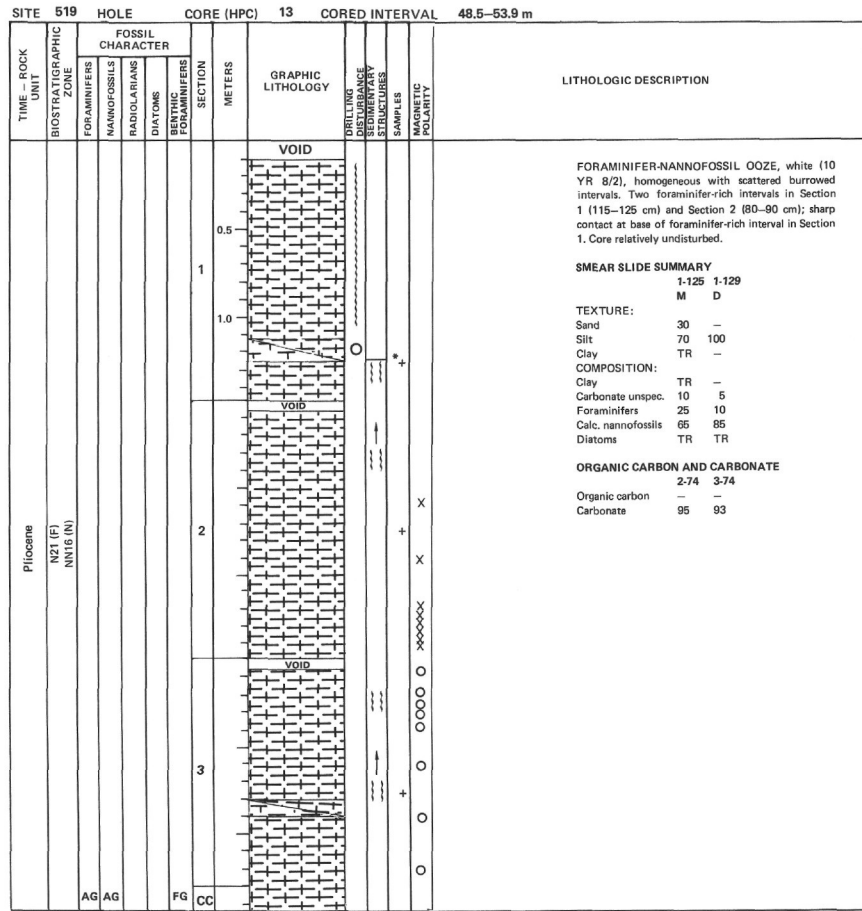


SITE 519 HOLE CORE (HPC) 5 CORED INTERVAL 15.3-19.3 m



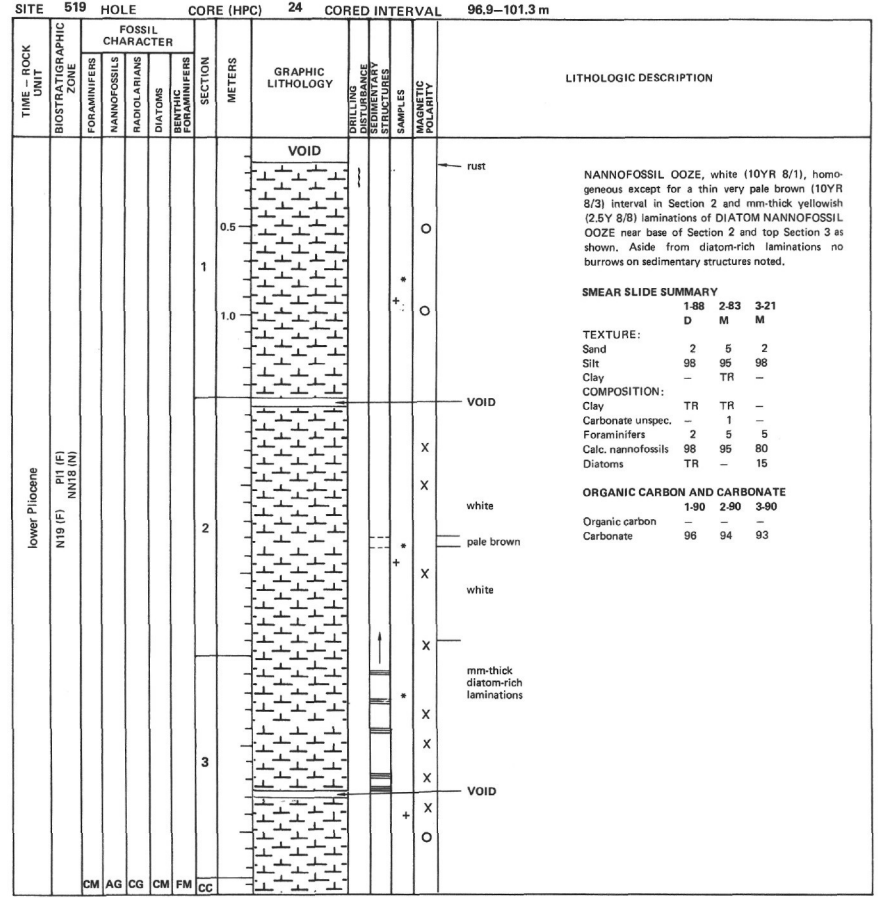
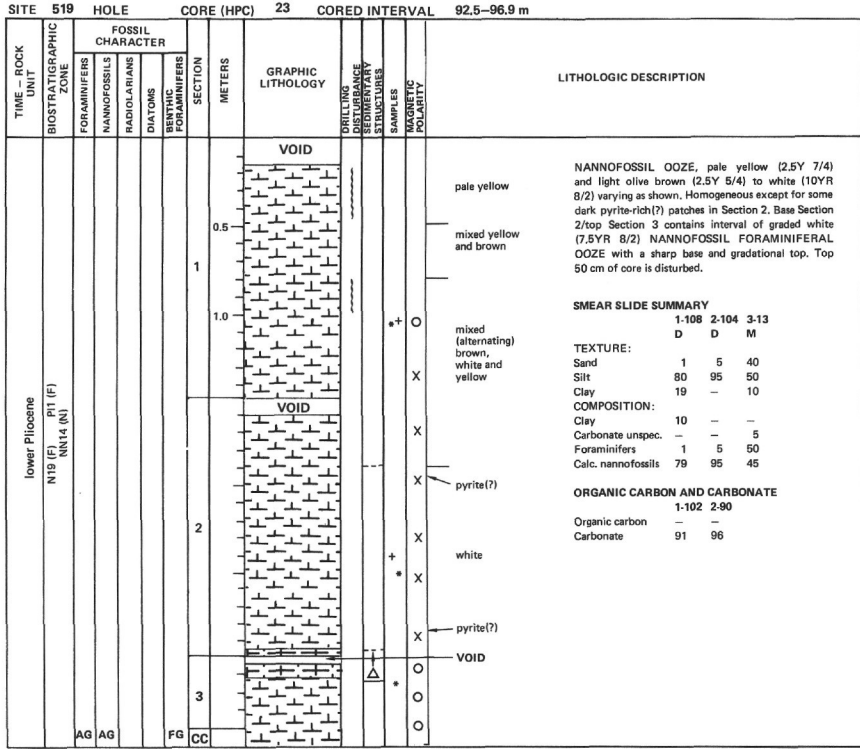
SITE 519 HOLE CORE (HPC) 6 CORED INTERVAL 19.3-23.3 m

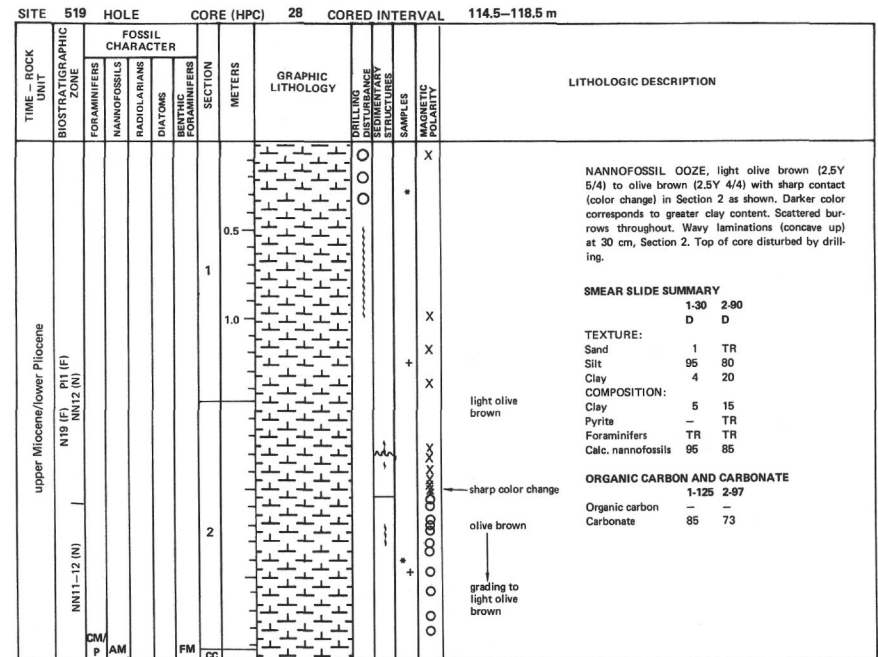
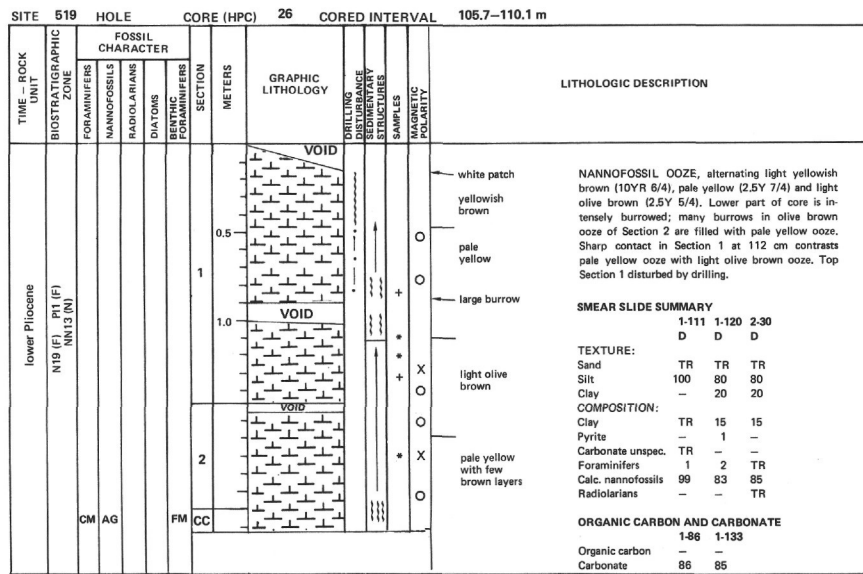
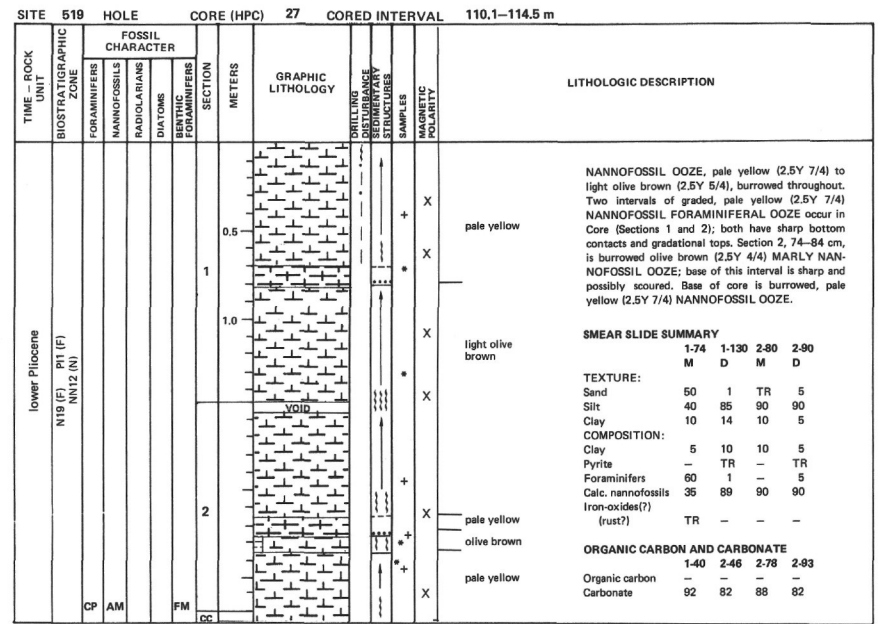
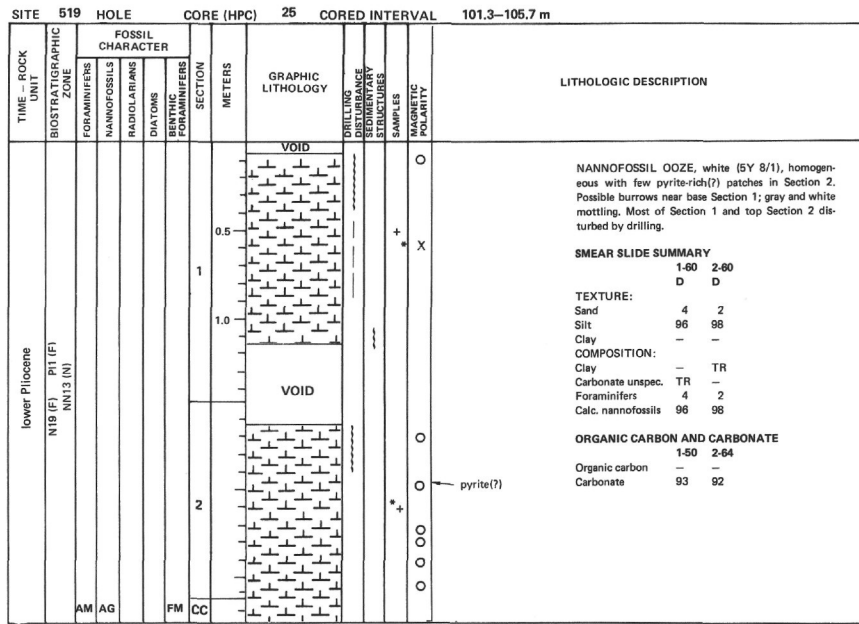




SITE 519 HOLE		CORE (HPC) 15		CORED INTERVAL 57.3-61.7 m							
TIME - ROCK UNIT	BIOSTRATIGRAPHIC ZONE	FOSSIL CHARACTER		SECTION	METERS	GRAPHIC LITHOLOGY	DRILLING DISTURBANCE	SEDIMENTARY STRUCTURE	SAMPLES	MAGNETIC POLARITY	LITHOLOGIC DESCRIPTION
		FORAMINIFERS	NANNOFOSSILS								
Pliocene	N19 (F) NN11/12 (N)				0.5	VOID					NANNOFOSSIL OOZE (mostly discoasters), very pale brown (10YR 7/4) to yellowish brown changing abruptly to white (10YR 8/2) at 140 cm, Section 2. Scattered burrowed intervals as marked. Otherwise core is homogeneous. Drilling disturbance in top of Section 1 only.
					1.0						
	AG AG	NN15 (N)				2	VOID				TEXTURE: Sand - - - Silt 100 100 100 Clay - - - COMPOSITION: Carbonate unspec. TR TR 5 Foraminifers TR 5 TR Calc. nannofossils 95 95 95 Iron-oxides 5 TR TR
	NN16 (N)				3						ORGANIC CARBON AND CARBONATE 1-138 2-135 Organic carbon - - Carbonate 91 95
		FG	CC								○ brown ○ sharp color change ○ white

SITE 519 HOLE		CORE (HPC) 16		CORED INTERVAL 61.7-66.1 m							
TIME - ROCK UNIT	BIOSTRATIGRAPHIC ZONE	FOSSIL CHARACTER		SECTION	METERS	GRAPHIC LITHOLOGY	DRILLING DISTURBANCE	SEDIMENTARY STRUCTURE	SAMPLES	MAGNETIC POLARITY	LITHOLOGIC DESCRIPTION
		FORAMINIFERS	NANNOFOSSILS								
Pliocene	N19 (F) N12-3 (F) NN18 (N)				0.5	VOID					NANNOFOSSIL OOZE, white (10YR 8/1-8/2), homogeneous except for thin, light brownish gray (10YR 6/2) laminations of DIATOM NANNOFOSSIL OOZE between 20 cm and 128 cm in Section 1. Some laminations disturbed by burrows. Sections 2 and 3 also contain scattered dark laminations that may also be diatom-rich. Remainder of core is homogeneous nannofossil ooze undisturbed by drilling.
					1.0						
	AG AG		CP	CP		2	VOID				TEXTURE: Sand - - - Silt 100 100 100 Clay - - - COMPOSITION: Carbonate unspec. 5 5 5 Foraminifers 5 TR TR Calc. nannofossils 85 80 95 Diatoms 5 35 40 Iron-oxides - 3 TR
		CP	FG		3						ORGANIC CARBON AND CARBONATE 1-138 2-138 3-138 Organic carbon - - - Carbonate 91 95 94
											○ + ○ X ○ X ○ X ○ X ○ X





SITE 519 HOLE CORE (HPC) 31 CORED INTERVAL 126.9-131.3 m																																
TIME - ROCK UNIT	BIOSTRATIGRAPHIC ZONE	FOSSIL CHARACTER				SECTION	METERS	GRAPHIC LITHOLOGY	DRILLING DISTURBANCE	SEDIMENTARY STRUCTURES	SAMPLES	MAGNETIC POLARITY	LITHOLOGIC DESCRIPTION																			
		FORAMINIFERS	NANNOFOSSILS	RADIOLARIANS	DIATOMS																											
upper Miocene	N17 (F) NN10-11 (N)	FM	AM			1	0.5 1.0	[Lithology: Nannofossil ooze with scattered white patches]					<p>NANNOFOSSIL OOZE, very pale brown (10YR 7/4-8/4) with scattered white (10YR 8/3) patches and burrows filled with white nannofossil ooze. Thin white layers of nannofossil ooze occurs in Section 2. Core is fairly homogeneous.</p> <p>SMEAR SLIDE SUMMARY</p> <table border="1"> <tr> <td></td> <td>1-80</td> <td>2-100</td> <td>3-74</td> <td>3-79</td> </tr> <tr> <td>D</td> <td>D</td> <td>D</td> <td>D</td> <td>D</td> </tr> </table> <p>TEXTURE:</p> <p>Sand - - - -</p> <p>Silt 100 100 100 100</p> <p>Clay - TR - TR</p> <p>COMPOSITION:</p> <p>Quartz TR TR TR TR</p> <p>Clay TR TR - TR</p> <p>Carbonate unspec. 5 5 10 5</p> <p>Foraminifers 10 10 5 5</p> <p>Calc. nannofossils 85 85 85 90</p> <p>Diatoms - - TR TR</p> <p>Iron-oxides TR TR TR TR</p> <p>ORGANIC CARBON AND CARBONATE</p> <table border="1"> <tr> <td></td> <td>1-145</td> <td>3-130</td> </tr> <tr> <td>Organic carbon</td> <td>-</td> <td>-</td> </tr> <tr> <td>Carbonate</td> <td>94</td> <td>94</td> </tr> </table>		1-80	2-100	3-74	3-79	D	D	D	D	D		1-145	3-130	Organic carbon	-	-	Carbonate	94	94
			1-80	2-100	3-74	3-79																										
		D	D	D	D	D																										
	1-145	3-130																														
Organic carbon	-	-																														
Carbonate	94	94																														
					2		[Lithology: Nannofossil ooze with thin white layer]					thin white layer																				
					3		[Lithology: Nannofossil ooze with sharp color change]					10YR 8/4 sharp color change 10YR 7/4																				
		FM	CC				[Lithology: Void]																									

SITE 519 HOLE CORE (HPC) 32 CORED INTERVAL 131.3-135.7 m																													
TIME - ROCK UNIT	BIOSTRATIGRAPHIC ZONE	FOSSIL CHARACTER				SECTION	METERS	GRAPHIC LITHOLOGY	DRILLING DISTURBANCE	SEDIMENTARY STRUCTURES	SAMPLES	MAGNETIC POLARITY	LITHOLOGIC DESCRIPTION																
		FORAMINIFERS	NANNOFOSSILS	RADIOLARIANS	DIATOMS																								
upper Miocene	N17 (F) NN10-11 (N)	CM	AM			1	0.5 1.0	[Lithology: Nannofossil ooze with occasional very pale brown patches]					<p>NANNOFOSSIL OOZE, light yellowish brown (10YR 6/4) with occasional very pale brown (10YR 8/3) patches and filled burrows. Core is homogeneous and undisturbed by drilling.</p> <p>SMEAR SLIDE SUMMARY</p> <table border="1"> <tr> <td></td> <td>1-100</td> </tr> <tr> <td>D</td> <td>D</td> </tr> </table> <p>TEXTURE:</p> <p>Sand -</p> <p>Silt 100</p> <p>Clay TR</p> <p>COMPOSITION:</p> <p>Clay TR</p> <p>Carbonate unspec. 15</p> <p>Foraminifers 5</p> <p>Calc. nannofossils 80</p> <p>Diatoms TR</p> <p>Iron-oxides TR</p> <p>ORGANIC CARBON AND CARBONATE</p> <table border="1"> <tr> <td></td> <td>1-126</td> <td>2-134</td> <td>3-116</td> </tr> <tr> <td>Organic carbon</td> <td>-</td> <td>-</td> <td>-</td> </tr> <tr> <td>Carbonate</td> <td>94</td> <td>93</td> <td>89</td> </tr> </table>		1-100	D	D		1-126	2-134	3-116	Organic carbon	-	-	-	Carbonate	94	93	89
			1-100																										
		D	D																										
	1-126	2-134	3-116																										
Organic carbon	-	-	-																										
Carbonate	94	93	89																										
					2		[Lithology: Nannofossil ooze]																						
					3		[Lithology: Nannofossil ooze]																						
		FM	CC				[Lithology: Void]																						

SITE 519 HOLE CORE (HPC) 36 CORED INTERVAL 144.1-148.5 m

TIME - ROCK UNIT	FOSSIL CHARACTER				SECTION	METERS	GRAPHIC LITHOLOGY	LITHOLOGIC DESCRIPTION
	BIOSTRATIGRAPHIC ZONE	FORAMINIFERS	NANNOFOSSILS	RADIOLARIANS				
upper Miocene	N17 (F) N10 (N)				1	0.5 1.0		<p>NANNOFOSSIL OOZE, light yellowish brown (10 YR 8/4) with scattered very pale brown (10YR 8/4) patches and filled burrows. Subtle color variations occur in Section 2. Core is homogeneous with only top disturbed by drilling.</p> <p>SMEAR SLIDE SUMMARY 1-140</p> <p>TEXTURE: Sand - Silt 85 Clay 15</p> <p>COMPOSITION: Quartz 5 Clay 5 Palagonite TR Carbonate unspec. 5 Foraminifers TR Calc. nannofossils 70 Iron-oxides 15</p> <p>ORGANIC CARBON AND CARBONATE 1-83 2-83 3-83</p> <p>Organic carbon - - - Carbonate 84 89 91</p>
					2			<p>subtle yellowish brown color variations</p>
					3			

SITE 519 HOLE CORE (HPC) 36 CORED INTERVAL 148.5-151.5 m

TIME - ROCK UNIT	FOSSIL CHARACTER				SECTION	METERS	GRAPHIC LITHOLOGY	LITHOLOGIC DESCRIPTION
	BIOSTRATIGRAPHIC ZONE	FORAMINIFERS	NANNOFOSSILS	RADIOLARIANS				
upper Miocene	N16-17 (F) N10 (N)				1	0.5 1.0		<p>MARLY NANNOFOSSIL OOZE, light yellowish brown (10YR 5/4) grading down core to dark brown (7.5Y 4/4). Color change corresponds to downward increase in clay, iron-oxide and quartz content of ooze. Occasional burrows noted. Core undisturbed except for upper 35 cm.</p> <p>SMEAR SLIDE SUMMARY 1-130 CC</p> <p>TEXTURE: Sand - Silt 70 50 Clay 30 50</p> <p>COMPOSITION: Quartz 5 10 Clay 5 15 Palagonite TR - Carbonate unspec. 5 5 Foraminifers TR 5 Calc. nannofossils 65 40 Diatoms - 5 Iron-oxides 25 30</p> <p>ORGANIC CARBON AND CARBONATE 1-67 2-62</p> <p>Organic carbon - - Carbonate 80 62</p>
					2			

SITE 519 HOLE CORE (HPC) 37 CORED INTERVAL 151.5-151.6 m

TIME - ROCK UNIT	FOSSIL CHARACTER				SECTION	METERS	GRAPHIC LITHOLOGY	LITHOLOGIC DESCRIPTION
	BIOSTRATIGRAPHIC ZONE	FORAMINIFERS	NANNOFOSSILS	RADIOLARIANS				
					CC			<p>Drilling breccia of very pale brown (10YR 8/3) and dark yellowish brown (10YR 4/4) NANNOFOSSIL OOZE with scattered fragments of basalt and basaltic glass, palagonite, and phillipsite.</p> <p>SMEAR SLIDE SUMMARY CC</p> <p>TEXTURE: Sand - Silt 100 Clay -</p> <p>COMPOSITION: Quartz TR Carbonate unspec. 5 Foraminifers 5 Calc. nannofossils 90</p>

SITE 519 HOLE A CORE 3 CORED INTERVAL 86.5-96.0 m

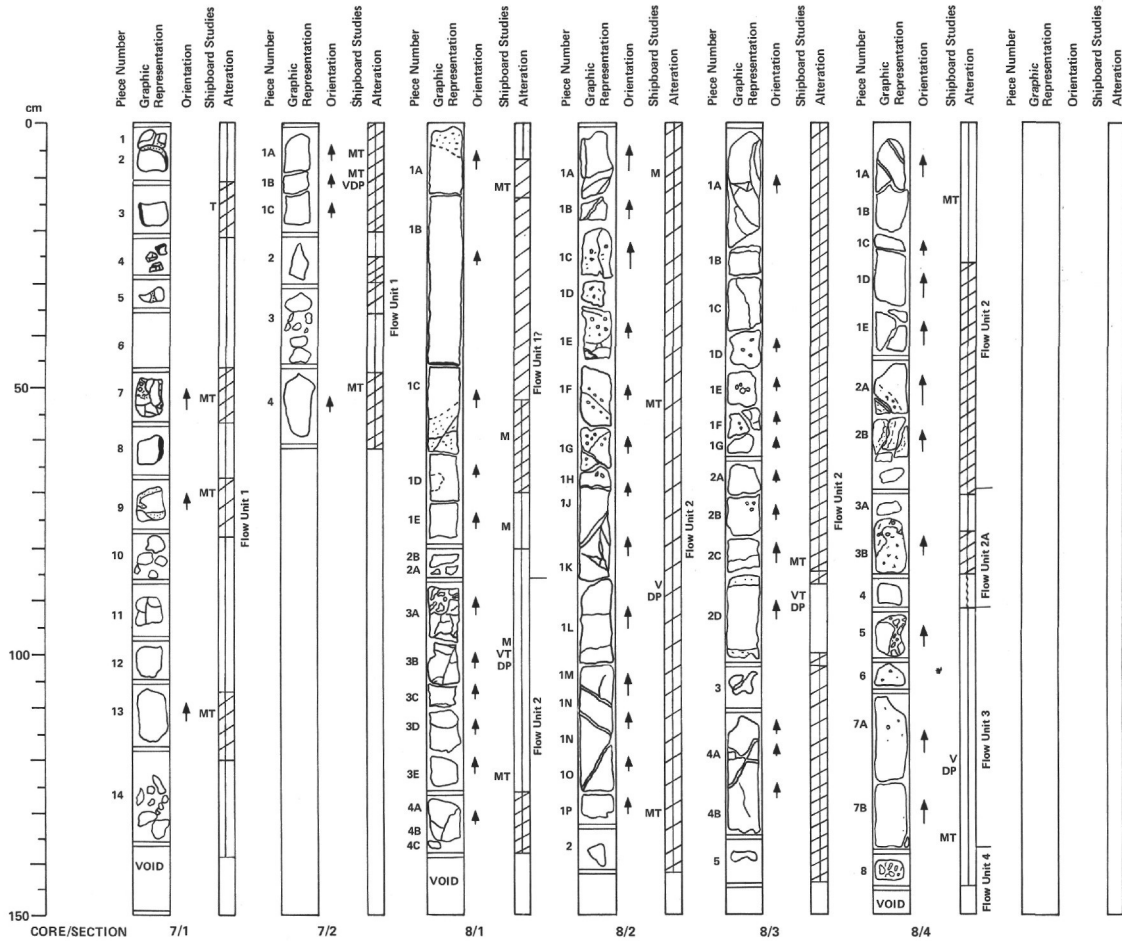
TIME - ROCK UNIT	BIOSTRATIGRAPHIC ZONE	FOSSIL CHARACTER			SECTION	METERS	GRAPHIC LITHOLOGY	DRELLING LOG OF SEDIMENTARY STRUCTURES	SAMPLES	MAGNETIC POLARITY	LITHOLOGIC DESCRIPTION
		FORAMINIFERS	NANNOFOSSILS	RADIOLARIANS							
Mixed Pliocene and Miocene	NN14 (N)					0.5					VOID
						1.0					NANNOFOSSIL OOZE, very pale brown (10YR 7/4) becoming lighter down core (10YR 7/3); light yellowish brown ooze in Sections 3 and 4. Core homogeneous except for burrowed intervals in Sections 4 and 5.
						2					SMEAR SLIDE SUMMARY 3-80 D
						3					TEXTURE: Sand - Silt 100 Clay -
						4					COMPOSITION: Quartz TR Clay TR Palagonite TR Carbonate unspec. 5 Foraminifers 5 Calc. nannofossils 90 Iron oxides TR
						5					very pale brown
						6					light yellowish brown
	NN11/12 (N)					7					
						CC					

SITE 519 HOLE A CORE 4 CORED INTERVAL 96.0-105.5 m

TIME - ROCK UNIT	BIOSTRATIGRAPHIC ZONE	FOSSIL CHARACTER			SECTION	METERS	GRAPHIC LITHOLOGY	DRELLING LOG OF SEDIMENTARY STRUCTURES	SAMPLES	MAGNETIC POLARITY	LITHOLOGIC DESCRIPTION
		FORAMINIFERS	NANNOFOSSILS	RADIOLARIANS							
Pliocene	NN14 (N)					0.5					VOID
						1.0					NANNOFOSSIL OOZE, white (10YR 8/1), homogeneous throughout except for faintly burrowed zone near base of Section 6 and top Section 7. Burrows filled with grayish ooze compositionally identical to surrounding white ooze.
						2					SMEAR SLIDE SUMMARY 2-20 6-115 D M
						3					TEXTURE: Sand 5 - Silt 95 100 Clay - -
						4					COMPOSITION: Clay TR - Carbonate unspec. 5 5 Foraminifers 5 5 Calc. nannofossils 90 90
						5					
						6					
				7							
						CC					

SITE 519		HOLE A		CORE 5		CORED INTERVAL 134.0-143.5 m					
TIME - ROCK UNIT	BIOSTRATIGRAPHIC ZONE	FOSSIL CHARACTER				SECTION	METERS	GRAPHIC LITHOLOGY	DISTURBANCE SEDIMENTARY STRUCTURES	DRILLING SAMPLER MAGNETIC POLARITY	LITHOLOGIC DESCRIPTION
		FORAMINIFERS	NANNOFOSSILS	RADIOLARIANS	DIAZOOMS						
						1	0.5 1.0	VOID brown white brown yellow brown brown			VOID brown yellow brown dark brown yellow brown very pale brown
						2		VOID brown yellow brown dark brown yellow brown			TEXTURE: Sand - Silt 60 Clay 40 COMPOSITION: Quartz TR Clay 5 Palagonite 5 Micronodules 5 Carbonate unsp. 5 Foraminifers TR Calc. nannofossils 70 Iron oxides 10
						3		VOID			
						4					
						5					
						6					
						7					
						8					white patch (downhole contamination?)

SITE 519		HOLE A		CORE 6		CORED INTERVAL 143.5-153.0 m				
TIME - ROCK UNIT	BIOSTRATIGRAPHIC ZONE	FOSSIL CHARACTER				SECTION	METERS	GRAPHIC LITHOLOGY	DRILLING SAMPLER MAGNETIC POLARITY	LITHOLOGIC DESCRIPTION
		FORAMINIFERS	NANNOFOSSILS	RADIOLARIANS	DIAZOOMS					
						1	0.5 1.0			NANNOFOSSIL OOZE, pale yellow (2.5Y 7/4), homogeneous throughout; no sedimentary structures.
						2				
						CC				



HOLE 519A, CORE 7, SECTIONS 1-2, 153.0-155.1 m

MAJOR ROCK TYPE - BASALT
MINOR ROCK TYPE - LIMESTONE

Macroscopic Description

Basalt - Single flow unit of aphyric, very fine-grained sparsely microporphyrritic and vesicular near top Sec. 1 (Pieces 1-8), grading to coarsely crystalline (diabasic texture) aphyric basalt in Section 2. Sparse plagioclase microphenocrysts in Pieces 1-10, Sec. 1, chiefly in 0.2-0.5 mm glomerocystic clusters. Pieces 1-4, 6, and 8 in Sec. 1 have black glassy margins; some altered to palaeogite. Moderately to badly altered with alteration concentrated in zones bounding fractures. Calcite filled some fractures (e.g. Piece 9, Sec. 1).

Limestone - Piece 4C and two fragments of Pieces 6 are tan crystalline limestone with suggestions of rounded microfossil relics.

Thin Section Summaries

Section 1: Sparsely microporphyritic (phenocrysts <1%) with plagioclase (An₇₀₋₈₀) microphenocrysts (0.04-4.1 mm) mostly in glomerocystic clusters; euhedral, not resorbed and with few inclusions. Main rock range textures from glassy (top of unit) through spherulitic, skeletal and dendritic, to subophitic, and from very fine-grained (<0.01

mm) to very coarse-grained (>0.5 mm) transitionally downward from top of unit. Subophitic, and some ophitic texture, occurs in very coarse-grained rocks (>0.5 mm). More fine-grained rocks (<0.5 mm) show various quench textures. In these plagioclase is typically skeletal, swallowtailed and occasionally chain-linked; pyroxene is plumose and comb-shaped dendritic, rarely chain-linked; and olivine is typically skeletal or chain-linked. Olivine ~Fo80-85 (2Vx ~85-90), plagioclase microlites ~An_{65±5}. Pyroxene normal augite. Rock slightly to badly altered, with olivine mostly gone to smectitic or iddingsitic phyllosilicates. Approximate mode of coarsest rock; Piece 13 = olivine 5, plagioclase 40, clinopyroxene 40, opaques 15.

Section 2: Aphyric (microphenocrysts of finer rocks higher in unit lost in coarsening of groundmass). Subophitic to ophitic interstitial, medium to very coarse-grained, coarsening downward from top of core. Olivine Fo-80 (2V~80), plagioclase An₇₀₋₇₅, pyroxene normal augite. Intersartal patches are a mixture of cryptocrystalline material, olivine, and opaques. Olivine much altered to smectite. Approximate mode: olivine 5, plagioclase 35-40, clinopyroxene 35-40, opaques 15, devitrified glass 5-10.

Shipboard Studies

Sample	D	P	V _L	V _I	NRM1	NRM2	S. I.
Sec. 1, Piece 7	-	-	-	-	19,514	76.7	79
Sec. 1, Piece 9	-	-	-	-	27,581	76.0	76.5
Sec. 1, Piece 13	-	-	-	-	12,872	66.1	75.5
Sec. 2, Piece 1A	-	-	-	-	10,091	77.6	75
Sec. 2, Piece 1B	2.84	10.9	5.48	5.46	8,020	66.4	71
Sec. 2, Piece 4	-	-	-	-	11,559	72.7	79

HOLE 519A, CORE 8, SECTIONS 1-4, 160.5-166.5 m

MAJOR ROCK TYPE - BASALT

Macroscopic Description

Basalt - Pieces 1A-E and 2A are even textured coarse-grained aphyric basalt with sparse calcite-filled veins and local alteration; continuation of Flow Unit 1, Core 7. Sec. 2, Piece 2B is badly altered very fine-

grained aphyric basalt with pink clay or siliceous coating on one end; base of Flow Unit 1 or top of Unit 2. Flow Unit 2 (Pieces 3A-4C, Sec. 1, all of Sec. 2 and 3, and Sec. 4 Pieces 1-2) is coarsening downward dark brownish gray basalt. Top of Unit 2 (Piece 3A, Sec. 1) is brecciated basalt cemented with calcite. This grades downward through fractured zone into massive, non-brecciated basalt laced with 1-3 mm wide smectite-coated calcite veins. Small zeolite(?) filled vesicles occur in Section 2 (Pieces 1C-H) and Sec. 3 (Pieces 10-F and 2B). Prominent conjugate fracture set oriented ~30° to core axis spaced ~5-15 cm apart throughout Sec. 2. Piece 3A Sec. 4 is aphyric basalt from base unit 2. Flow Unit 2A (Pieces 3B and 4, Sec. 4) is badly altered aphyric very fine-grained basalt. Underlying Flow Unit 3 (Pieces 5-7, Sec. 4) has a brecciated top of fine-grained badly altered aphyric basalt set in calcite matrix (Piece 5) followed by aphyric badly altered basalt with sparse zeolite(?) filled vesicles. Top of Flow Unit 4 (Piece 8, Sec. 4) is dark orange-brown glass breccia composed of black tachylyte fragments (0.5 mm-2.5 cm) rimmed with concentric bands of orange-brown palaeogite and iron-oxides(?) set in matrix of clear, glassy bladed crystals (phillipsite).

Thin Section Summaries

Section 1: Piece 1A - same as Piece 4 (Core 7, Sec. 2) but bit finer-grained. Piece 3A - flow top breccia of monolithologic fragments of basalt set in calcite matrix. Fragments identical to rock below them; breccia grades downward through minutely fractured and veined rock to more massive material. Aphyric with fine-grained quench texture (swallowtails, dendritic, skeletal, chain-linked and in radiating clusters); augite has finely plumose and comb dendritic texture interstitially between plagioclase. Olivine occupies cores of many plagioclase sheaves. Much interstitial material is glass devitrified to cryptocrystalline mass with faint plumose structure. Approximate mode: olivine <1, plagioclase 20, clinopyroxene 10-20, devitrified glass 60-70. Piece 3E - aphyric intersertal, coarse quench, subophitic to ophitic. Plagioclase shows faint radial sheaves and some skeletal features (chain link crystals and central core of inclusions). Pyroxene is subophitic and ophitic but clearly developing from coarsening of plumose structure; plumose and comb augite visible in glassy patches. Approximate mode: olivine 5, plagioclase 35-40, clinopyroxene 35-40, opaques 5-10, glass 10-20.

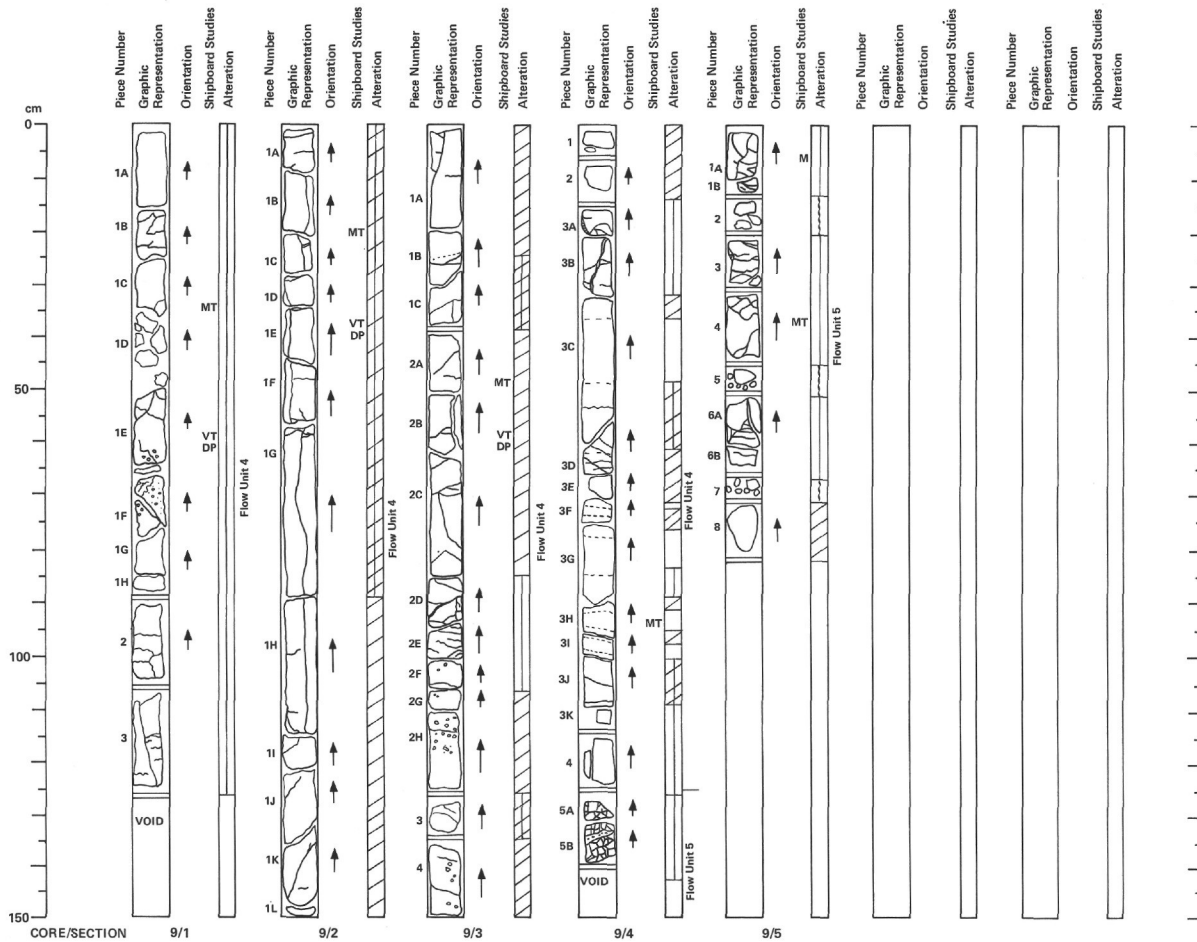
Section 2: Aphyric intersertal ranging from coarse quench to subophitic; coarse- to very coarse-grained. Pieces 1E-F show transition from fine quench to subophitic. Olivine relatively fresh; composition <Fo85 (2V x <90), central inclusions in each grain. Augite finely plumose dendritic to ophitic and intergranular with subophitic dominant. Sparse irregular calcite-filled vesicles. Piece 1P is more coarse-grained (up to 1.04 mm) subophitic and intersertal with faint plumose texture in some augite. Smectite lines vesicles and replaces rims of olivines. Approximate mode: olivine 8-10, plagioclase 35-40, clinopyroxene 35-40, opaques 10-15, devitrified glass 3-5.

Section 3: Aphyric, ophitic and intersertal, very coarse-grained. Texture and mineralogy same as Piece 1P, Sec. 2, but slightly more coarse-grained. Plagioclase shows strong normal zoning An₇₂₋₇₃.

Section 4: Piece 1B - aphyric, intersertal, coarse quench; texture and mineralogy same as Pieces 1E-F, Sec. 2. Piece 7B - aphyric intersertal, coarse quench, incipient subophitic; texture between those of Pieces 3A and 3E, Sec. 1. Sparse single plagioclase microphenocrysts (0.3-1.5 mm). Sparse calcite-filled vesicles. Approximate mode: olivine 5, plagioclase 30-35, clinopyroxene 35, opaques 10, devitrified glass 20.

Shipboard Studies

Sample	D	P	V _L	V _I	NRM1	NRM2	S. I.
Sec. 1, Piece 1A	-	-	-	-	9,811	-3.1	68
Sec. 1, Piece 1C	-	-	-	-	9,886	24.2	69
Sec. 1, Piece 1E	-	-	-	-	10,693	68.7	58
Sec. 1, Piece 3A	2.72	12.4	4.57	4.47	38,943	79.6	-
Sec. 1, Piece 3E	-	-	-	-	51,802	82.4	81.5
Sec. 2, Piece 1A	-	-	-	-	25,400	75.6	-
Sec. 2, Piece 1F	-	-	-	-	13,123	63.7	68
Sec. 2, Piece 1L	2.84	7.6	5.93	5.52	-	-	-
Sec. 2, Piece 1P	-	-	-	-	17,969	38.7	53
Sec. 3, Piece 2C	-	-	-	-	10,026	38.1	50
Sec. 3, Piece 2D	2.86	4.9	5.88	5.79	-	-	-
Sec. 4, Piece 1B	-	-	-	-	7,865	15.2	42
Sec. 4, Piece 7A	2.81	9.5	5.32	4.78	-	-	-
Sec. 4, Piece 7B	-	-	-	-	4,847	46.1	45.5



HOLE 519A, CORE 9, SECTIONS 1-5, 171.0-177.8 m
MAJOR ROCK TYPE - BASALT

Microscopic Description

Basalt - Aphyric coarse-grained through Piece 4, Sec. 4; essentially a continuation of Flow Unit 4 from Core 8. Pieces 1D, E, and F (Sec. 1) have finer-grained zones enclosed by more coarsely crystalline basalt; finer-grained areas have spherulitic texture with spherulites increasing and merging away from coarser phase. Fine-grained zones intrude coarser ones and are chilled against them. Most pieces of this flow unit are moderately to badly altered with relatively fresh basalt commonly surrounded by dark brownish gray to dark brown altered basalt in single pieces. Calcite- and zeolite(?) -filled vesicles (1 mm-1 cm) are scattered throughout, but especially concentrated in Pieces 1E-F (Sec. 1) and Pieces 2E-H and 4 (Sec. 3). Calcite- and smectite-lined fractures also common; largest one in Pieces 1B-H (Sec. 2). Finer-

grained aphyric basalt again in Pieces 3K and 4 (Sec. 4) at base of Flow Unit 4. Pieces 5A-B (Sec. 4) are flow top breccia of very fine-grained badly altered basalt in calcite matrix (top of Flow Unit 5). Breccia grades downward to dark brown very fine-grained aphyric basalt in Section 5 that is microporphyritic with plagioclase glomerocrysts. Pieces 1, 3, 4, and 6 (Section 5) are altered basalt; Piece 8 (Sec. 5) is similar but less altered. Pieces 2, 5, and 7 (Sec. 5) basalt rubble coated with smectite and powdery calcite.

Thin Section Summaries

Section 1: Aphyric interstitial coarse quench. Texture and mineralogy same as Pieces 1E-F in Section 2, Core 8, except this rock is slightly coarser-grained.

Section 2: Aphyric subophitic intersertal. Texture and mineralogy same as Piece 1P, Sec. 2, Core 8 but slightly coarser-grained.

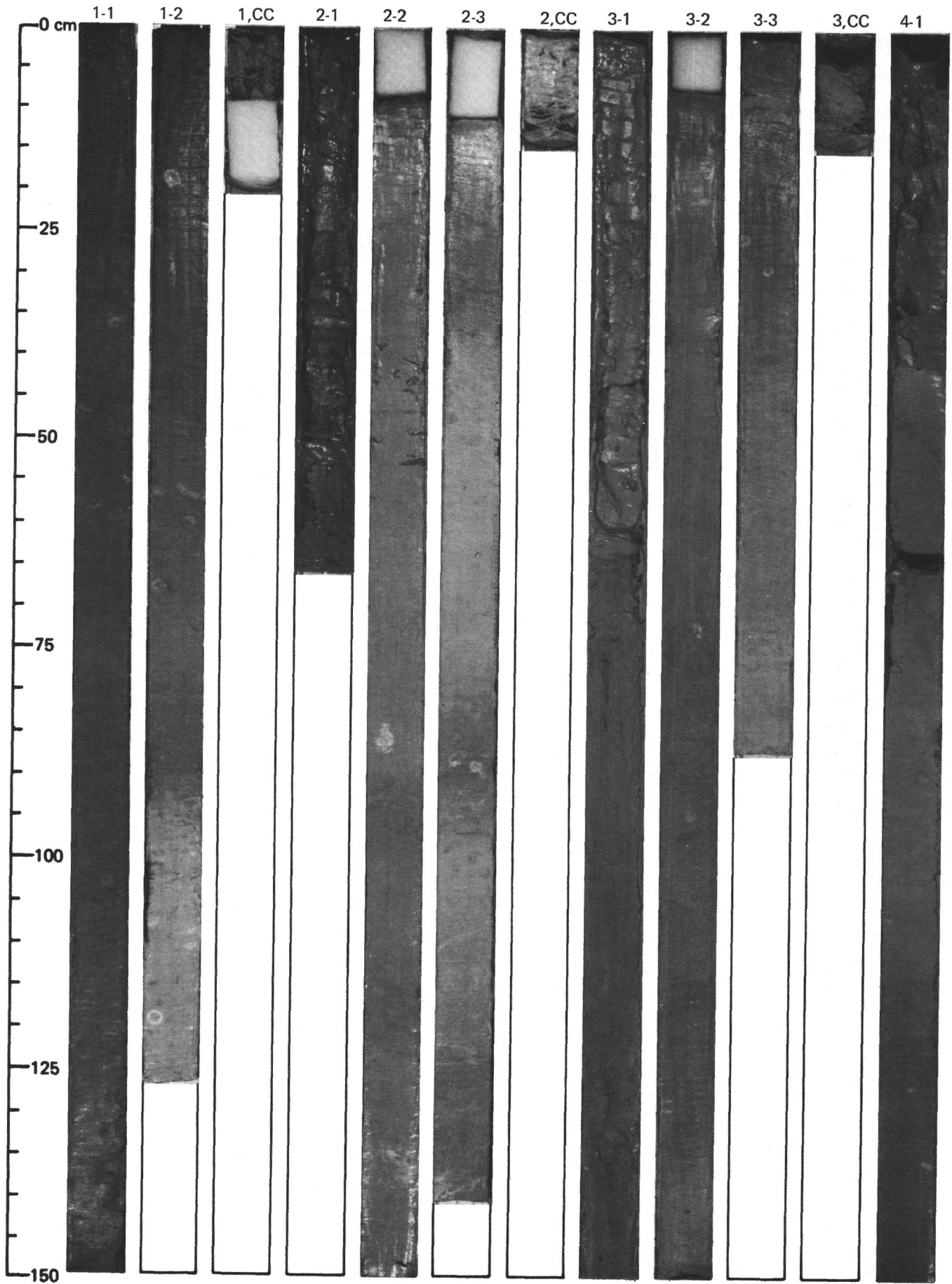
Section 3: Aphyric ophitic intersertal, coarse- to very coarse-grained. Olivine completely altered to smectite. Two generations of opaques: 1) intergranular, (0.005-0.12 mm), and; 2) dusting devitrified interstitial glass, ($l \leq 0.001$ mm). Plagioclase An₇₀. Approximate mode: olivine 5+, plagioclase 30, augite 30, opaques 10+, devitrified glass 20+.

Section 4: Aphyric ophitic intersertal. Texturally and mineralogically similar to Pieces 2A-B, Sec. 3 of this core but slightly fresher and finer-grained.

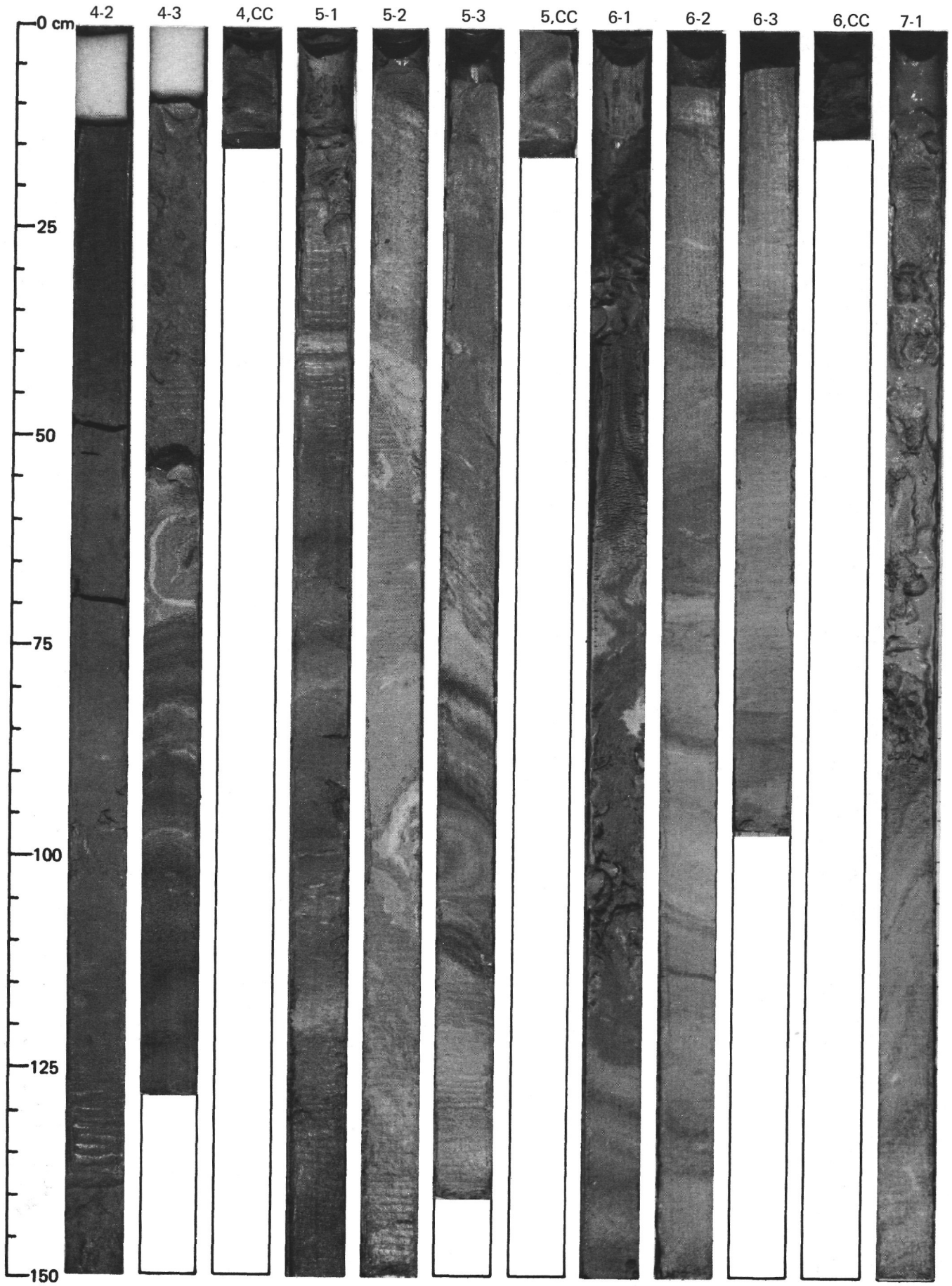
Section 5: Aphyric hyaloplitic or intersertal, with flow alignment of plagioclase microlites. Sparse (<1%) microphenocrysts of plagioclase (0.08-0.96 mm, An₆₀) and orthopyroxene (hypersthene? - 0.07-0.16 mm, 2Vx>90, birefringent <0.010). Plagioclase somewhat tapered with thin inclusion cores. Augite has plumose and fine comb texture in intersertal space between plagioclase microlites. Olivine completely altered to chlorite and smectite. Devitrified glass appears to be a mass of ultrafine augite and plagioclase fibers. Approximate mode: olivine 3-5, plagioclase 35-40, clinopyroxene 35-40, devitrified glass 25.

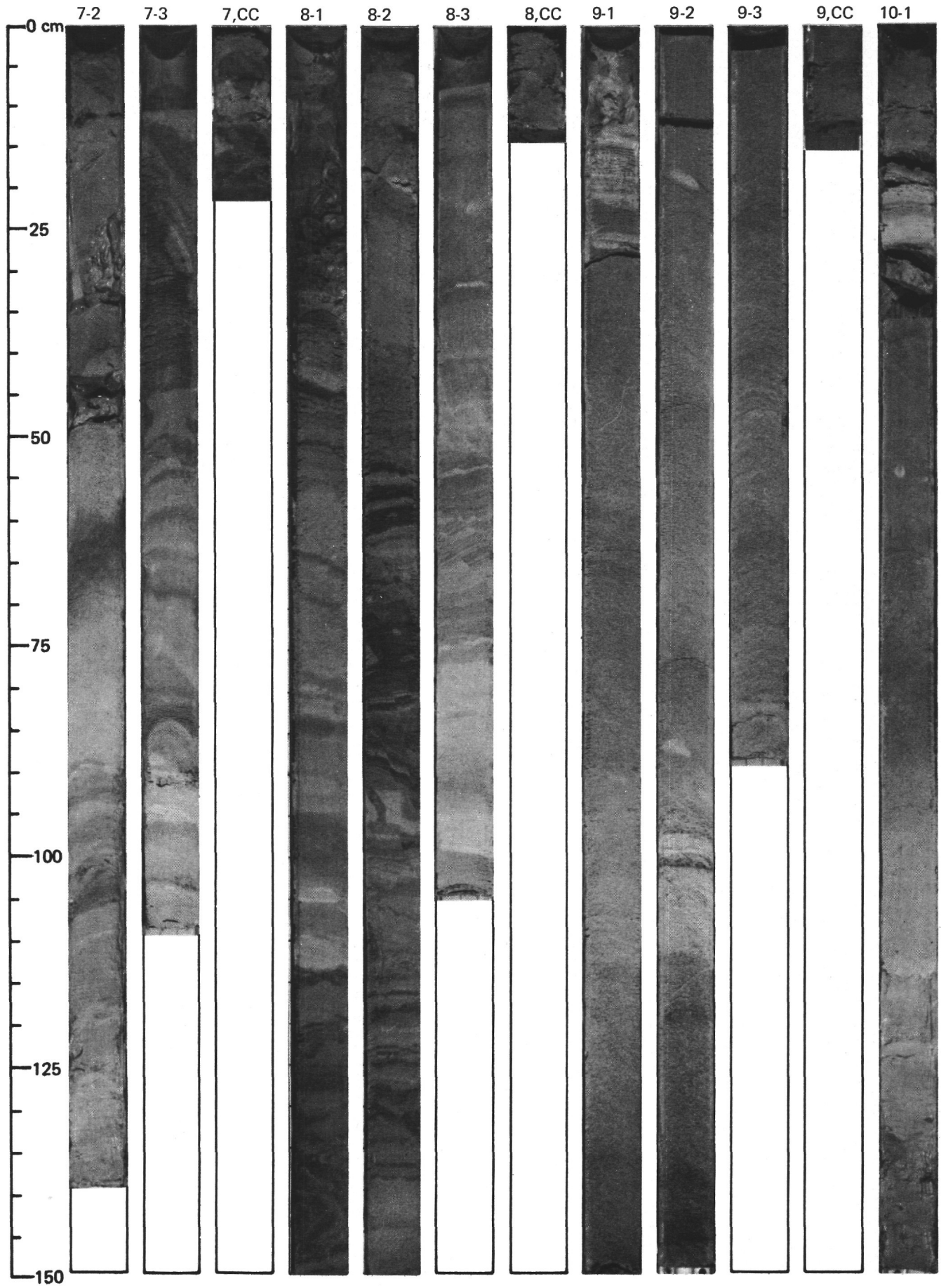
Shipboard Studies

Sample	D	P	V _L	V _H	NRM1	NRM2	S. I.
Sec. 1, Piece 1C	-	-	-	-	13,079	-9.3	-5
Sec. 2, Piece 1C	-	-	-	-	15,630	-6.0	3
Sec. 2, Piece 1E	2.80	3.1	5.51	5.49	-	-	-
Sec. 3, Piece 2A	-	-	-	-	13,438	-30.3	+0
Sec. 3, Piece 2B	2.80	3.4	5.87	5.60	-	-	-
Sec. 4, Piece 3H	-	-	-	-	7,124	-30.4	-0.5
Sec. 5, Piece 1A	-	-	-	-	10,590	-4.5	-2
Sec. 5, Piece 4	-	-	-	-	12,437	0.6	-1

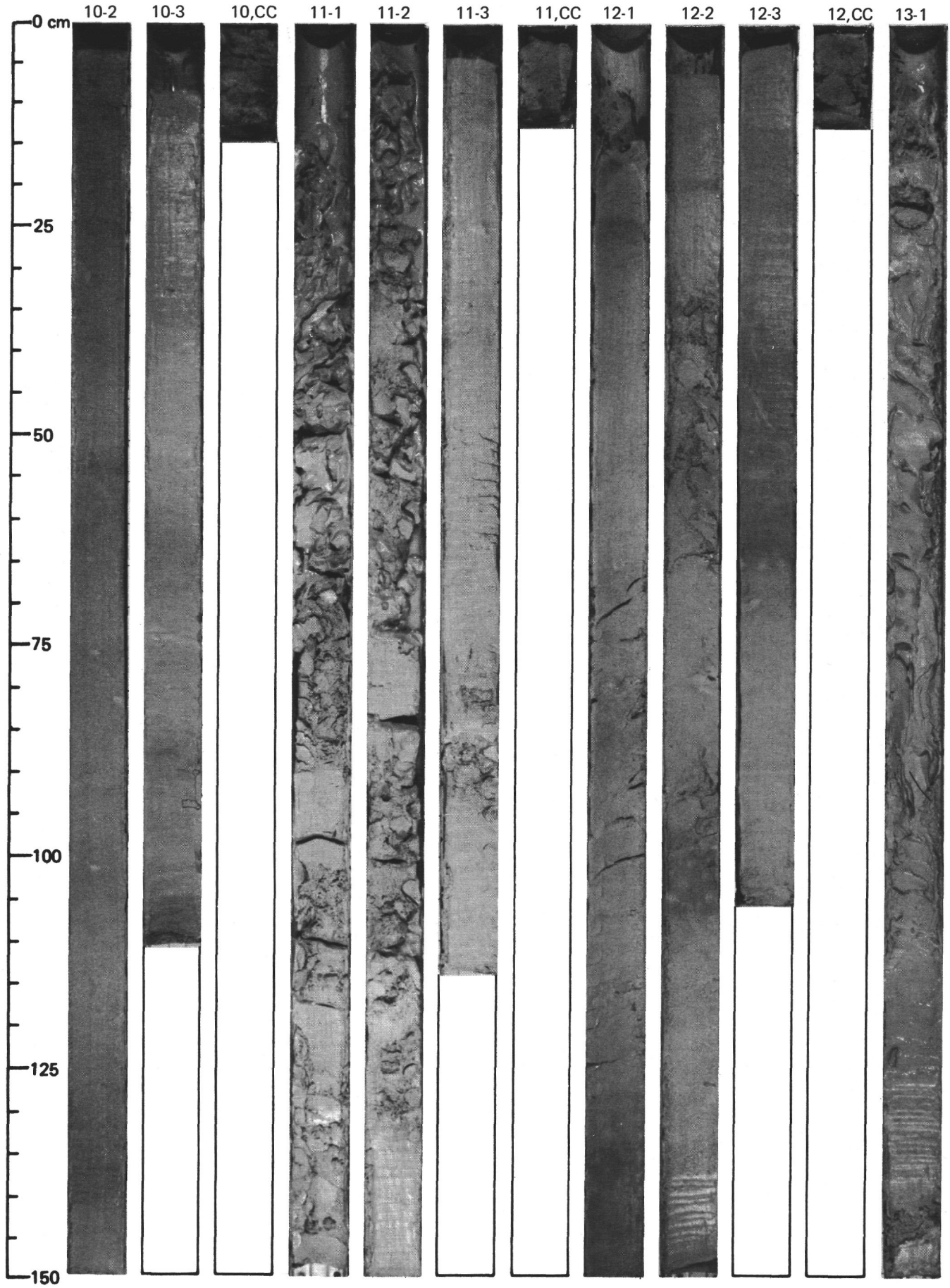


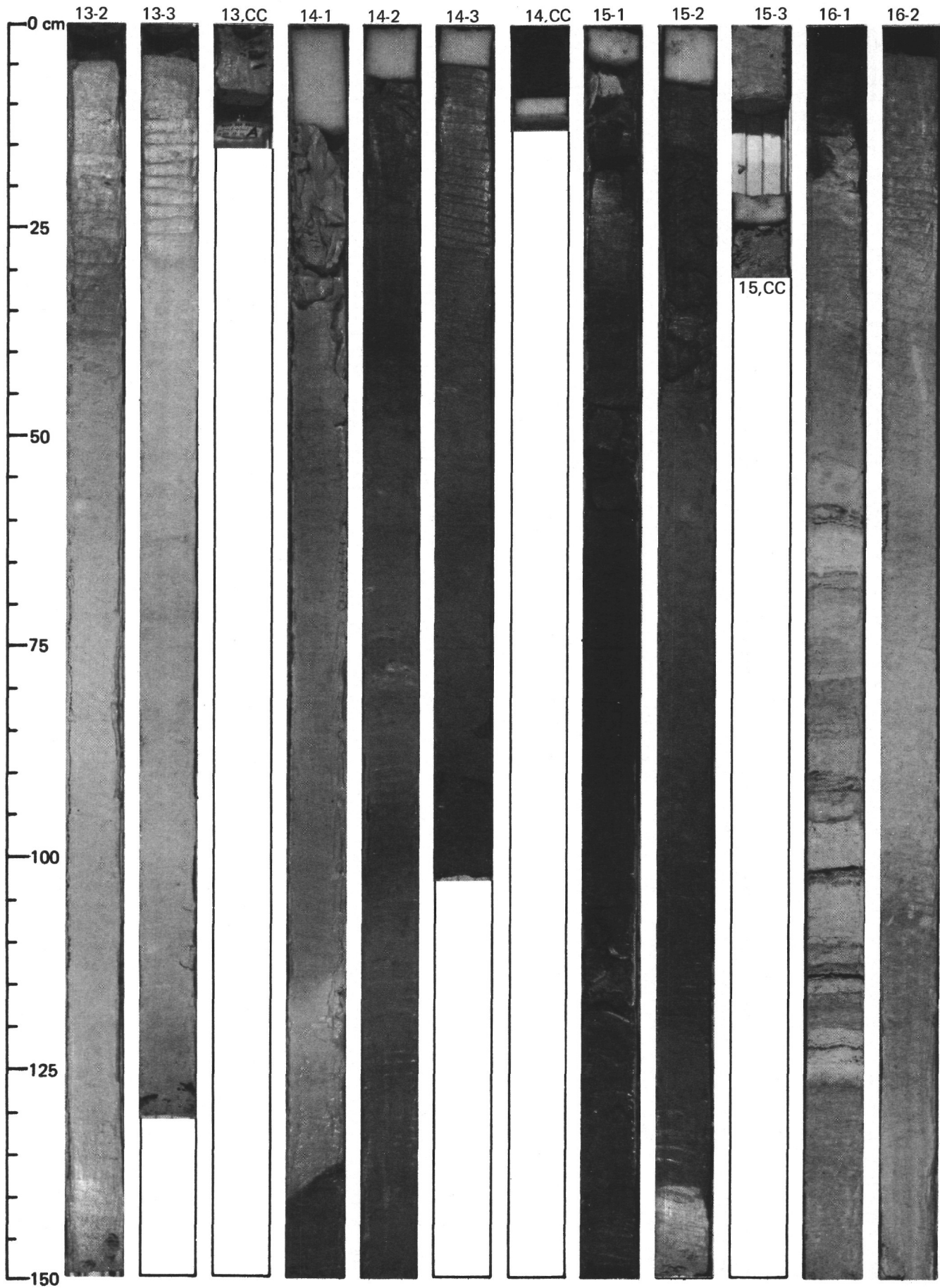
SITE 519 (HOLE 519)

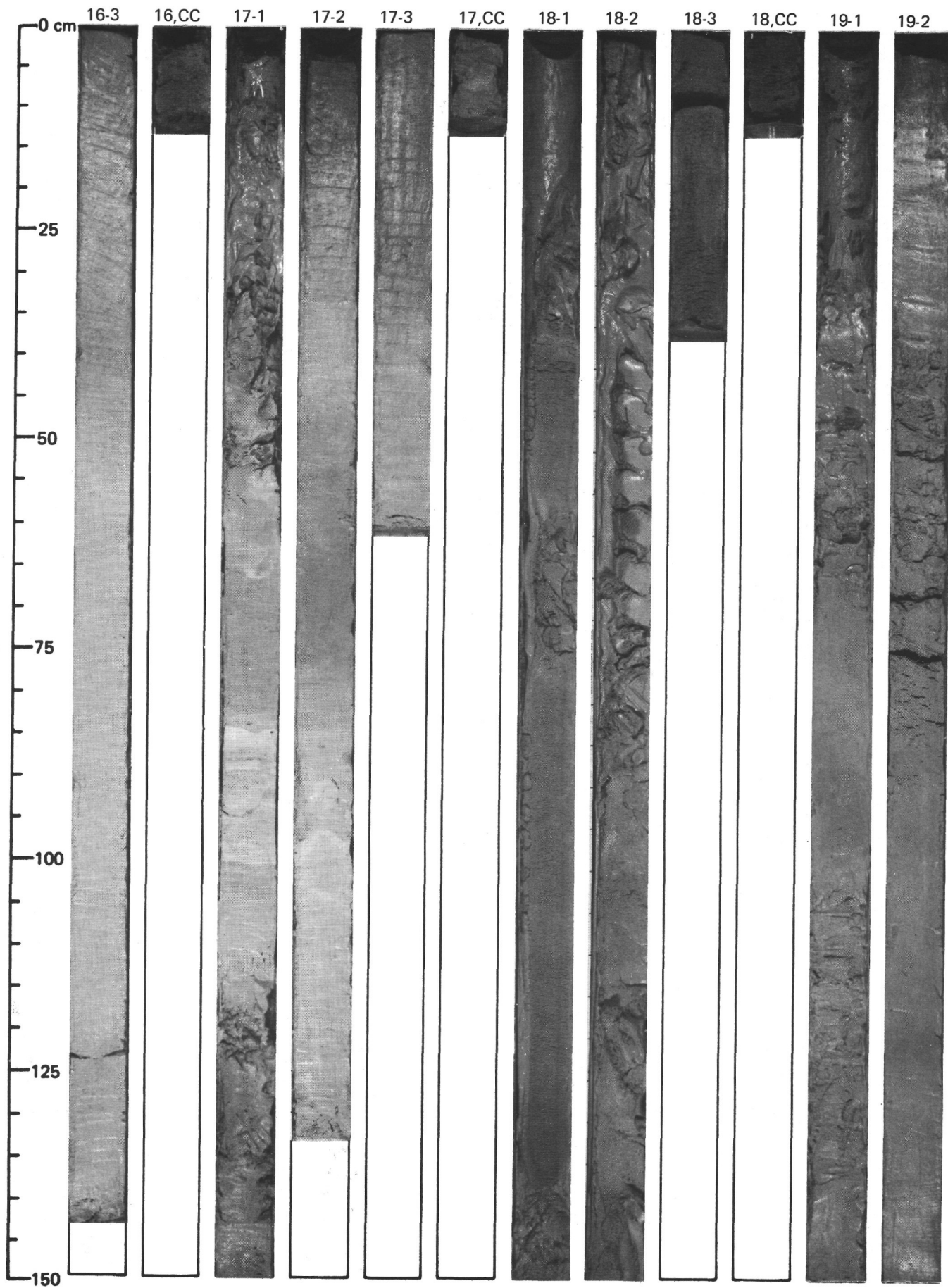


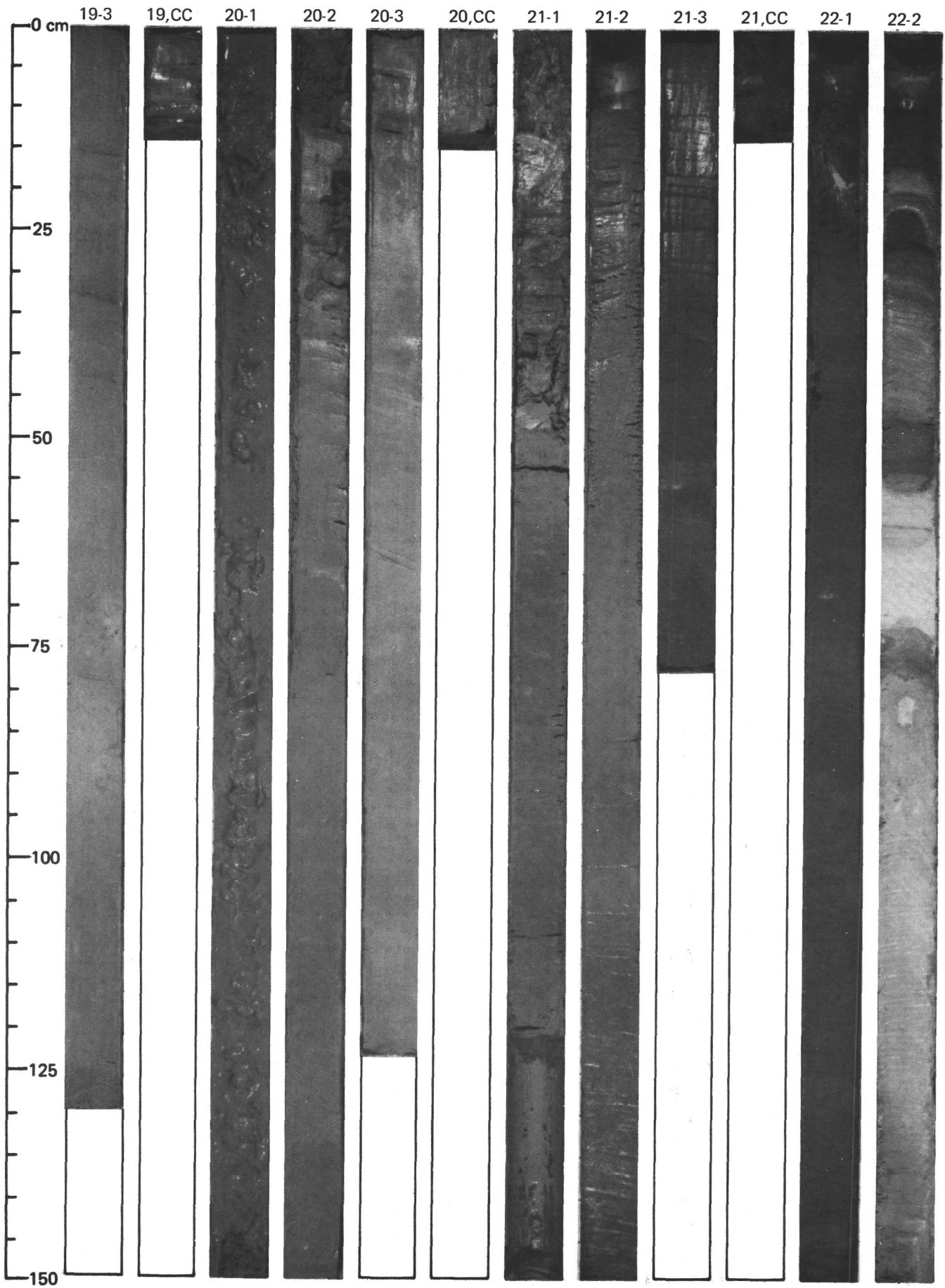


SITE 519 (HOLE 519)

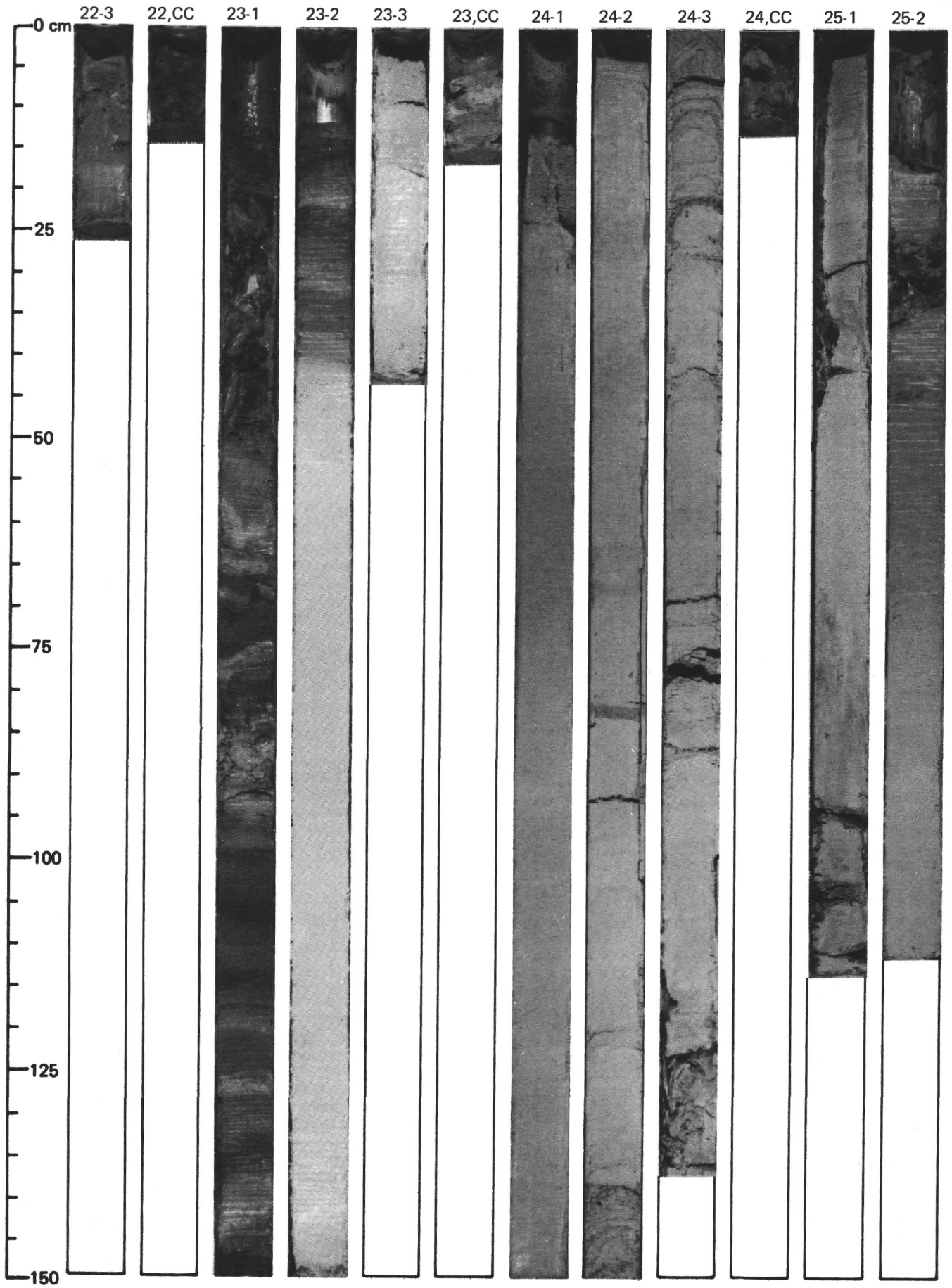


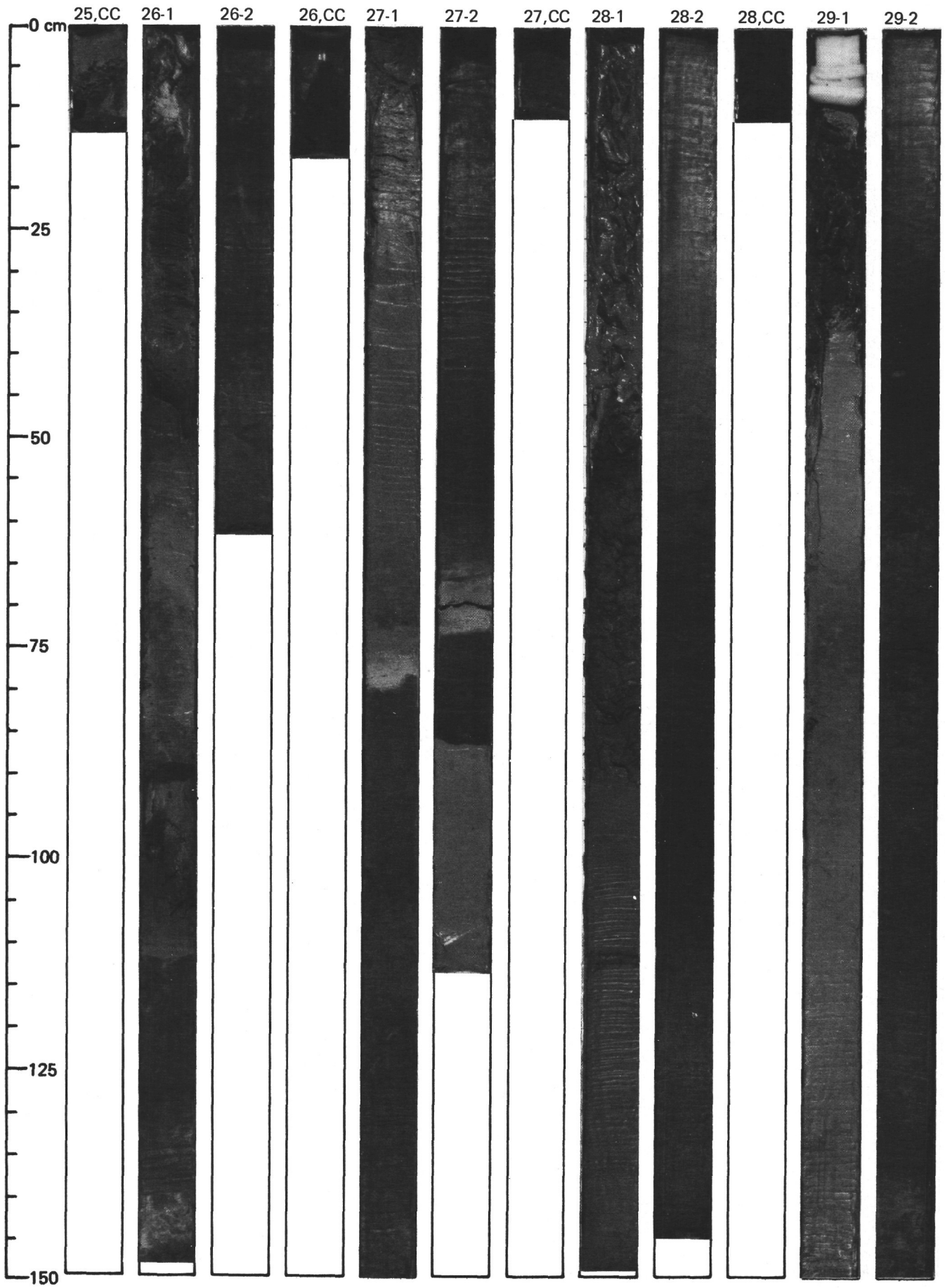


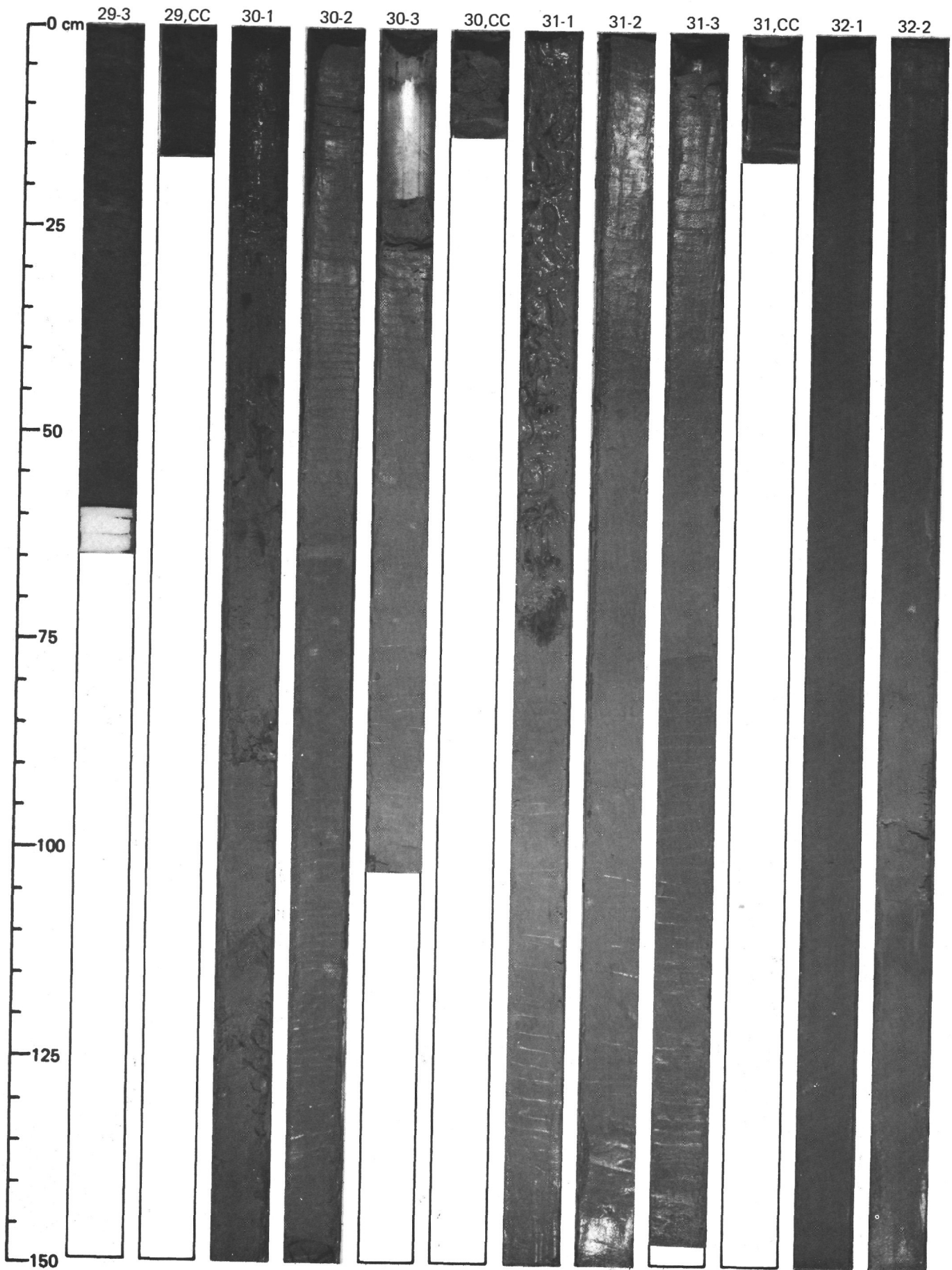


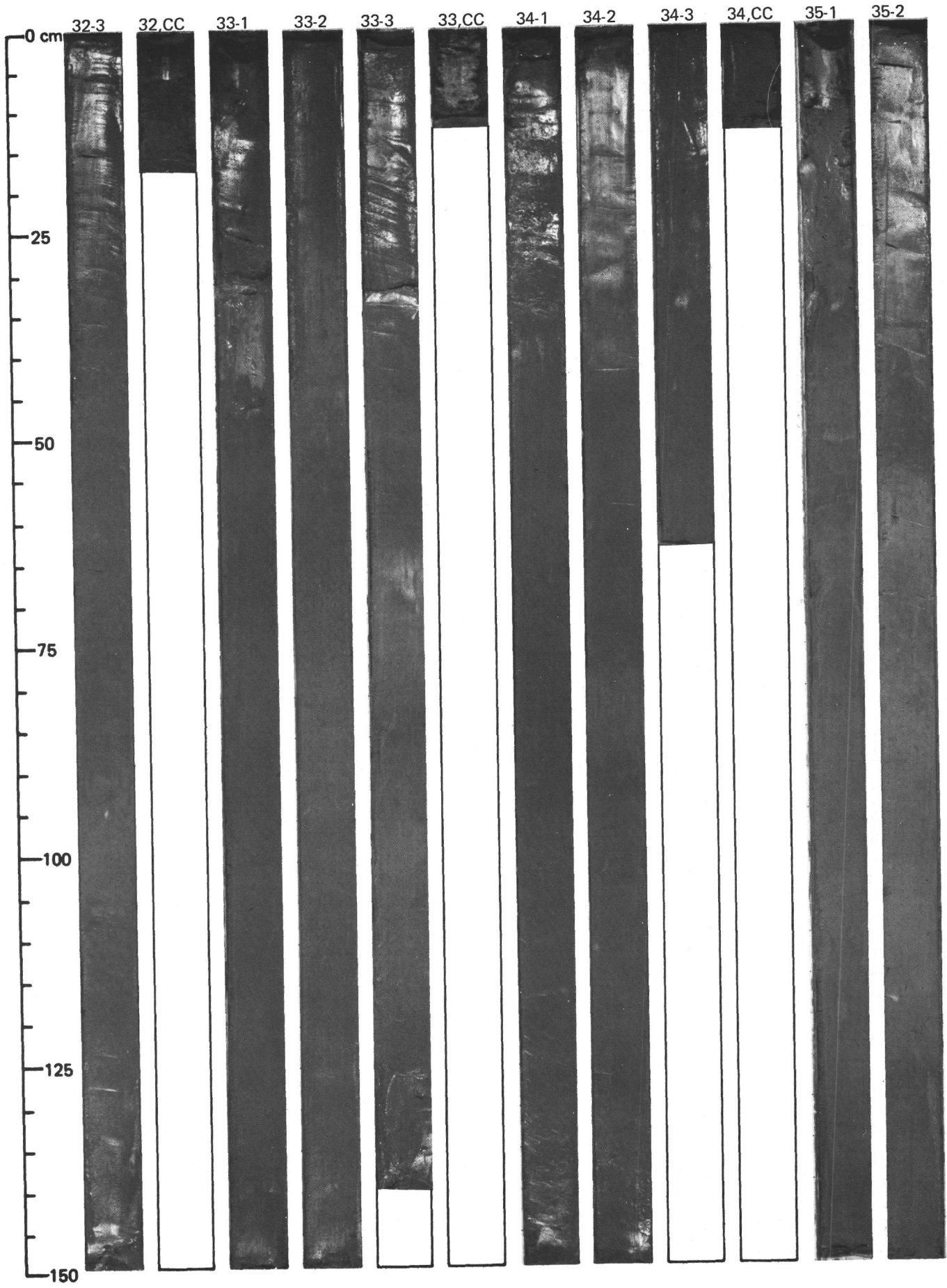


SITE 519 (HOLE 519)

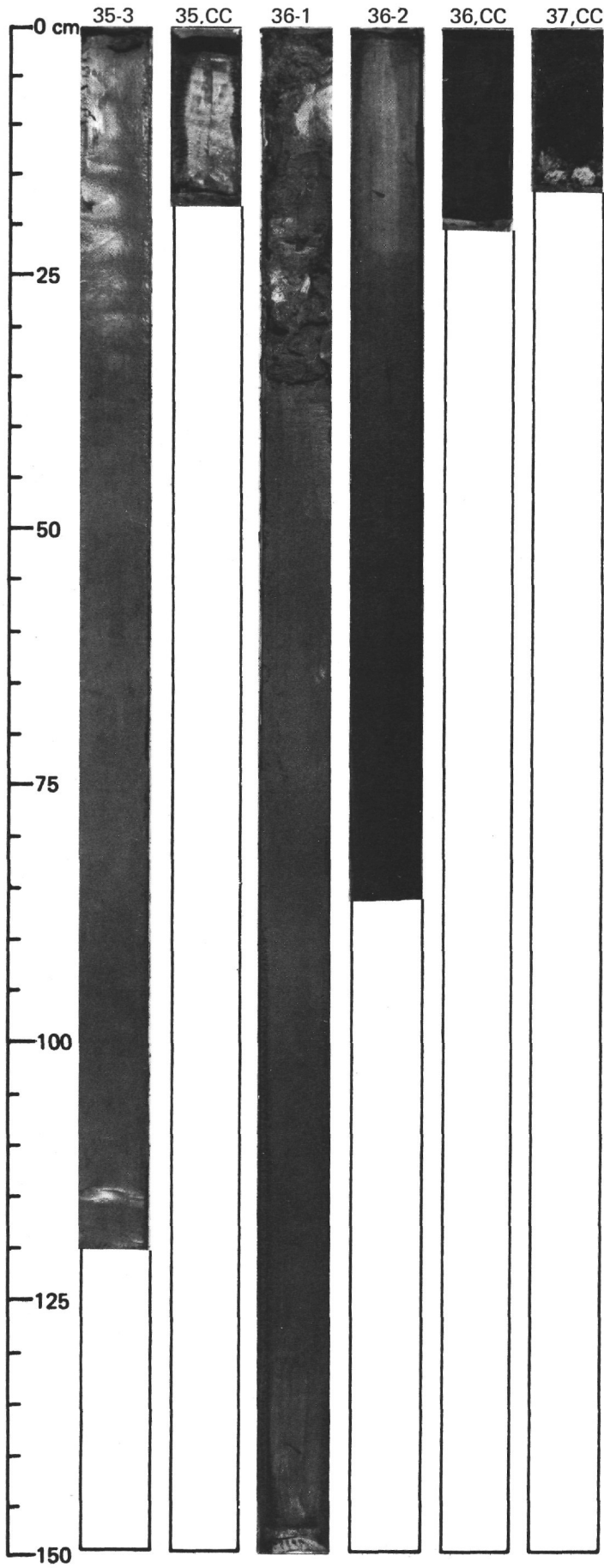


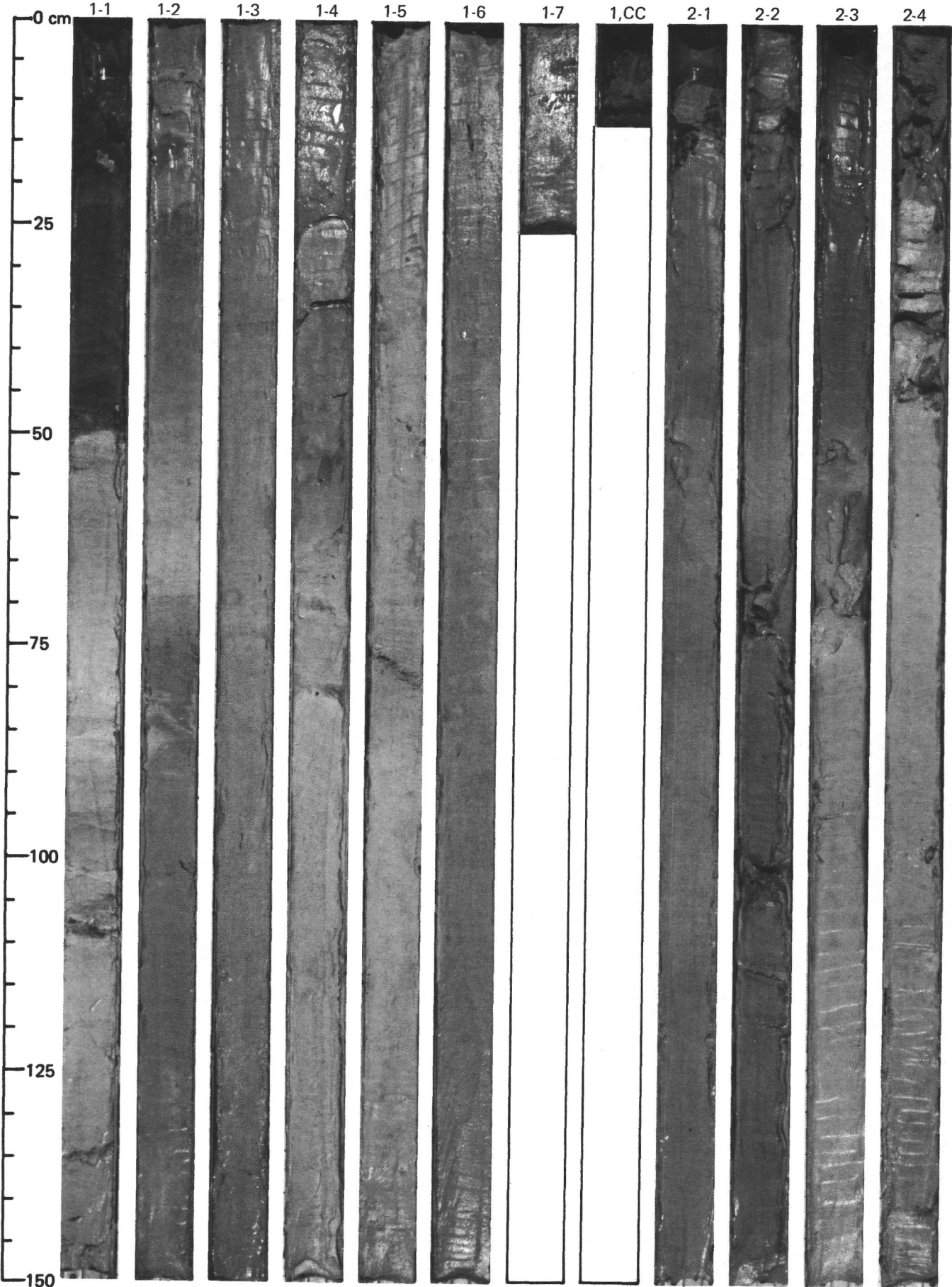


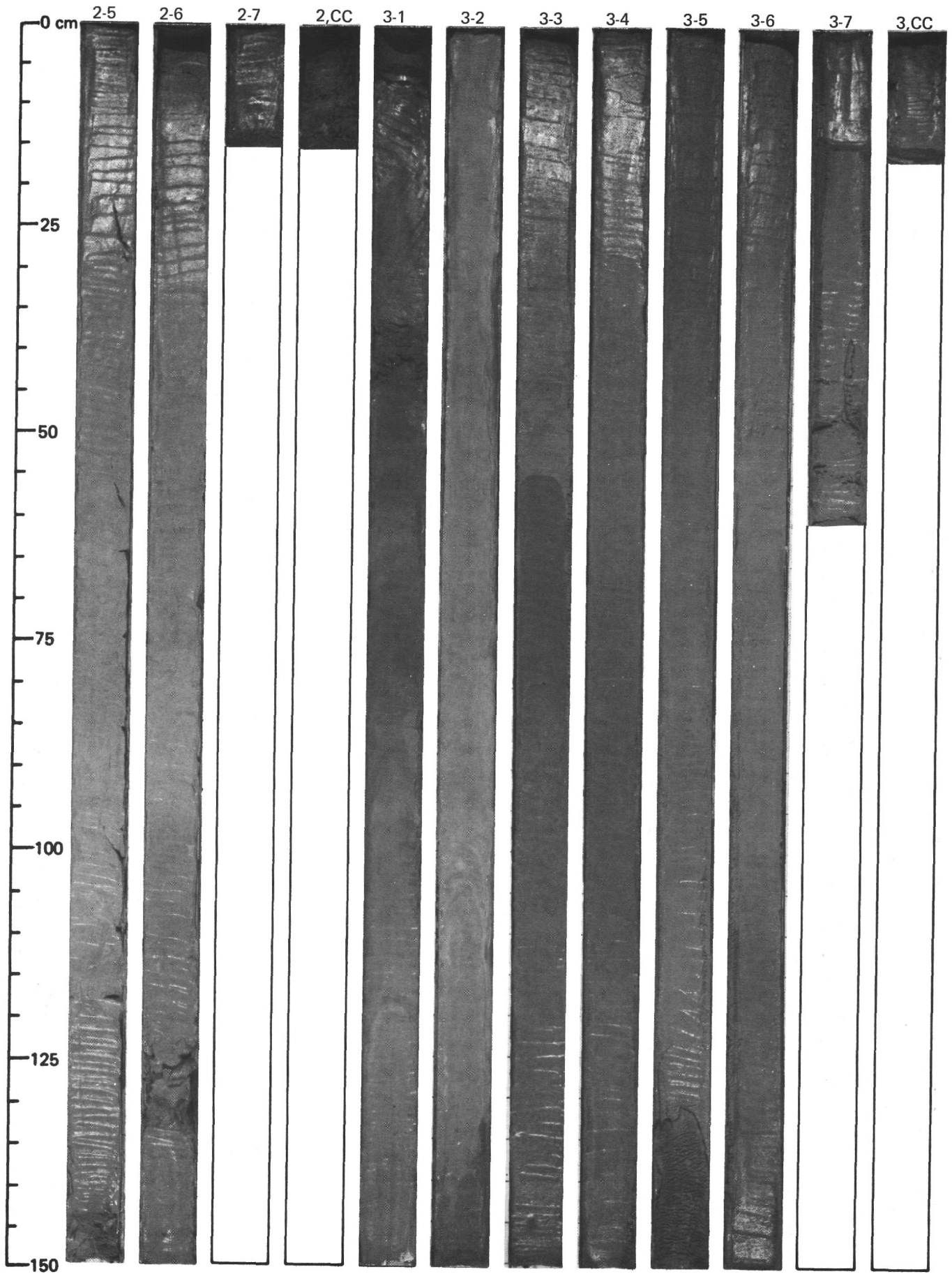


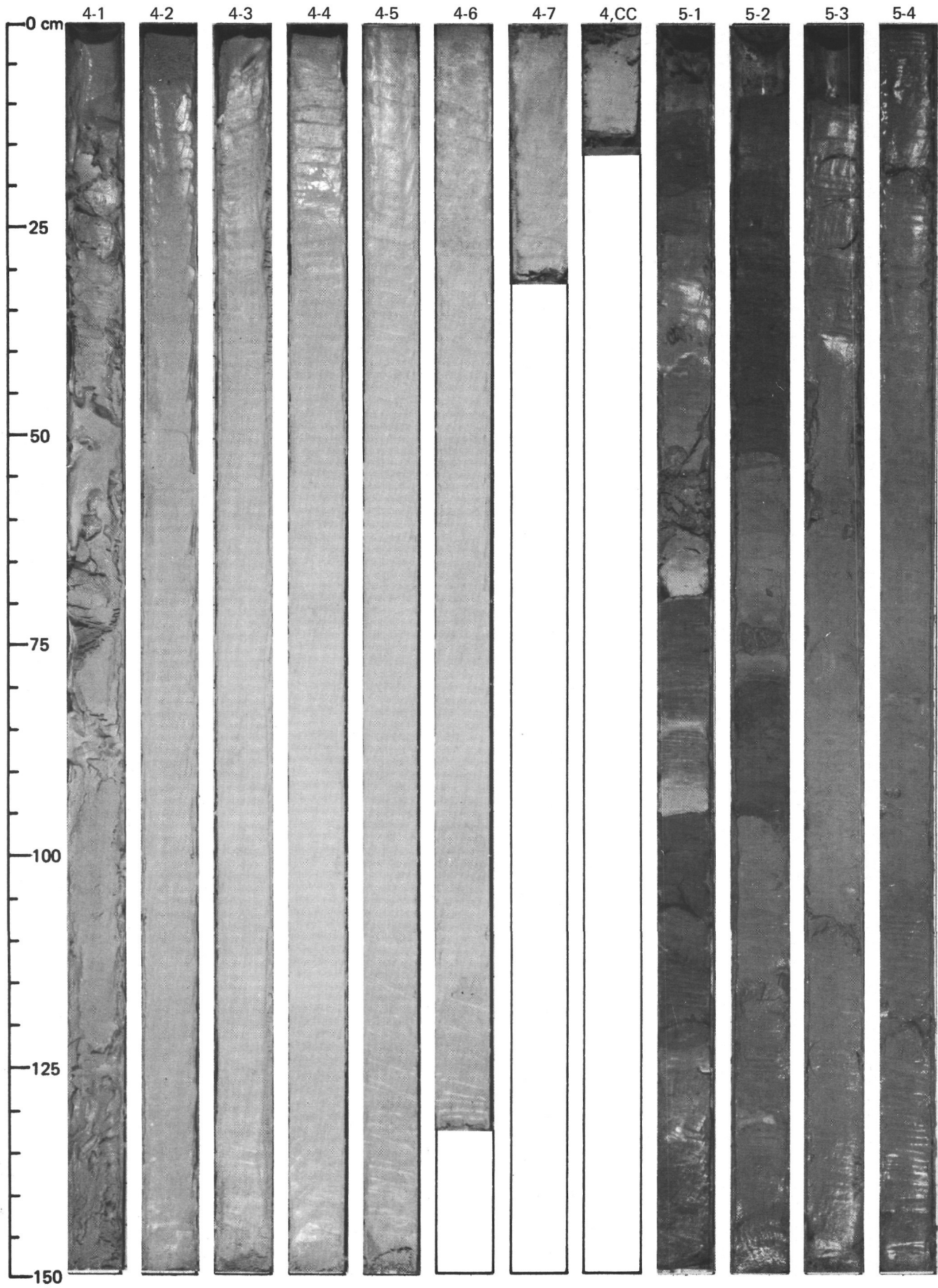


SITE 519 (HOLE 519)









SITE 519 (HOLE 519A)

